

N O T I C E

THIS DOCUMENT HAS BEEN REPRODUCED FROM
MICROFICHE. ALTHOUGH IT IS RECOGNIZED THAT
CERTAIN PORTIONS ARE ILLEGIBLE, IT IS BEING RELEASED
IN THE INTEREST OF MAKING AVAILABLE AS MUCH
INFORMATION AS POSSIBLE

"Made available under NASA sponsorship
in the interest of early and wide dis-
semination of Earth Resources Survey
Program information and without liability
for any use made thereof."

81-10083

CR-163781

SEA SURFACE TEMPERATURE OF THE COASTAL
ZONES OF FRANCE

Heat Capacity Mapping Mission - HCMM
Investigation n° 15
Progress Report n° 4

P.Y. DESCHAMPS and R. FROUIN
Laboratoire d'Optique Atmosphérique - Université de Lille I

J. CASSANET and F. VERGER
Laboratoire de Géographie - Ecole Normale Supérieure

M. CREPON
Laboratoire d'Océanographie Physique - Muséum d'Histoire
Naturelle

J.M. MONGET and L. WALD
Centre de Télédétection et d'Analyse des Milieux Naturels,
Ecole des Mines.

(E81-10083) SEA SURFACE TEMPERATURE OF THE
COASTAL ZONES OF FRANCE Progress Report
(Lille Univ.) 94 p HC A05/MF A01 CSCL 08J

N81-13436

Unclass

G3/43 00083

August 1980

RECEIVED

DEC 1 1980
SIS/902.6

HCMM-015
TYPE II

SEA SURFACE TEMPERATURE OF THE COASTAL
ZONES OF FRANCE

Heat Capacity Mapping Mission - HCMM
Investigation n° 15
Progress Report n° 4

P.Y. DESCHAMPS and R. FROUIN
Laboratoire d'Optique Atmosphérique - Université de Lille I

J. CASSANET and F. VERGER
Laboratoire de Géographie - Ecole Normale Supérieure

M. CREPON
Laboratoire d'Océanographie Physique - Muséum d'Histoire
Naturelle

J.M. MONGET and L. WALD
Centre de Télédétection et d'Analyse des Milieux Naturels,
Ecole des Mines.

August 1980

EROS Data Center
57198

SUMMARY

1 - INTRODUCTION

2 - RESULTS

2.1. Residual flow through the Dover Strait

2.2. Upwelling at the continental shelf break in the Bay of Biscay.

2.3. Mesoscale variability of the SST field.

2.4. Diurnal heating of the ocean surface layer.

3 - CONCLUSIONS

Appendice A - Permanent addresses of the investigators.

Appendice B - Satellite determination of the meso scale variability of the sea surface temperature.

Appendice C - Large diurnal heating of the sea surface observed by the HCMM experiment.

Appendice D - List of the received HCMM data.

LIST OF ABBREVIATIONS

AVHRR - Advanced Very High Resolution Radiometer on Tiros-N and NOAA-6 satellites.

CCT - Computer Compatible Tape.

CMS - Centre de Météorologie Spatiale.

CTAMN - Centre de Télédétection et d'Analyse des Milieux Naturels.

HCMM - Heat Capacity Mapping Mission.

HCMR - Heat Capacity Mapping Radiometer.

SST - Sea Surface Temperature.

VHRR - Very High Resolution Radiometer on NOAA-1 to 5 satellites.

1 - INTRODUCTION

The objectives of this investigation are to map the various thermal gradients in the coastal zones of France with regard to natural phenomena and man-made thermal effluents : to study and map the mesoscale thermal features in the English Channel, the Bay of Biscay and the North Western Mediterranean Sea ; to study and map the evolution of the thermal gradients generated by the main estuaries of the french coastal zones ; and to contribute to the modelling of diurnal heating of the sea surface and its influence on the oceanic surface layers.

The investigation is conducted by the followings : Dr P.Y. DESCHAMPS (Principal Investigator) and Dr M. CREPON, Mr J.M. MONGET and Professor F. VERGER (Co-Investigators).

Appendix A give related organizations and addresses.

This progress report is the last one before final report of the investigations. Results have been emphasized, while methods and problems have not been discussed.

2 - RESULTS

2.1. Residual flow through the Dover Strait

Time sequence of HCMM scenes allowed us to outline the influence of meteorological conditions on the residual current which flows to the N.E., from the British Channel into the North Sea, through the Dover Strait.. S.W. winds enhance this residual flow, and, as a result, the thermal effluent of the Rhine River is kept to the Dutch coast in a very narrow coastal band. N.E. winds contrary the residual flow which is slow down and deviated to the English coast : then the Rhine thermal effluent propagates offshore at a distance of up to 25 nautical miles. A close correlation exists between wind speed direction and the offshore width of the effluent.

2.2. Upwelling at the continental shelf break in the Bay of Biscay

HCMM data confirm the existence of a permanent upwelling at the continental shelf break in the Bay of Biscay. The upwelling is outlined by the appearance of cold water in summertime. This was previously mentioned from VHRR data. From HCMM scenes, a more complete description and interpretation of the upwelling has been obtained.

(1) The upwelling is probably permanent, but is enhanced by upwelled colder water in summertime when a seasonal thermocline is formed. On one occasion, January 16, 1979, warmer water appeared in wintertime at the shelf break (HCMM scene n° 265 - 1090) : this water is probably a "mediterranean" water, warmer and salted, flowing out of the mediterranean sea, from the Gibraltar Strait, into the Atlantic, at a depth of several hundred meters.

(2) Upwelling is enhanced after spring tides, which suggests that the basic mechanism for the upwelling is a tidal one. On two occasions after spring tides, August 25 and September 21, 1978, HCMM scenes (ID n° A-A0121 - 13260 and A-A0148 - 13320) show very similar patterns of cold water at the shelf break, with a maximum intensity between 48N-8E and 46.30N-5E where the tidal currents are at a maximum.

2.3. Mesoscale variability of the SST field.

Using VHRR and HCMR infrared digital data, a statistical two-dimensional analysis of the mesoscale variability of the SST field has been performed in order to characterize the random properties of this field. The power law exponent, n , of the spatial variance density spectrum, $E(k) \sim k^{-n}$ (k is wave-number), is deduced from the computation of the structure function of the SST. The study was first started on VHRR/NOAA-5 in the range of scales 40-100 km. HCMR data allowed us to extend the study down to a scale of 3 km. In the range of scales 3-100 km, n was found to vary from 1.5 to 2.3, with a mean

value of 1.8, over a study of 11 VHRR and 9 HCMR scenes. These values of n are of the order of the predicted values by the two-dimensional turbulence theories. However a discrepancy exists and we need further advanced theories to explain this experimental determination of the mesoscale SST variability.

The feasibility of the spectral analysis in the range of scales 3-30 km was made possible by the only low noise level of the HCMR data. A detailed manuscript is given as Appendix B.

2.4. Diurnal heating

Daytime HCMR data occasionally exhibit warmer sea surface areas which extend over 10 to 100 km. The warming is of several °C and is easily detected on photographic products because the warmer areas have usually smooth boundaries and cannot be confused with the sharper oceanic thermal boundaries.

These warmer areas are interpreted as a large diurnal heating of the upper surface layer under low wind speed conditions. Evidence of that is supported by several arguments.

(1) Meteorological observations and analysis show that warmer areas are associated with low wind speed conditions - i.e. anticyclonic conditions or coastal breeze effects.

(2) Glitter - i.e. direct solar radiation reflected by the wavy sea surface towards the sensor - has been used to derive an equivalent wind speed from the HCMR visible channel, where feasible (observation must be close to the specular reflection of a flat sea). Warmer areas are always associated with changes in the glitter patterns and decreasing wind speeds.

(3) Warmer areas disappear on consecutive nighttime HCMR data.

Under these low wind speed conditions, turbulence induced in the surface layer by the wind stress is strongly reduced, and most of the solar radiation absorbed is stored without downwards propagation. Theoretical simulations using a radiative and heat transfer model have been performed and predict large heating rates in the upper meter, and a maximum heating of several °C in the upper layer which is confirmed by a few in-situ measurements. Large heating only occurs in a few tens of cm and is very rapidly destroyed by the nighttime cooling.

4

HCMR data allowed us to discover that a diurnal heating of more than 1° C could affect large areas. Frequencies of occurrence are relatively high in the Western Mediterranean Sea where more than 10 % of marine surface are affected one day or another, while a large diurnal heating is very unlikely in the North Sea (only one scene). In such strongly affected areas, daytime satellite data could consequently give meaningless SST fields, and observations should be restricted to nighttime, or early in the morning when the surface layer is the most homogeneous. A detailed manuscript is given as Appendix C.

3 - CONCLUSIONS

During the reporting period, HCMM photographic products proved to be very useful :

- (1) to interpret the influence of wind direction on the mean residual flow through the Dover Strait,
- (2) to understand the upwelling occurring at the continental shelf break in the Bay of Biscay, and its relation with tidal currents.

A multitemporal analysis of HCMM digital products is on progress

- (1) to obtain a mean value of diurnal heatings observed in the Western Mediterranean Sea, during summer months,
- (2) to obtain a quantitative assessment of the intensity of the shelf break upwelling in the Bay of Biscay as function of tidal conditions.

Appendix A

Permanent addresses and organizations of the investigators

Dr. M. CREPON

Laboratoire d'Océanographie Physique
Muséum d'Histoire Naturelle
43, rue Cuvier
75231 PARIS Cedex 05 (France)

Dr. P.Y. DESCHAMPS

Laboratoire d'Optique Atmosphérique
Université des Sciences et Techniques
U.E.R. de Physique Fondamentale
59655 VILLENEUVE D'ASCQ (France)

Mr. J.M. MONGET

Centre de Télédétection et d'Analyse des milieux naturels
Ecole des Mines
Sophia-Antipolis
06560 VALBONNE (France)

Pr. F. VERGER

Laboratoire de Géographie
Ecole Normale Supérieure
1, rue Maurice Arnoux
92410 MONTRouGE (France)

SATELLITE DETERMINATION OF THE MESOSCALE VARIABILITY
OF THE SEA-SURFACE TEMPERATURE

P.Y. DESCHAMPS⁽¹⁾, R. FROUIN⁽¹⁾, L. WALD⁽²⁾

(1) Laboratoire d'Optique Atmosphérique, Equipe associée au C.N.R.S.,
Université des Sciences et Techniques de Lille,
59655 Villeneuve d'Ascq Cédex, France.

(2) Centre de Télédétection et d'Analyse des Milieux Naturels,
Ecole Nationale Supérieure des Mines de Paris, Sophia-Antipolis,
06560 Valbonne, France.

29 août 1980

60

ABSTRACT

Satellite infrared data have been used to investigate the mesoscale variability of the SST (Sea Surface Temperature) field. A statistical two-dimensional analysis of the SST field has been performed by means of the structure function. Results give the equivalent power law exponent, n , of the spatial variance density spectrum, $E(k) \sim k^{-n}$. n was found to vary from 1.5 to 2.3 with a mean value of 1.8 in the range of scales 3-100 km, in agreement with previous one-dimensional analysis from shipborne and airborne measurements. These observed values of n are discussed and compared to the values predicted by turbulence theories.

1. Introduction

The present capability of satellite infrared radiometers permits the determination of the mesoscale SST (Sea Surface Temperature) field on an operational basis thanks to their improved radiometric performances, which are typically a few tenths of ($^{\circ}\text{C}$) for a nadir resolution of 1 km^2 . This gives a potential tool for a systematic investigation of mesoscale thermal features such as thermal fronts and gradients which have already been detected and studied by means of infrared imageries or derived SST maps. Besides these observable features, a part of the SST field must be considered as random and containing some other information which can only be retrieved by a statistical analysis - e.g. the spectral density of variance.

Attempts to compute the spatial spectrum of the SST have been previously made by Mc Leish (1970), Saunders (1972 a) and Holladay and O'Brien (1975), from airborne infrared measurements along the aircraft track. Examples of mesoscale spectra have also been given from shipborne measurements (Voorhis and Perkins, 1966, Fieux et al., 1978), but more frequently for time series than for spatial variations. On the other hand, the satellite observations give the unique opportunity of investigating the mesoscale variability of the SST field, in the two-dimensions, down to scales of 1 km , at any given time, with a frequency which is limited only by the cloud cover. In this study, we intend to demonstrate the feasibility of using satellite data to obtain statistical parameters of the mesoscale SST field.

2. Statistical analysis of the SST field

Studies of the variability of the temperature (or any scalar) field

usually make an extensive use of spectral methods - i.e. the computation of the spectrum of the density of the scalar variance by means of Fourier transform or autocorrelation function, to obtain a typical power law which characterizes the variability of the temperature field and which can be referred to turbulence theories. In the present study, the structure function has been preferably used to determinate more accurately the power law exponent in the presence of the large noise level of satellite infrared data.

2.1 - Structure function

The SST field is considered as an isotropic random process with homogeneous increments (locally homogeneous) for which the structure function can be computed as :

$$D_{TT}(h) = \frac{1}{2} E \{ T(x+h) - T(x) \}^2 \quad (1)$$

where $T(x)$ = temperature at x ,

h = scale, $k = h^{-1}$ = wavenumber,

E = average operator.

The main advantage of the structure function, $D(h)$ when compared to the spectrum of the variance density, $E(k)$, or the autocorrelation function, $B(h)$, is that the experimental determination of the structure function is more accurate and much less affected by random variations because only increments are taken into account (Panchev, 1971). An example is given in Fig. 1 where both $E_T(k)$ and $D_{TT}(h)$ have been computed and are shown for the same sample of the SST field, measured by the AVHRR (Advanced Very High Resolution Radiometer) experiment on board the TIROS-N satellite. This example shows

clearly that the structure function is more regular than the spectrum, allowing an easier determination of the characteristic parameters - e.g. the power law exponent given by the slope when using logarithmic coordinates.

2.2 - Interpretation of the structure function

The structure function $D(h)$ statistically represents the influence of a point upon the h -distant points. For an homogeneous and isotropic random process, $D(h)$ and $B(h)$ are linked by the following relationship :

$$D(h) = B(0) - B(h) \quad (2)$$

As $B(h)$ and $E(k)$ are the Fourier transforms of each other, $D(h)$ may thus be related to $E(k)$ (Panchev, 1971) :

$$D(h) = 2 \int_0^{\infty} (1 - J_0(kh)) E(k) dk \quad (2\text{-dimension field}) \quad (3a)$$

$$D(h) = 4 \int_0^{\infty} \left(1 - \frac{\sin kh}{kh}\right) E(k) dk \quad (3\text{-dimension field}) \quad (3b)$$

where $J_0(kh)$ is the zero order Bessel function of the first kind.

In geophysics, the spectrum is usually expressed in the following way :

$$E(k) = B k^{-n} \quad (4)$$

and then, from (3a), (3b), the structure function may be written as :

$$D(h) = A h^p \quad (5)$$

where A and B are constants,

n and p are exponents, which may be deduced from each other by :

$$n = p + 1 \quad . \quad (6)$$

so that the exponent, n, of the spectrum can be alternately determined from the structure function, using (6), as far as the field under study is homogeneous.

Two kinds of error may affect the determination of the SST field obtained from satellite : instrumental data noise, atmospheric effect. .

Although the structure function has the advantage of being much more regular than the spectrum, the study of the structure function and of its shape is generally limited by the noise level at the smallest scales. This effect is illustrated in Fig. 1b, where the observed slope giving the power law exponent of the structure function decreases from about 1 at larger scales, to 0 at smaller scales. This is due to the fact that the structure function of the instrumental noise adds to the SST one. As far as this noise is white, its structure function is a constant (p=0) and its addition restricts the statistical analysis at smaller scales. This effect can be reduced by spatial smoothing with a corresponding degradation of the ground resolution.

Smoothing also introduces a bias in the determination of the structure function. If $D_F(h)$ is the structure function of the smoothed field, and Q is the convolution square of the smoothing function F, it may be shown (Matheron, 1970) that :

$$D_F(h) = D * Q - A \quad (7)$$

where \otimes means convolution and A is a constant, :

$$A = \int_{-\infty}^{+\infty} D(u) Q(u) du \quad (8)$$

In the particular case where F is the spatial average in $\sqrt{3}$ square and where the structure function $D(h) \sim h^p$, with $0.5 < p < 1.5$, the influence of smoothing on the amplitude of the structure function $D(h)$ increases with p, but decreases rapidly when h increases, and is less than 10 % when h is equal to 5 times the dimension of the smoothing square. The influence of spatial smoothing was thus neglected in the present study.

As far as the variations of the atmosphere can be neglected within the mesoscale oceanic range, the observed satellite variations of the SST field are reduced by the atmospheric infrared transmittance, τ (Deschamps and Phulpin, 1980) :

$$T(x+h) - T(x) = \tau(T_S(x+h) - T_S(x)) \quad (9)$$

where T_S is the actual SST,

T is the measured SST from space.

Then :

$$D_{TT}(h) = \tau^2 D_{TT}^S(h) \quad (10)$$

where D_{TT}^S is the actual structure function. τ depends on the atmospheric water vapor content and ranges between typical values of 0.9 to 0.3 for the 10.5 - 12.5 μm channel mostly used on satellites. This atmospheric effect will affect the determination of the amplitude of the structure function, but not the determination of the power law exponent, p. Because the atmospheric transmittance cannot be accurately determined over the oceans, only one parameter of

the structure function can be determined from satellite, and this is the power law exponent, p , obtained from the slope of the curve in a log-log plot.

The hypothesis of the homogeneity of the random field must be verified, otherwise erroneous determinations of the exponent could be obtained. For example, a frontal zone would have a spectrum $E_{TT}(k) \sim k^{-2}$ and a structure function $D_{TT}(h) \sim h$, while a non-removed trend would also give $E_{TT}(k) \sim k^{-2}$, but $D_{TT}(h) \sim k^2$. Because these exponents are close to the values physically expected, it is necessary to check carefully the homogeneity of the SST field and to remove the existing trend when necessary.

3. Results

The results of two independent but complementary studies are hereby presented. The first one deals with data obtained from the VHRR (Very High Resolution Radiometer) on board NOAA-5 and the study was limited to the range of scales 40-100 km because of the large level of instrumental noise. The improved radiometric performances of the HCMM (Heat Capacity Mapping Mission) data, - i.e. a nadir resolution of 0.5 km and NEDT = 0.3° K (see Table 1) - allowed us to extend the study down to scales of 3 km.

Cloudfree satellite data were selected in homogeneous study areas, Northeastern Atlantic Ocean and Mediterranean Sea. Locations are shown in Fig. 2 and dates are given in Table 2. At each one of these locations, the unidimensional structure functions were computed in four directions, $\theta=0$ (across the satellite track - i.e. approximately east to west), $\pi/4$, $\pi/2$ (along the satellite track) and $3\pi/4$. More details on the processing of the data may be

found in Frouin (1980) and Wald (1980). Examples of the computed structure functions are given in Fig. 3 for VHRR/NOAA-5 and in Fig. 4 for HCMM. The results generally show that the SST field is not exactly isotropic. Nevertheless, the structure functions, if not equal, are roughly parallel on a log-log plot, so that the anisotropy is confined in the amplitude, $A(\theta)$:

$$D_{TT}(\theta, h) = A(\theta) h^p \quad (11)$$

but the slope p remains very isotropic.

Values of p from 0.5 to 1.3 have been observed in this study with an estimated accuracy of about 0.1. Using VHRR/NOAA-5 data, 44 estimations of p were made in the range of scales 40-100 km, and 37 estimations in the range of scales 3-30 km with HCMM data. The corresponding histograms of the observed p are given in Fig. 5a and Fig. 5b. The most frequent values are 0.9-1.0 and the mean values are 0.8 (3-30 km) and 0.9 (40-100 km) with a standard deviation of about 0.2. About 90 % of the observed values are distributed between 0.5 and 1.1. The results correspond to a mean value of the power law exponent of the spectrum, n , of 1.8 in the wavenumber range 0.01-0.3 km^{-1} .

The amplitude of the structure functions varied from 10^{-2} to $10^{-1} (\text{°C})^2$ at $h = 40$ km. Even after spatial smoothing, it was noted that the noise level had a slight tendency of reducing the estimated of values of p because the structure function of the noise is a constant ($p=0$). This is particularly effective when the noise level ($5 \cdot 10^{-3} (\text{°C})^2$ for the HCMM data, $3 \cdot 10^{-2} (\text{°C})^2$ for the VHRR/NOAA-5 after smoothings) is of the same order as the structure function (see Fig. 1). Whenever possible, the estimates of p were corrected for this effect, but the effect could partly explain the lowest values of p .

On the other hand, a mean horizontal thermal gradient would give $D(h) \sim h^2$. The areas studied were carefully selected to avoid the existence of such thermal gradients which would increase the estimate of p towards larger values ; but here again some influence on the data could remain. Both these two effects, noise level and horizontal thermal gradients, could partly but not totally explain the spread of the results around the mean value, between 0.5 and 1.3, which remains significant. There is no evidence of correlation between the estimates of p and the corresponding geographical locations or seasons, but nevertheless, we would guess that it is probably necessary to involve physical processes in the explanation of the observed p values.

4. Discussion

Using Eq. 6 and the result from this structure function analysis, we obtain $1.5 < n < 2.3$ for the power exponent of the spectrum. This agrees fairly well with the previous results reported by several authors either from shipborne measurements (Fieux et al, 1978), or from airborne infrared measurements (Saunders, 1972a), for the one-dimensional temperature spectra (see Table 3). Holladay and O'Brien (1975) also made an attempt to reconstruct the two dimensional SST field from the tracks of the aircraft survey and found $n = 3$ for the isotropic part of the two-dimensional spectrum, a value which is probably overestimated because of the smoothing of high wavenumbers produced by the SST mapping procedure.

It would be interesting to relate the computed values of n to those given by turbulence theories in geophysics. All these theories assume the existence of an inertial range, i.e. the considered ^{scales} are far from the energy sink and source scales. It is not evident that the range of scales 3-100 km in the ocean is an inertial one. The upper limit of the dissipation scale

is of the order of 500 m and can be related to the wavelength of surface and internal waves via breaking processes. This scale is about one decade smaller than the lower limit of the studied range and we consider that there is no interaction between these two scales. The scales of input of kinetic energy and of temperature variance remain puzzling. Input of kinetic energy related to the wind is found at scales of the order of the wind waves (100 m) and at scales of the meteorological systems (1000 km or more). Energy inflow due to thermodynamic forcing is found at even larger scales. All these scales are one or two order of magnitude smaller or greater than those studied. At some location, interior processes such as baroclinic eddies or baroclinic instability may also play an important role in converting energy through non-linear mechanisms. The scales of these phenomena are of the same order as the internal radius of deformation or two to six times greater, depending on initial conditions. This radius is^{of} about 50 km in the open ocean and 10 km in the Mediterranean sea. If these physical processes are of importance in the area studied, the range 3-100 km is not an inertial one. In fact, we cannot precisely determine this from our observations : by looking at Fig. 3 and 4, one can notice that the structure functions do not exhibit any peak characterizing a very^{energetic} scale in the range we deal with, but this may only mean that the energy inputs are outside the studied range.

In the range of scales 3-100 km, horizontal scales are larger compared to vertical ones and the observed variability may be considered as being a quasi two-dimensional process. Therefore the observations can be related to the n -values predicted by the theories of bidimensional turbulence (Kraichnan, 1971) and of geostrophic turbulence in the atmosphere (Charney, 1971). These theories take into account either the conservation of energy and the conservation of enstrophy (half of the mean square of the vorticity) in the case of Kraichnan's theory or the pseudo-potential enstrophy (Charney). Both these theories agree when predicting the power law of the kinetic energy spectrum : $E_K(k) \sim k^{-3}$.

But the relations between current and temperature are not obvious and the different mechanisms involved lead to drastically different theoretical power laws for the temperature variance spectrum. In Kraichnan's theory, considering that temperature is a passive contaminant implies that $E_T(k)$ only depends upon k and upon the dissipation rates of enstrophy and temperature variance. Then, from a dimensional analysis, $E_T(k)$ must follow a k^{-1} power law. Charney made use of the perfect gas law and of the hydrostatic relation to compute a relation between the temperature and the stream function and he found the same law for $E_T(k)$ as for $E_K(k)$ - i.e. $E_T(k) \sim E_K(k) \sim k^{-3}$. Furthermore, assuming also $E_K(k) \sim k^{-3}$, Saunders (1972b) exhibited a temperature variance spectrum $E_T(k) \sim k^{-5}$, by the use of the thermal wind equation. These examples show that the results may be very different according to various authors. In this study, the mean observed value of 1.8 for n is far from the assessment ($n=5$) made by Saunders but falls between the Kraichnan and Charney predictions ($n=1$ and 3). This discrepancy may be due to the fact that the theories hypotheses have not been respected, in particular the hypothesis that the range studied is not an inertial one.

Some three-dimensional theories of turbulence (Kolmogorov, 1941, Bolgiano, 1962) or space-time variability theories of internal waves (Garrett and Munk, 1972, 1975) report values of n close to those found in our study (respectively 1.7, 1.4 and 2), but their physical basic hypothesis can hardly be extended in the mesoscale range.

We may also notice that several studies of atmospheric temperature fields mention values of n in agreement with our study at similar range of scales (100-1000 km). One may refer to the reviews by Gage (1979) and Panchev (1971). Some of these results are obtained by using spectral analysis

on time-series data and equivalent wavenumbers are computed by using Taylor's relation. As the validity of this relation is dubious for such scales, these time-series results must be considered carefully. But as for the oceanographic observations, there is no atmospheric theory to explain the observed results.

In summary, the power law exponent n of the spectral temperature variance observed in the range of scales 3-100 km is nearly 2. A large discrepancy exists with the predicted values from the 2 - dimensional turbulence theories which are widely spread around this value, and we need further advanced theories to explain the experimental determination of the mesoscale SST variability.

5. Conclusion

In this study, it has been proved feasible to estimate the random properties of the SST field in the mesoscale range 3-100 km from satellite infrared data. Compared to previous 1-dimension analysis from shipborne and airborne observations, the use of satellite data allowed us to perform a 2 - dimensional analysis. Using the structure function, the power law exponent, n , of the spectrum of the variance density of the SST field can be retrieved within a good accuracy (± 0.1). A mean value of 1.8 and a standard deviation of 0.2 have been found in the range 3-100 km, and extreme values of 1.5 and 2.3 have been observed.

The results give rise to several questions : (i) Is the range 3-100 km an inertial one ? (ii) If yes, is there any turbulence theory to explain the spectrum power law observed ? (iii) If not, at which scales are the inputs of energy and to which processes are they related ? At the present time, further investigations, both theoretical and experimental, are needed to interpretate

the physical mechanisms and parameters involved in the mesoscale variability of the SST field.

ACKNOWLEDGEMENTS

The authors are indebted to the receiving station of the "Météorologie Nationale" at Lannion, France, for providing them the infrared data from meteorological satellites. HCMM data have been received from NASA as a support to HCMM investigation number 15. They wish also to acknowledge the helpful advices of J.M. Monget and the fruitful suggestions of M. Crepon. Supports for this work have been provided by the following french agencies : CNRS (Centre National de la Recherche Scientifique), CNES (Centre National d'Etudes Spatiales) and CNEXO (Centre National pour l'Exploitation des Océans).

REFERENCES

BOLGIANO, R., 1962 : Structure of turbulence in stratified media. J. Geophys. Res., 67, 8, 3015-3023.

CHARNEY J.G., 1971: Geostrophic turbulence. J. Atmos. Sci., 28, 1087-1095.

DESCHAMPS, P.Y. and T. PHULPIN, 1980 : Atmospheric correction of infrared measurements of sea surface temperature using channels at 3.7, 11 and 12 μ m. Boundary-Layer Meteorol., 18, 131-143.

FIEUX, M., S. GARZOLI and J. GONELLA, 1978 : Contribution à la connaissance de la structure spatiale des courants superficiels au large du golfe du Lion. J. Rech. Oceanogr., 3,4.

FROUIN, R., 1980 : Contribution apportée par l'expérience spatiale HCMM à la télédétection de la température de surface de la mer. Thèse de 3e cycle, Université de Lille I.

GAGE, K.S., 1979 : Evidence for a $k^{-5/3}$ law in inertial range in mesoscale two dimensional turbulence. J. Atmos. Sci., 36, 1950-1954.

GARRETT, C. and W. MUNK, 1972 : Space time scales of internal waves. Geophys. Fluid Dynamics, 3, 225-264.

GARRETT, C. and W. MUNK, 1975 : Space time of internal waves : a progress report. J. Geophys. Res., 80, 3, 291-297.

HOLLADAY, C.G. and J.J. O'BRIEN, 1975 : Mesoscale variability of sea surface temperature. J. Phys. Oceanogr., 5, 761-772.

KOLMOGOROV, A.N., 1941 : The local structure of turbulence in incompressible viscous fluid for very large Reynolds numbers. Dokl. Akad. Nauk. SSSR, 30, 301-305.

KRAICHNAN, R.H., 1971 : Inertial-range transfer in two-and three-dimensional turbulence. J. Fluid Mech., 47,3, 525-535.

- KRAICHNAN R.H., 1974 : Convection of a passive scalar by a quasi-uniform random straining field. *J. Fluid Mech.*, 64, 4, 737-762.
- Mc LEISH, W., 1970 : Spatial spectra of ocean surface temperature. *J. Geophys. Res.* 75, 6872-6877.
- MATHERON G., 1970 : La théorie des variables régionalisées et ses applications. Cahiers du Centre de Morphologie Mathématiques de Fontainebleau. Ecole des Mines de Paris, Editors.
- PANCHEV, S., 1971 : Random functions and turbulence. Pergamon Press, 444 p.
- SAUNDERS, P.M., 1972 a : Space and time variability of temperature in the upper ocean. *Deep-Sea Res.*, 19, 467-480.
- SAUNDERS, P.M., 1972 b : Comments on "Wavenumber-frequency spectra of temperature in the free atmosphere". *J. Atmos. Sci.*, 29, 197-199.
- VOORHIS, A.D. and PERKINS H.T., 1966 : The spatial spectrum of short-wave fluctuations in the near surface thermocline. *Deep-Sea Res.*, 13, 641-654.
- WALD, L., 1980 : Utilisation du satellite NOAA-5 à la connaissance de la dynamique océanique. Etude de ses variations saisonnières en Mer Iigure et de ses variations spatiales en Méditerranée. Thèse de 3e cycle, Université de Paris VI.

Table 1. Radiometer performances of the satellite experiments used in this study.

Satellite experiment	Ground resolution at nadir (km) ²	Noise equivalent temperature difference (°C)
VHRR/NOAA-5	1	0.8
HCMR/HCSM	0.25	0.3
AVHRR/TIROS-N	1	0.1

Table 2. Summary of the different areas studied

Area	Date	Location	Experiment
Eastern Mediterranean Sea	19 Mar., 1978	33°00'N-28°00'E	VHRR
"	05 May, 1978	34°00'N-15°00'E	"
"	08 May, 1978	33°00'N-29°00'E	"
"	14 May, 1978	33°30'N-28°30'E	"
"	17 May, 1978	33°30'N-26°00'E	"
Western Mediterranean Sea	29 Sep., 1977	41°00'N-04°00'E	"
"	29 May, 1978	39°05'N-07°15'E	HCMR
"	29 May, 1978	40°05'N-06°55'E	"
"	11 Jul., 1978	38°55'N-04°50'E	"
"	11 Jul., 1978	41°55'N-06°55'E	"
"	26 Jul., 1978	39°20'N-06°15'E	"
"	28 Jul., 1978	38°15'N-03°45'E	"
"	28 Jul., 1978	38°35'N-05°05'E	"
"	28 Jul., 1978	37°40'N-07°25'E	"
"	14 Aug., 1978	38°30'N-03°00'E	VHRR
"	14 Sep., 1978	40°25'N-06°30'E	HCMR
"	1. Sep., 1978	40°35'N-11°55'E	"
"	14 Sep., 1978	41°40'N-06°45'E	"
Northeastern Atlantic Ocean	11 Sep., 1977	46°00'N-06°30'W	VHRR
"	14 Sep., 1977	45°00'N-07°00'W	"
"	06 Jan., 1978	46°30'N-09°00'W	"
"	10 May, 1978	46°00'N-08°00'W	"
"	11 May, 1978	45°15'N-04°40'W	HCMR
"	11 May, 1978	38°35'N-11°45'W	"
"	18 Jun., 1978	46°00'N-08°35'W	"

Table 3. Summary of observed mesoscale SST variability.

Authors	Range of scales (km)	Power law exponent n	Comments
SAUNDERS (1972)	3 - 100	2.2 ± 0.1	1-D, surface temperature, airborne infrared sensor.
HOLLADAY and O'BRIEN (1975)	3 - 20	3	2-D, SST maps from aircraft surveys.
FIEUX and AL. (1978)	1 - 64	2	1-D, surface temperature, ship-towed sensors.
This study	3 - 100	$1.5 < n < 2.3$; $\bar{n} = 1.8$	2-D, surface temperature, satellite data.

CAPTIONS

Figure 1 - Comparison between the density of temperature variance $E_T(k)$ (a) and the structure function $D_{TT}(h)$ (b), computed from AVHRR data, July 17, 1979, over the Bay of Biscay ($45^{\circ} 30' N - 4^{\circ} 30' W$). The dashed line indicates the radiometer noise level.

Figure 2 - Geographical locations of the different study areas for HCMM data (∇), and VHRR data (\bullet).

Figure 3 - Example of structure functions computed from VHRR data.

Figure 4 - Example of structure functions computed from HCMM data.

Figure 5 - Histograms of the observed values of the power law exponent p of the structure function in the range of scales 40 - 100 km (a) and in the range of scales 3-30 km (b).

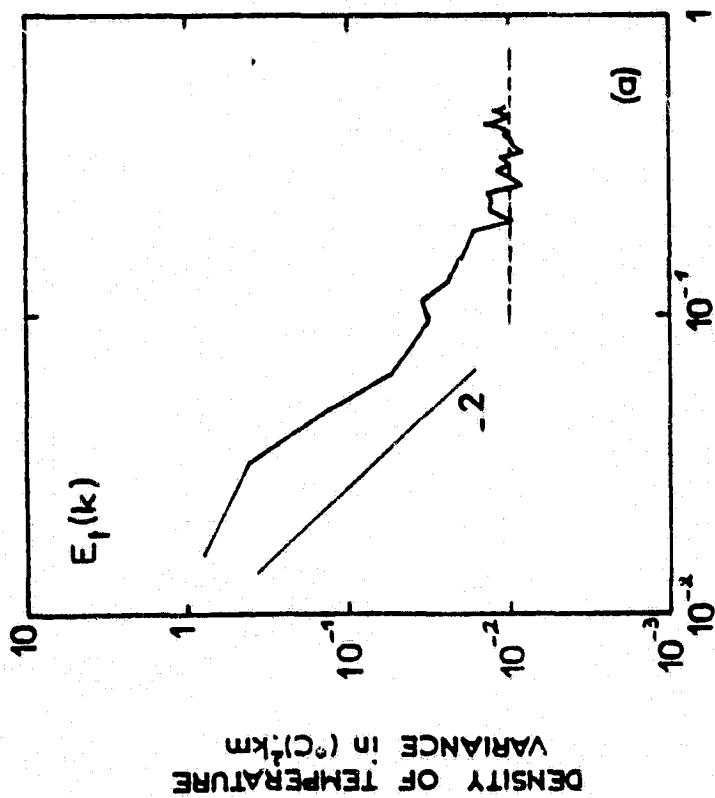


Fig. 1a

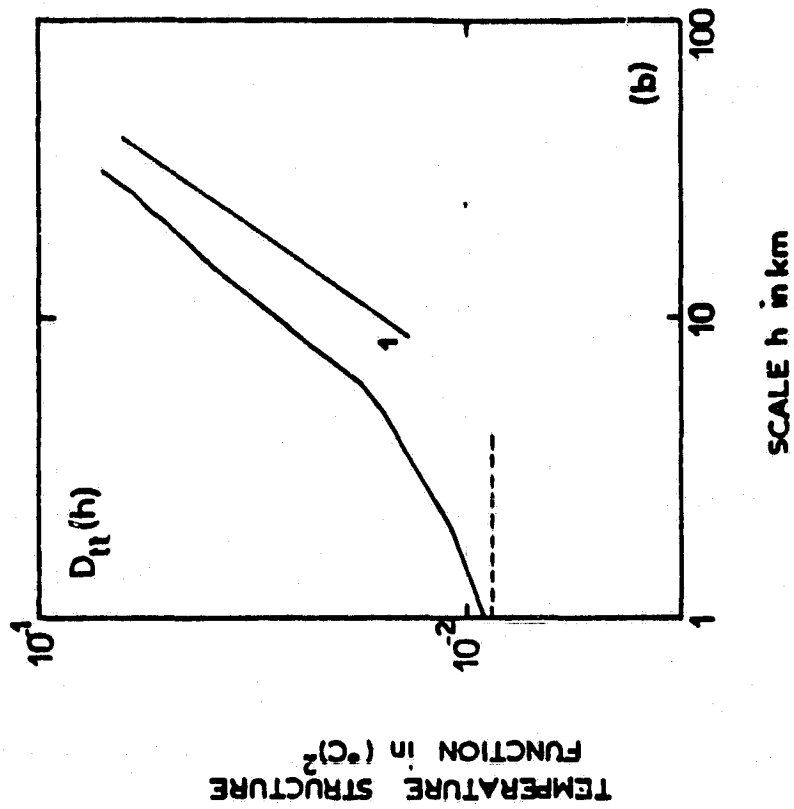


Fig. 1b

Figure 1 - Comparison between the density of temperature variance $E_t(k)$ (a) and the structure function $D_{tt}(h)$ (b), computed from AVHRR data, July 17, 1979, over the Bay of Biscay ($45^\circ 30' \text{ N} - 4^\circ 30' \text{ W}$). The dashed line indicates the radiometer noise level.

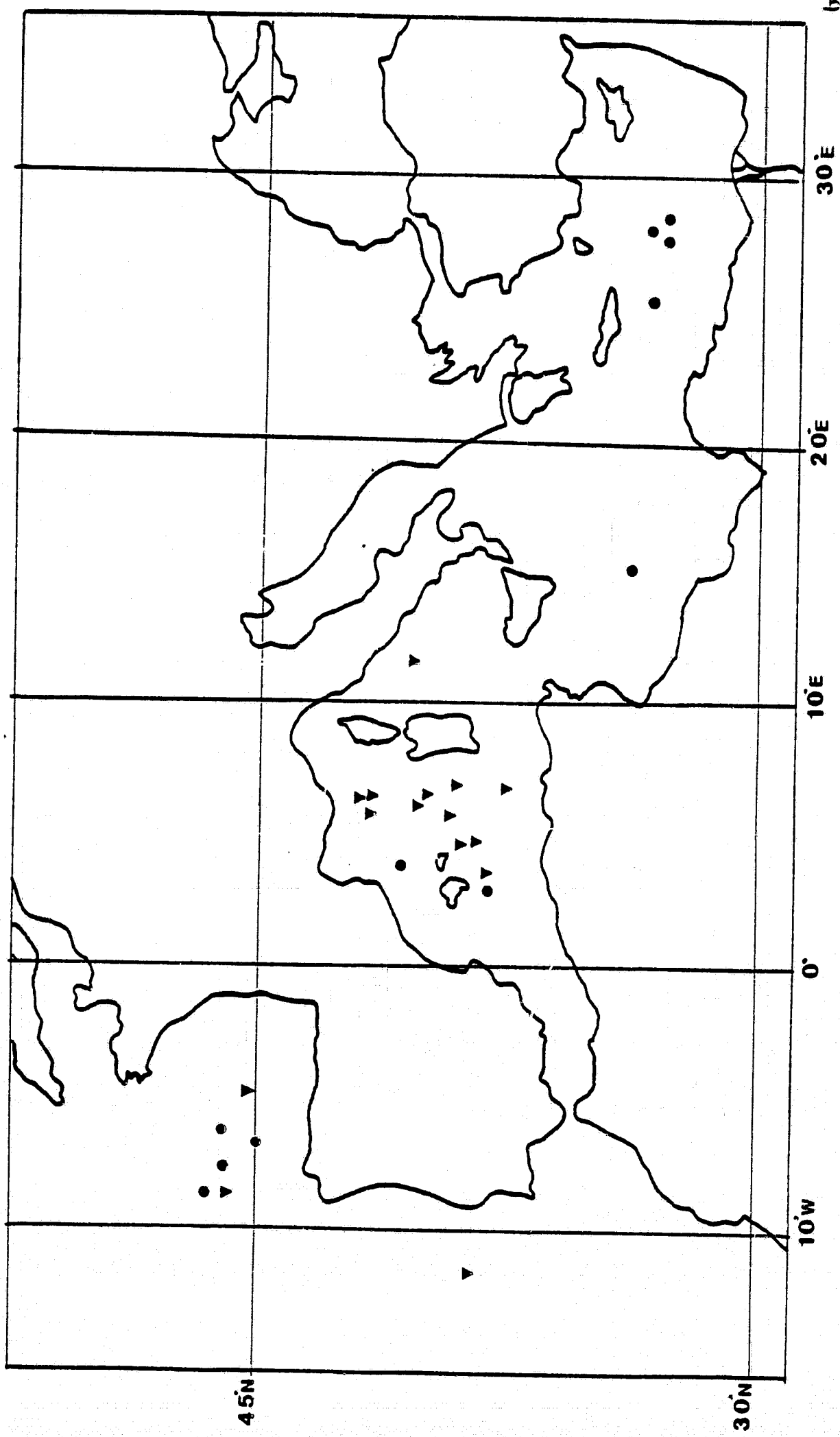


Figure 2 - Geographical locations of the different study areas for HCMH data (▼), and VHR data (●).

Fig. 2

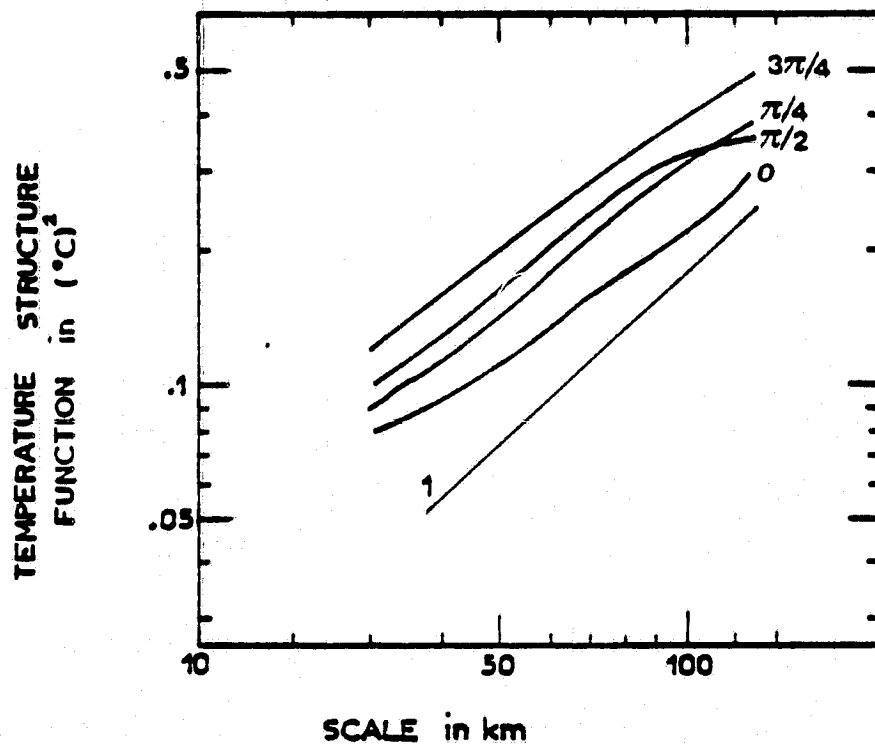


Fig. 3

Figure 3 - Example of structure functions computed from VHRR data.

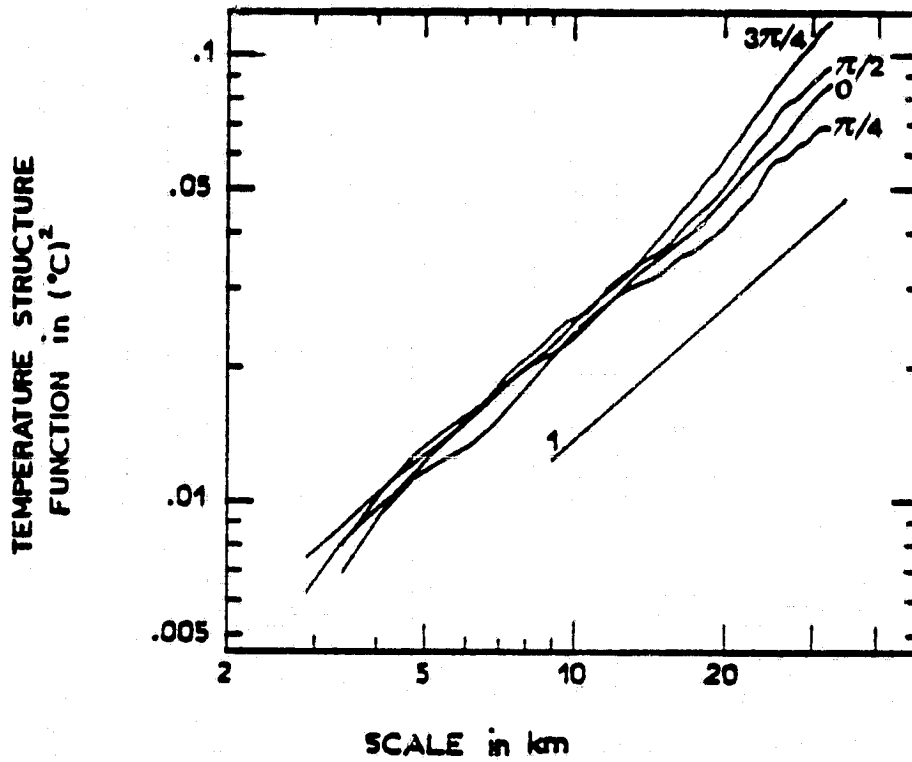


Fig. 4

Figure 4 - Example of structure functions computed from HCMM data.

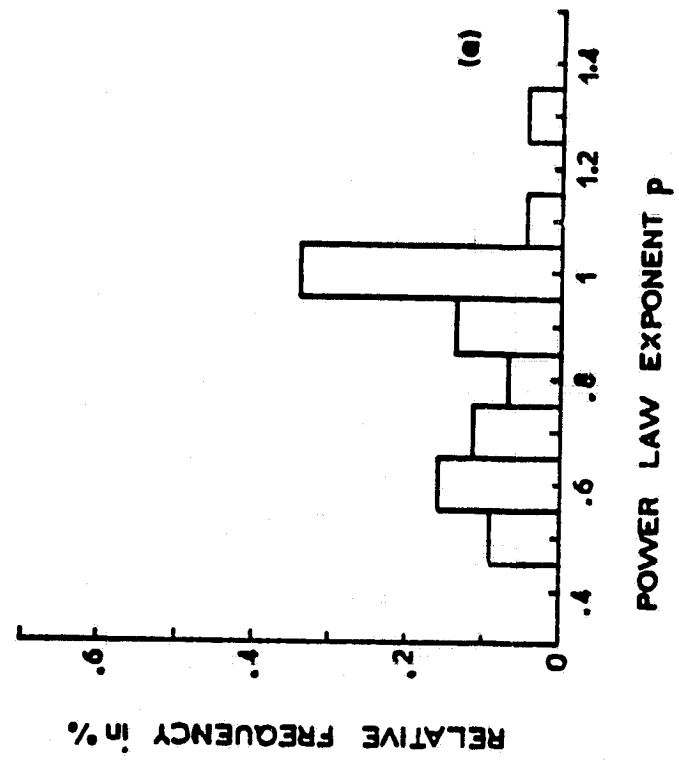


Fig. 5a

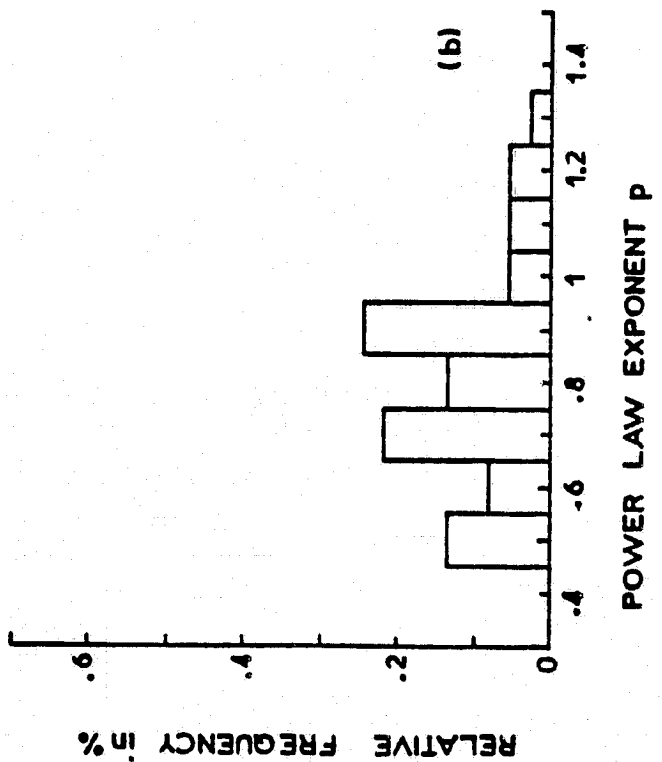


Fig. 5b

Figure 5 - Histogram of the observed values of the power law exponent p of the structure function in the range of scales 40 - 100 km (a) and in the range of scales 3-30 km (b).

LARGE DIURNAL HEATING OF THE SEA SURFACE OBSERVED
BY THE HCMM EXPERIMENT

P.Y. DESCHAMPS AND R. FROUIN

Laboratoire d'Optique Atmosphérique,
Equipe Associée au CNRS n° 466,
Université des Sciences et Techniques de Lille,
59655 Villeneuve d'Ascq Cédex, France

ABSTRACT

Day-night surface temperature differences have been measured in the infrared (10.5 - 12.5 μm channel) by the HCMM satellite experiment, which show large diurnal heating (several $^{\circ}\text{C}$) of the upper layer of the ocean, very frequently during summer months in the Mediterranean Sea, when the wind speed is low. When observed in the 0.5 - 1.1 μm channel, glitter reflectance - i.e. direct solar radiation specularly reflected towards the sensor - correlates with diurnal heating. Glitter reflectance has been modeled to retrieve an equivalent wind speed, and observed diurnal heatings, ΔT , rapidly decrease with the wind speed, U , from a maximum value of about 5°C . An empirical law is given : $\Delta T_{(^{\circ}\text{K})} \approx 3.5 \cdot 10^{-3} Q_{(\text{W.m}^{-2})} / (0.7 + U_{(\text{M.s}^{-1})})$ where Q is the irradiance at sea level. A mean diurnal heating of nearly 1°C is calculated for the marine coastal areas of the south France, in summer time. During this period, satellite observations should be restricted to night and early morning times, and to the only high wind speed ($U > 5 \text{ m.s}^{-1}$) at noon and during the afternoon.

I - INTRODUCTION

A daily variation of the temperature in the surface layer of the oceans is known to be produced by the diurnal heating of the absorbed solar radiation. The amplitude of the daily temperature is usually small because of the large turbulent mixing which usually prevails over the molecular thermal diffusivity. A solar irradiance of 1000 W.m^{-2} when absorbed in a mixed layer of 10 m would only give a heating rate of 0.1° C per hour, and a daily variation of less than 0.5° C . While if the turbulent mixing is reduced and the mixed layer thickness is restricted to less than 1 m, a heating rate of 1° C per hour may be expected and daily variations of several $^\circ \text{ C}$ should be observed. With the exception of very shallow waters, large diurnal heatings in open oceans thus correspond to the case of lower wind speeds as far as turbulence in the upper surface layer is mostly locally induced by the surface wind stress.

From a theoretical simulation of radiative and heat transfer in the upper ocean layer, HASSE (1971) has predicted ^{that} the deviation of the sea surface temperature (SST) T_0 from the bulk temperature T_{10} taken at 10 meter-depth should vary as :

$$T_0 - T_{10} = C_2 Q U^{-1} \quad (1)$$

where Q is the solar irradiance, U , the wind speed, and $C_2 = 3.5 \cdot 10^{-3}$ when Q is expressed in W.m^{-2} , U in m.s^{-1} . According to ^{HASSE}, Eq. (1) is only valid for $U \geq 2 \text{ m.s}^{-1}$, but the evidence that the SST diurnal variations increase when U decreases is supported by several observations : ROMER (1969), STOMMEL et al (1970) where large diurnal variations of more than 1° C are occasionally found at very low wind speeds - i.e. for $U < 2 \text{ m.s}^{-1}$. These obser-

vations are nethertheless restricted to a single location and limited time occasions.

Satellite infrared radiometers offer the opportunity to investigate more systematically such large diurnal variations of the SST. The first satellite experiment to provide adequate capability for this purpose was the HCMR (Heat Capacity Mapping Radiometer) experiment launched in late April 78 with an improved temperature resolution (0.3° C) and a nearly noon overpass. Results from this experiment are hereby reported in order (i) to investigate large diurnal SST variations at low wind speeds (ii) to give an assessment of the relation frequency of such an event and its impact on the determination of the SST field in such area ^{like} ~~the~~ Mediterranean Sea where the occurence of diurnal heating is rather large.

II - OBSERVATIONS OF DIURNAL HEATING FROM HCMR SATELLITE DATA

II-1 - The HCMR experiment

The basic objectives of the HCMR experiment are to measure diurnal variations of the earth surface temperature for applications to earth resources (geology, hydrology...). For this purpose, the satellite is sun-synchronous and ^{its} orbit was chosen to cross the equator at about 2 a.m and 2 p.m local time so that surface temperature data are obtained close to the minimum and the maximum of the diurnal variation. Satellite altitude is 620 km, and orbit inclinasion is 98.87° . The HCMR consists of a two-channel scanning radiometer, with a 0.5 - 1.1 μm spectral bandwith in the visible and 10.5 - 12.5 μm in the thermal infrared. Similar channels have been used on previous meteorological satellites, but the interests of the HCMR experiment are (i) a

large improvement of the radiometric performances in the thermal infrared channel for which the temperature resolution is 0.3° C and the nadir ground resolution is 500 m as compared to respectively 0.7° C and 1 km for the previous VHRR/NOAA satellite, (ii) the facility offered to the user to obtain differential surface temperature maps between day and night at 12 or 36 hours intervals. The HCMR experiment was originally designed to produce thermal inertia data for soil and geology applications but the very good performances of HCMR are suitable also for oceanographic studies. Data were received from NASA (National Administration for Space Research) through an investigation concerned with sea surface temperatures of the coastal zones of France.

Available HCMR data are photographic or digital products covering a 700 x 700 km² square scene. The following informations are displayed :

- (1) surface diffuse albedo or reflectance in the visible channel (day only),
- (2) surface temperature from the infrared channel, (3) surface temperature difference between day and night, (4) thermal inertia, which was not used in the present study.

About 1000 scenes covering the coastal zones of France were received for the period May 1978 - May 1979. Examples of the photographic products are given for two areas in the Western Mediterranean Sea (Fig. 1) ^{and} in the North Sea (Fig. 2)) where large diurnal variations of the SST were observed.

II-2 - Diurnal heating and glitter (sun glint) patterns

A large number of the received data from May to July 1978, over the Mediterranean Sea exhibited very interesting and similar features in both the visible and the infrared channels, as shown in Fig. . between Corsica Island and the south coast of France, and also close to the east coasts of

of Corsica and Sardinia Islands.

Warmer areas in the thermal channel are associated with changes of brightness in the visible.

The observed changes of brightness in the visible are identified as glitter or sunlint patterns - i.e. specular reflexion of direct solar radiation by the wavy sea surface. During the concerned period around the summer solstice, the observation angle of the HCMR imagery was allowed to be very close to the specular reflection of direct solar radiation, in the western part of the scenes, which is favorable for observations of glitter patterns. Most of the time, the glitter increases from rough to calm seas, when the wind decreases and the sea surface becomes more specular, and exhibits a maximum brightness when the observation angle is close ^{to} the specular reflexion of solar radiation : a homogeneous bright area is thus noted in the south-west part of Fig. ^{1-a} 2a. But for very calm seas, the surface reflexion becomes nearly specular, and a decrease of the brightness may also be observed because it is very unlikely that the observation angle is strictly towards the specular reflexion. Such a darkening is observed in the northwest part of Fig. ^{1a} 2a, where the two processes are present with both bright and dark areas corresponding respectively to weak and nul wind speeds. The fact that smoothing of the surface could produce either an increase or a decrease of the glitter brightness was previously mentionned by LA VIOLETTE ^{et al.} ~~and GILBERT~~ (1980). A physical and detailed description is given in Appendix, to support a further quantitative analysis of the data. The dark patterns in a mean bright glitter can thus be clearly interpreted as nul wind and calm sea areas, which obviously are favourable to a larger diurnal heating of the upper layer of the ocean because the heat transfer to deeper ocean layers is limited by a low turbulent mixing and thermal diffusivity.

II-3 - Meteorological observations

Evidence of a large diurnal heating corresponding to low wind speed conditions is also given by correlative meteorological observations. Surface observations are presented in Fig. 1-d for the case in the Mediterranean Sea, and in Fig. 2-d^c for an other case found in the North Sea where, due to higher latitudes, glitter is almost always unobservable. On Fig. 2-b^a a large warm spot was detected by HCMR in the middle of the North Sea which is coincident with the center of high anticyclonic situation pressure where nul wind speed is reported. Warmer areas observed in the Mediterranean Sea on Fig. 1-b are also coincident with low or nul wind speeds, but the observed wind field is much more complicated because most of the reporting coastal weather stations are affected by some breeze effect, which surimpose to an anticyclonic circulation. Cloudfree satellite SST observations are frequently acquired during similar anticyclonic situations with moderate wind speeds. It must be outlined that satellite estimations of SST may thus be systematically affected by diurnal heating, and a tentative statement of this is discussed in section III-4.

II-4 - Day-Night observations

Heat loss during the night very rapidly destroy most of the diurnal heating, at least in the upper layer, which was produced during day time. Evidence of a diurnal heating may thus be found from a comparative analysis of two successive day and night observations at 12 hours intervals. For the two cases given in Fig. 1-c and 2-b, nighttime observations show a much more constant SST field and the noticeable daytime warmer features disappear.

Figure 1-d gives the result of the computed day-night temperature differences after the proper calibration algorithms have been applied by NASA. These differences present the advantage to be independent of the mean mesoscale SST field and allow to enhance the diurnal heating, which again closely correlate with glitter patterns in the visible channel. Day-night temperature differences are used in the followings for a more quantitative analysis of diurnal heating.

III - DEPENDENCE OF DIURNAL HEATING ON SEA STATE AND WIND SPEED

The observed diurnal heatings were further quantitative^{ly} analysed to derive its relationship with the sea state and the wind speed. Day-night temperature difference were correlated to the reflectance of the 0.5 - 1.1 μm channel. This reflectance, mostly due to sun glitter, is related to the surface slope variance and to a mean wind speed using the statistical model from COX and MUNK (1955).

III-1 - Diurnal heating and glitter reflectance

Day-night temperature differences (Fig. 1-d) - i.e SST diurnal variations - show patterns similar to the glitter patterns (Fig. 1-^a~~b~~), on June 3, 1978. Fig. 3 gives the result of the correlation obtained when the diurnal heating, ΔT , is plotted as function of the glitter reflectance, ρ_g , in a small study area, east of Sardinia. Most evidently a close correlation exists and ΔT rapidly decreases when ρ_g increases. To further interpret that fact, ρ_g has to be related to the wind speed, or more exactly to the statistics of surface slopes.

Using the statistical distribution of surface slopes from COX and MUNK (1955), a model was developed to relate the glitter reflectance to the wind speed. This model is detailed in Appendix. Results indicate that ρ_g could either increase or decrease with wind speed : ρ_g presents a maximum value for a given wind speed value which both of them depend on solar and observation angles through θ_n ($\text{tg } \theta_n$ is the surface slope allowing specular reflection toward the sensor). Fig. 4 give the relationship between ρ_g and the wind speed, U, for $\theta_n = 8^\circ, 10^\circ,$ and 12° , which correspond to the area previously studied for $\Delta T = f(\rho_g)$. In this case ρ_g increases rapidly at the lower wind speeds and then is rather constant for $U > 3 \text{ m.s}^{-1}$ so that U can be estimated with a good accuracy from ρ_g , only for $U < 3 \text{ m.s}^{-1}$. The study has thus to be limited to this wind speed range. It should also be noted that ρ_g is physically linked to the surface slope variance, and only statistically to the wind speed. Local anomalies may thus occur, in particular when the fetch of the wind over the sea is variable. Keeping in mind these cautions, we may now transform $\Delta T(\rho_g)$ in $\Delta T(U)$ which is given in Fig. 5.

III-2 - Diurnal heating and the wind speed

The first point to be noted on Fig. 5 which gives the diurnal heating as a function of the wind speed, is that ΔT rapidly decreases from several °C to 1° C when U increases up to 2 m.s^{-1} . The scatter of observations on Fig. 5 is remarkably less than on Fig. 3 for $\Delta T(\rho_g)$, because the variations of ρ_g with changes of observation angles within the study area have been eliminated. A fit of $\Delta T(U)$ on Fig. 5 would give :

$$\Delta T = 0.4 U + 1.1 \tag{2}$$

(in °C for U in m.s^{-1})

Some uncertainties related to the model $\rho_g(U)$ have been previously outlined. Additional errors may be due to atmospheric effects on the measured radiances. An aerosol atmospheric reflectance^{of} about 0.02 was estimated from the minimum reflectance within the scene ($\rho_g = 0$) and subtracted in the 0.5 - 1.1 μm channel. Day-night temperature differences have not been corrected for atmospheric emission in the infrared. This approximation would be valid only if the atmosphere remains the same between the two satellite overpasses, but a bias due to a change of atmospheric parameters - i.e temperature and water vapor concentration - could have occur which would possibly explain the 1.1° C constant found in (2). Last, the observed ΔT are certainly underestimated by a factor τ , the atmospheric transmittance in the 10.5 - 12.5 μm , which is typically $\tau = 0.7$ for a midlatitude summer atmosphere.

The results may be compared to the predicted values from HASSE (1971). Using a mean solar irradiance at sea level $Q = 900 \text{ W.m}^{-2}$ in (1), ΔT is found to vary like $U^{3.2}$ (U in m.s^{-1}) which fits the measured values in the wind speed range 1-3 m.s^{-1} , but overestimates ΔT for $U < 1 \text{ m.s}^{-1}$. As pointed out by HASSE, the results of the model given in (1) can not be applied to the lower wind speed range because the model used by HASSE refers to a steady state assumption which is then not respected at scales of a few hours.

III-3 - Limit value of the diurnal heating

Fig. 5 and other HCMM scenes with large diurnal heatings indicate that diurnal heating do not exceed about 5° C, and that a limit value should exist at low wind speed. This value may be obtained by solving the heat transfer equation :

$$\frac{d}{dz} (k(z) \frac{dT(z,t)}{dz}) + \frac{dF(z,t)}{dz} = \rho c \frac{dT(z,t)}{dt} \quad (3)$$

for $k(z) = k_m$ the thermal molecular diffusivity - i.e no turbulent diffusivity at $U = 0$. Eq. (3) was solved using the following conditions :

$$F(z,t) = F(0,t) g(z) - F_0 \quad (4)$$

where $F(0,t)$ is the solar irradiance at sea level, F_0 the heat loss by the surface, and

$$g(z) = \sum a_i \exp(-k_i z) \quad (5)$$

where a_i, k_i are given in Table 1 and were obtained from a fit of $g(z)$ according to the work by PRUVOST (1976). $g(z)$ is taken as independent of time in (4) which is a rather good approximation since the underwater penetration of the direct solar radiation is close to the nadir even at low solar elevation angles. An homogeneous layer defined by $F(0,t) g(z_0) = F_0$ was set just below the surface for which $(\frac{dT}{dz}) = 0$ (z_0 is a few centimeters for $F_0 = 100 \text{ W.m}^{-2}$, $F(0,t) = 1000 \text{ W.m}^{-2}$). Under these conditions, ΔT was found to vary nearly with the net heat budget of the surface :

$$\Delta T_{\max} = C \int_0^{t_0} (F(0,t) - F_0) dt \quad (6)$$

with $C = 0.65 \cdot 10^{-6} \text{ K.j}^{-1} \text{ m}^2$. For the HCMM observations or ^{June 3}, 1978, $\int_0^{t_0} (F(0,t) - F_0) dt$ was estimated to about 600 W.m^{-2} during 4 hours (in fact a maximum value of 900 W.m^{-2} at noon at satellite overpass) and

$$\Delta T_{\max} = 5.6 \text{ }^\circ\text{C} \quad (7)$$

The Hasse's formula (1) may be simply accommodated to account for the limit found in (6) by writing :

$$\Delta T = 3.5 \cdot 10^{-3} Q / (U_0(t) + U) \quad (8)$$

where $U_0(t)$ will depend of the given hour during the day. In our case, U_0 should be about 0.7 m.s^{-1} and when plotted in Fig. 5, Eq. (8) fits pretty well the observations.

III-4 - Frequency of diurnal heating

From May 13 to August 28, 1978, 60 HCMM scenes taken over the Western Mediterranean Sea were examined, of which about 34 scenes exhibited large diurnal (typically more than 1° C) heating of particular areas of 10 to 100 km width. Relative frequency of the event is rather large, and is enhanced in some areas affected by a breeze effect where the wind systematically becomes nul at some distance of the coast. Table 2 give relative frequencies of low wind speeds ($U < 3 \text{ m.s}^{-1}$) at some stations along the Coast of France during the summer months (from DARCHEN (1974)). Frequency of nul wind allowing a diurnal heating of more than 1° C are between 10 to 30 %. Frequency of low wind speed ($1 < U < 3 \text{ m.s}^{-1}$) is from 20 to 50 %, allowing a diurnal heating of about 1° C . From these frequencies, N_1 and N_2 , a mean diurnal heating $\bar{\Delta T}$ was calculated as .

$$\bar{\Delta T} = 2.5 N_1 + N_2$$

and is given also in Table 2. The mean diurnal heating range from 0.5 to 1.5° C along the south coast of France with a maximum on the French Riviera (Cap Ferrat).

IV - CONCLUSION

The present investigation, using SST satellite observations from the HCMM experiment has shown a high frequency of large diurnal heatings (more than 1° C) of the sea surface during summer months in such areas like the Mediterranean Sea where low wind speed are very frequent. This shows that satellite observations at noon and during the afternoon should be rejected, or at least checked to eliminate those corresponding to low wind speed ($U < 3 \text{ m.s}^{-1}$). If not, a systematic bias could be introduced in the SST analysis of ^{some} ~~some~~ areas, particularly the marine coastal areas affected by a sea-^eland breeze effect.

Using simultaneous observations of the glitter reflectance, the diurnal heating was correlated to the wind speed. Diurnal heatings of about 1° C were found for $U = 2 \text{ m.s}^{-1}$, which fits the formulation given by HASSE (1971). A maximum diurnal heating of 5° C is found for nul wind conditions, which is in agreement to the value calculated from the radiative and heat transfer, assuming the thermal diffusivity is only molecular.

2-5

APPENDIX

Glitter refers to direct solar radiation reflected by the sea surface. This reflection is specular for a planar surface. When there is wind, the surface is agitated and consists of elements which are statistically distributed around the horizontal plane. This produces a more or less bright spot of variable dimensions which is commonly called glitter.

The radiance L_g reflected by the agitated sea surface can be expressed (COX and MUNK, 1956)

$$L_g = \frac{E_s R(\omega)}{4 \mu_v \mu_n} p \quad (A-1)$$

and the equivalent reflectance ρ_g will be expressed as

$$\rho_g = \frac{\pi L_g}{\mu_s E_s} = \frac{\pi R(\omega)}{4 \mu_s \mu_v \mu_n} p \quad (A-2)$$

where E_s is the direct solar radiation at sea level,
 $R(\omega)$ is the reflection coefficient of water at a given incidence ω ,
 p is the probability of encountering a properly oriented surface element,

$\mu_v = \cos\theta_v$, $\mu_s = \cos\theta_s$, $\mu_n = \cos\theta_n$, respectively define the zenithal angles of the observation direction, the direction of incidence, and their bisector,

φ is the angle between the planes of incidence and observation :

$$\mu_n = \frac{\mu_s + \mu_v}{2 \cos \omega} \quad (\text{A-3})$$

$$\cos 2\omega = \mu_s \mu_v + \left(1 - \mu_s^2\right)^{\frac{1}{2}} \left(1 - \mu_v^2\right)^{\frac{1}{2}} \cos \varphi \quad (\text{A-4})$$

From a study of aerial photographs of glitter patterns, COX and MUNK (1955) developed p in a Gram Charlier series which in a first approximation is reduced to a gaussian distribution , with revolution symmetry :

$$p = \frac{1}{\pi \sigma^2} \exp - \frac{(\text{tg } \theta_n)^2}{\sigma^2} \quad (\text{A-5})$$

$$\text{with } \sigma^2 = 0,003 + 5,12 \cdot 10^{-3} U_{\text{m.s}}^{-1} \pm 0,004 \quad (\text{A-6})$$

for $1 < U < 14 \text{ m.s}^{-1}$

Figure 6 gives an example of the glitter spot ρ_g thus computed as a function of solar zenithal angle for different values of W , and for a nadir viewing ($\theta_v = 0$). In accordance with the reciprocity principle, by permutation ($\theta_s; \theta_v$), Fig.6 also gives ρ_g as a function of observation angle for a sun at the zenith ($\theta_s = 0$). For a given angle ρ_g presents a maximum, ρ_{gm} , at a certain value of σ_m which is related to wind speed. σ_m and ρ_{gm} are given by :

$$\sigma_m^2 = \text{tg}^2 \theta_n = \mu_n^{-2} - 1 \quad (\text{A-7})$$

$$\rho_{gm} = \frac{R(\omega)}{4 \mu_s \mu_v \mu_n^2 (1 - \mu_n^2)} \quad (\text{A-8})$$

The dashed curve in Fig.6 envelops the preceding curves and represents the maximum glitter ρ_{gm} as defined by (A-8).

277

REFERENCES

- 1 - COX, C., MUNK, W., 1955 - Slopes of the sea surface deduced from photographs of the sun glitter. Bulletin of the Scripps Institution of Oceanography, California, 6 (9), 401-488.
- 2 - COX, C., MUNK, W., 1956 - Journal of Marine Research 14 (1), 63-78.
- 3 - DARCHEN, J., 1974 - ^Eléments climatologiques concernant les côtes de la France métropolitaine (Méditerranée). Monographie n° 93 de la Météorologie Nationale, France.
- 4 - HASSE, L., 1971 - The sea surface temperature deviation and the heat flow at the sea-air interface. Boundary Layer Meteorology 1, 368-379.
- 5 - LA VIOLETTE, P.E., PETEHERYCH, S., GOWER, J.F.R., 1980 - Oceanographic implications of features in NOAA satellite visible imagery. Boundary Layer Meteorology 18, 159-175.
- 6 - PRUVOST, P., 1975 - Etude du flux solaire et de l'échauffement radiatif dans la mer par temps clair. Annales Hydrologiques 5ème série vol. 3 (1), 25-34.
- 7 - ROMER, J., 1969 - Variations de la température de surface de la mer au voisinage de la surface. Note EERM n° 262, Météorologie Nationale, France.
- 8 - STOMMEL, H., SAUNDERS, K., SIMMONS, W., COOPER, J., 1969 - Observations of the diurnal thermocline. Deep. Sea Research, Supplement vol. 16, 269-284.

Table 1 - Coefficients a_i , k_i in (5) for solar irradiance underwater penetration.

	a_i	k_i (m^{-1})
$i = 1$.041	3365.9
$i = 2$.139	201.18
$i = 3$.211	13.05
$i = 4$.24	1.22
$i = 5$.37	.07

Table 2 - Relative frequencies of low wind speeds :

N_1 : nul ; N_2 : Beaufort forces 1 and 2 ($1 < U < 3 \text{ m.s}^{-1}$),
 during June, July and August in the French mediterranean
 coastal area from DARCHEN (1974). An estimate of the mean diurnal
 heating $\bar{\Delta T}$ is given in column (3).

Station	N_1 %	N_2 %	$\bar{\Delta T}$ °C
Cap Bear	16.0	26.9	0.67
Sète	9.5	42.3	0.66
Panègues	21.3	26.8	0.80
Cap Camarat	10.8	46.6	0.74
Cap Ferrat	35.1	50.4	1.38
Cap Corse	18.4	35.5	0.82
Pertusato	6.4	21.0	0.37
42° N-6E	7.6	/	0.5 ?

FIGURES CAPTIONS

Figure 1 - Diurnal heating in the Western Mediterranean Sea :

- (a) - HCMM scene A-A0038 - 12440 on June 3, 1978 at 12.40 TU, image center is at 40.54 N, 011.04 E. Visible channel : darker tones are lower reflectances. Note the bright patterns East and West of Corsica and Sardina.
- (b) - Same as (a) but infrared channel : darker tones are colder sea surface temperatures. Note warmer waters East of Corsica and Sardina.
- (c) - Day-night temperature differences between HCMM scenes obtained on June 3, 1978 at 1.50 TU (night) and 12.40 TU (day). Darker tones are smaller diurnal heatings.
- (d) - Meteorological situation, on June 3, 1978 at 12.00 TU.

Figure 2 - Diurnal heating in the North Sea :

- (a) - Day HCMM scene A-A0034 - 13120, on May 30, 1978 at 13.10 TU. Image center is at 54.27 N, 00.01E. Infrared channel : darker tones are colder waters. Note the warm (bright) spot between Scotland and the top right of the image where a thermal front is shown close to Norway.
- (b) - Night HCMM scene A-A0035 - 02280, on May 31, 1978 at 2.30 TU. Image center is at 56.13 - 03.00E. Infrared channel : darker tones are colder waters. The warm spot disappeared during the night.
- (c) - Meteorological situation on May 30, 1978.

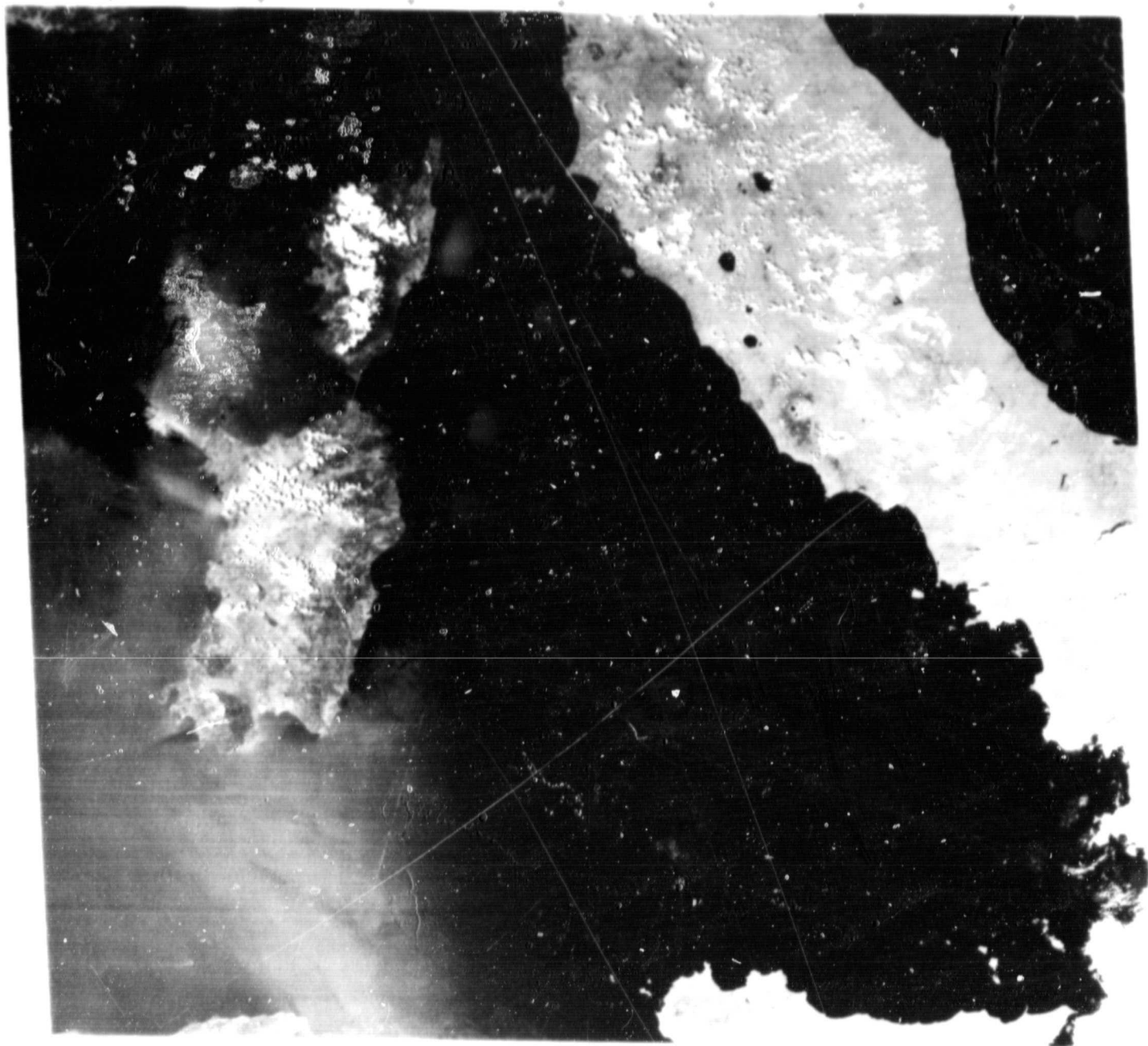
Figure 3 - Day-night temperature difference vs glitter reflectance on June 3, 1978, for a study area East of Sardina.

Figure 4 - Retrieved wind speed vs glitter reflectance for the study area.

Figure 5 - Day-night temperature difference vs retrieved wind speed for the study area. Dashed line is from HASSE (1971). Full line is (8) : the HASSE's formula after modification to account for a low wind speed limit of ΔT .

Figure 6 - Glitter reflectance vs zenithal viewing angle, for a sun at zenith, and several wind speeds from 0 to 15 m.s^{-1} . Maximum glitter reflectance is given by a dashed line.

FIG. 1a



GENUS: *...*
SPECIES: *...*

FIG 16

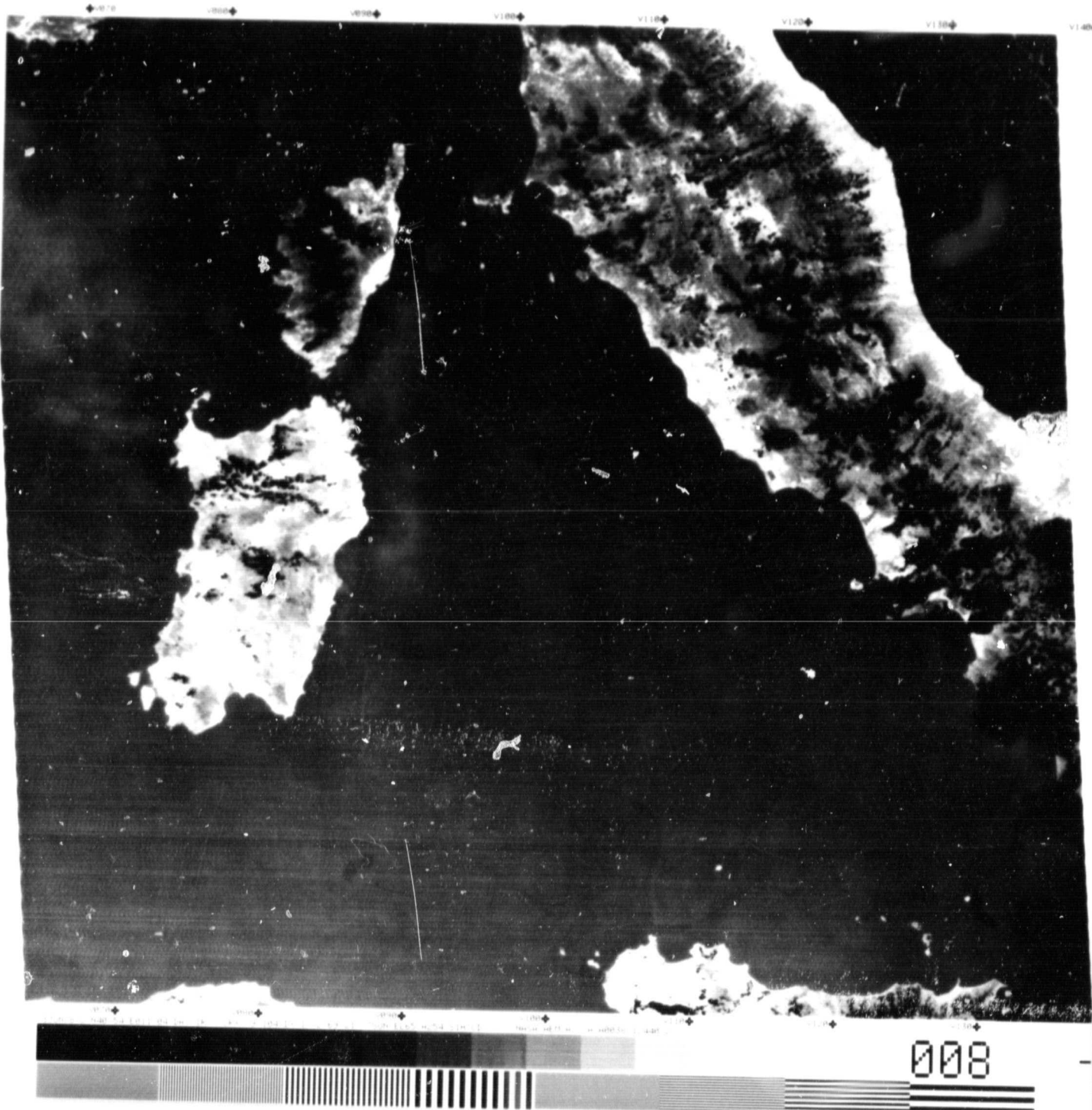


FIG. 1c



ORIGINAL PAGE IS
OF POOR QUALITY

FIG. 1d

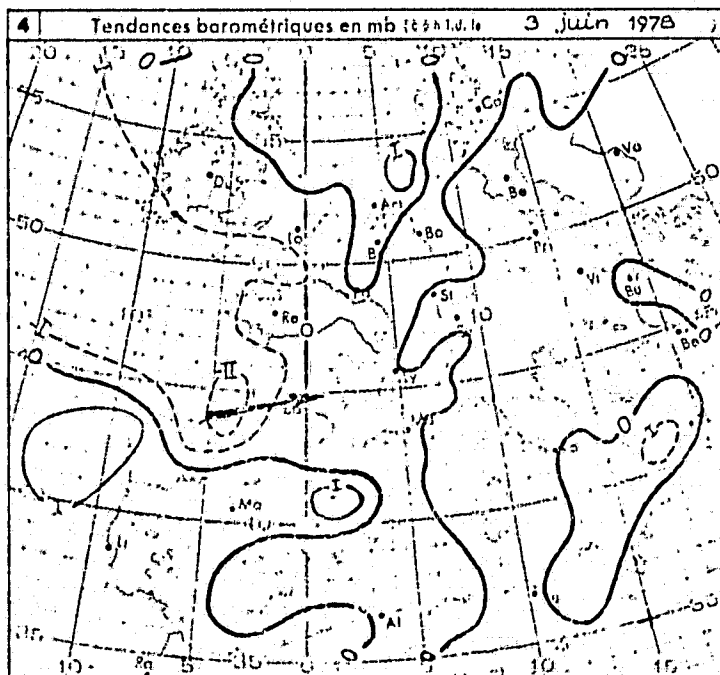
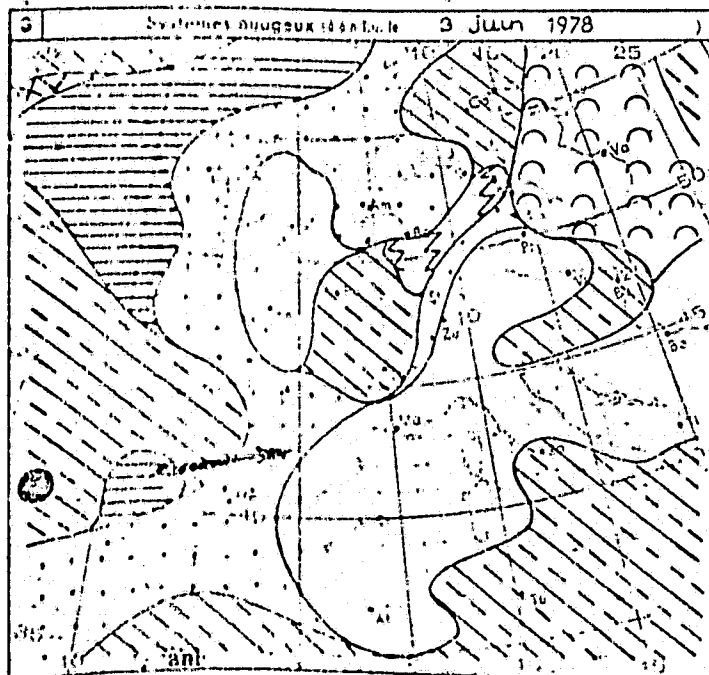
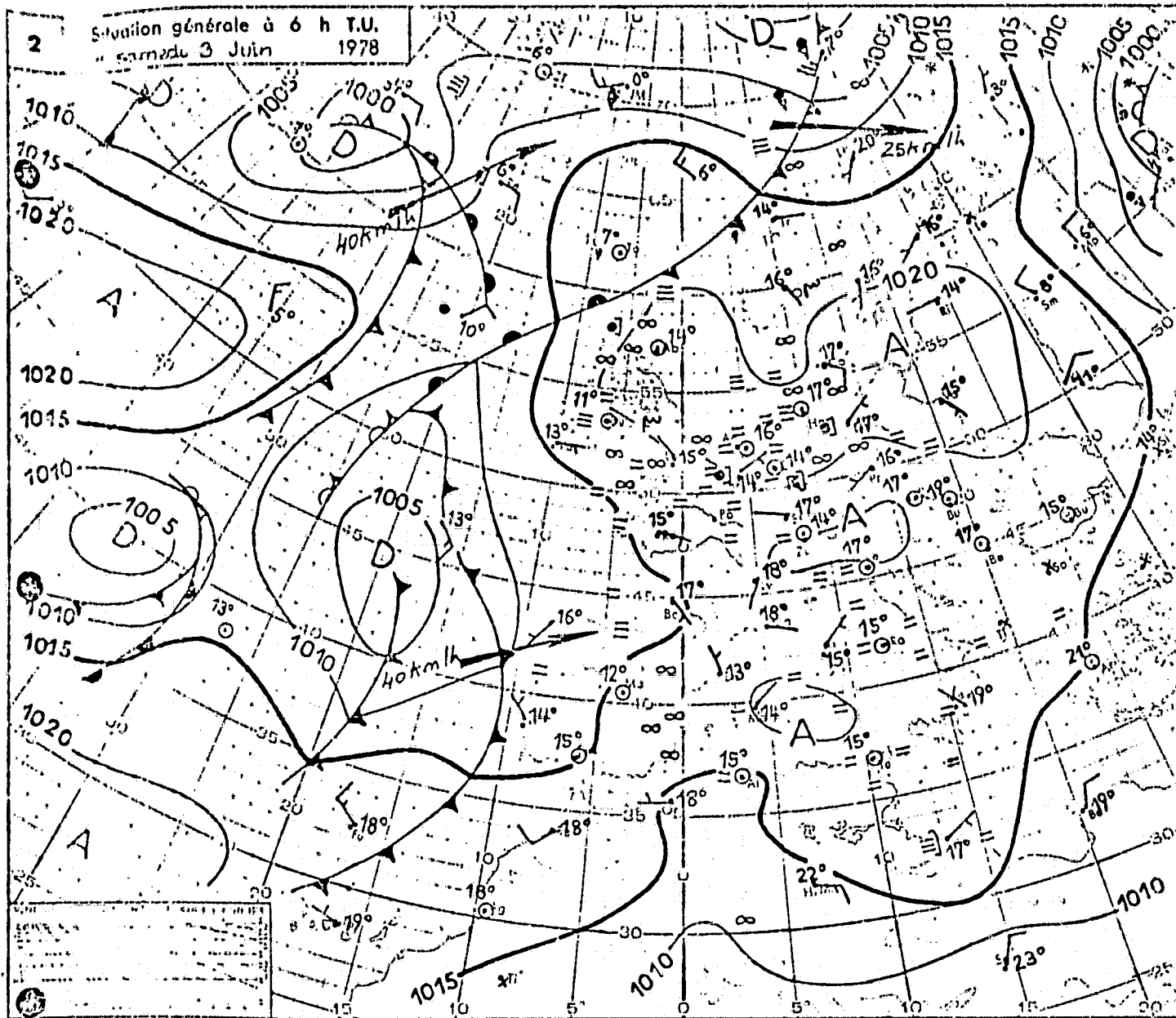
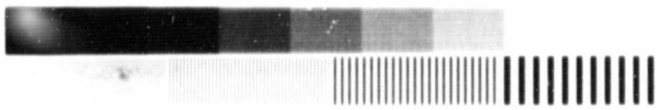
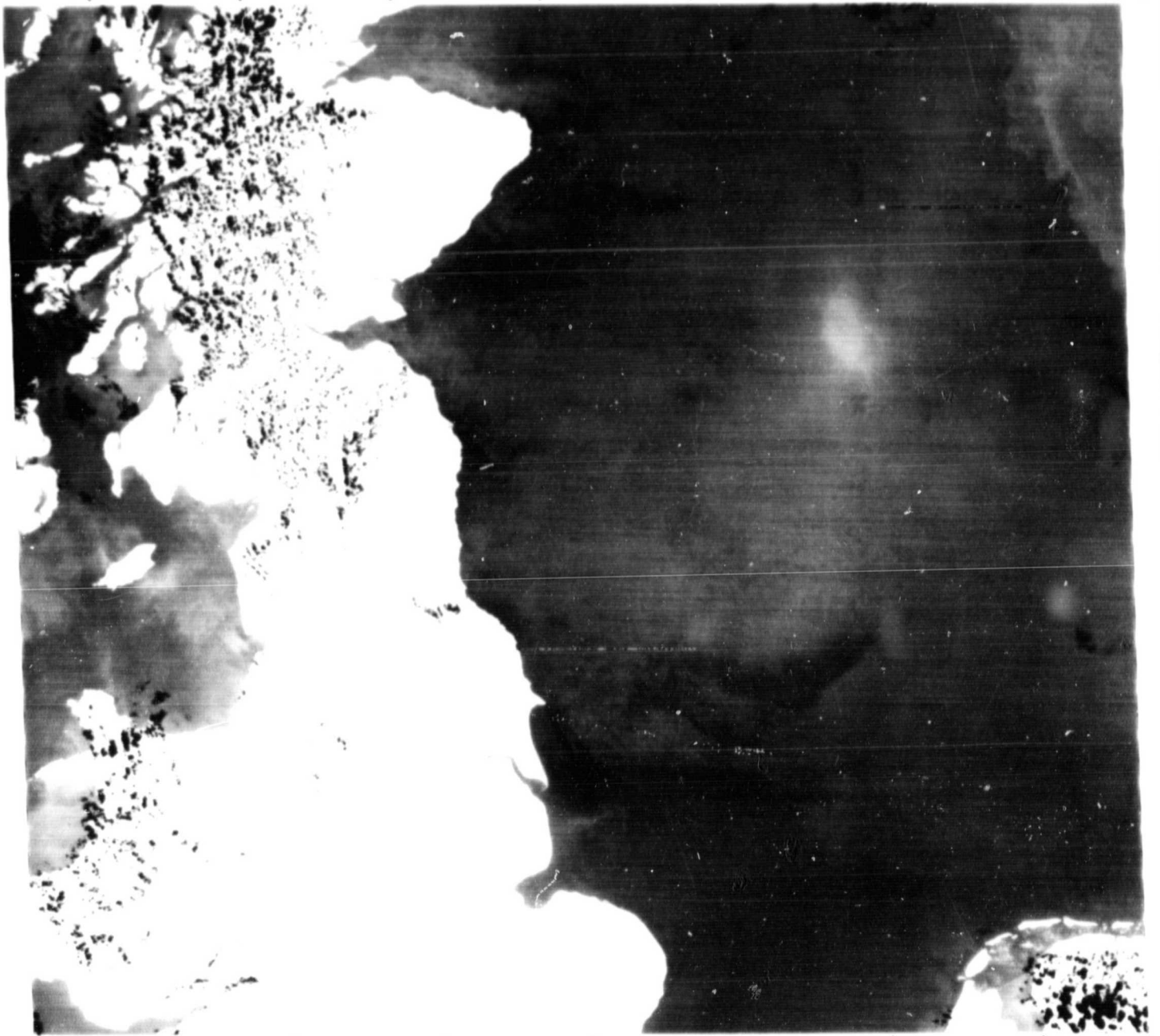


FIG. 2a

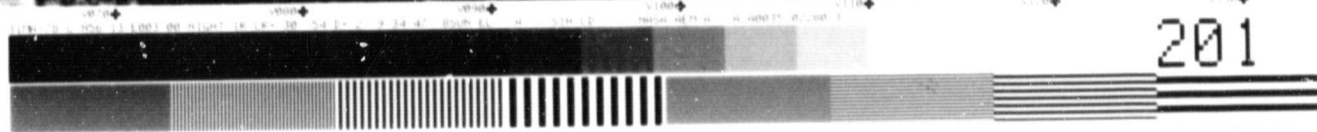
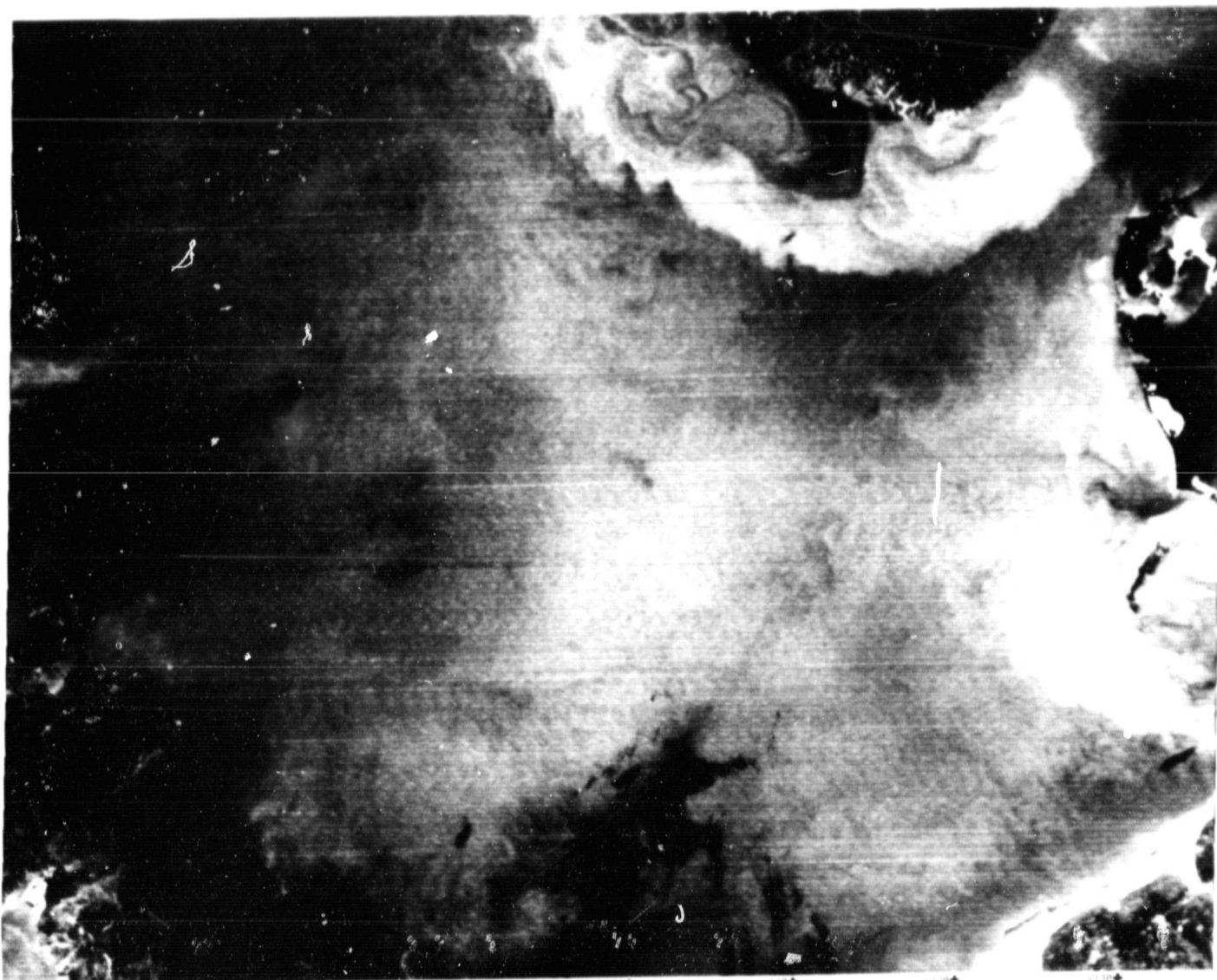


043

+

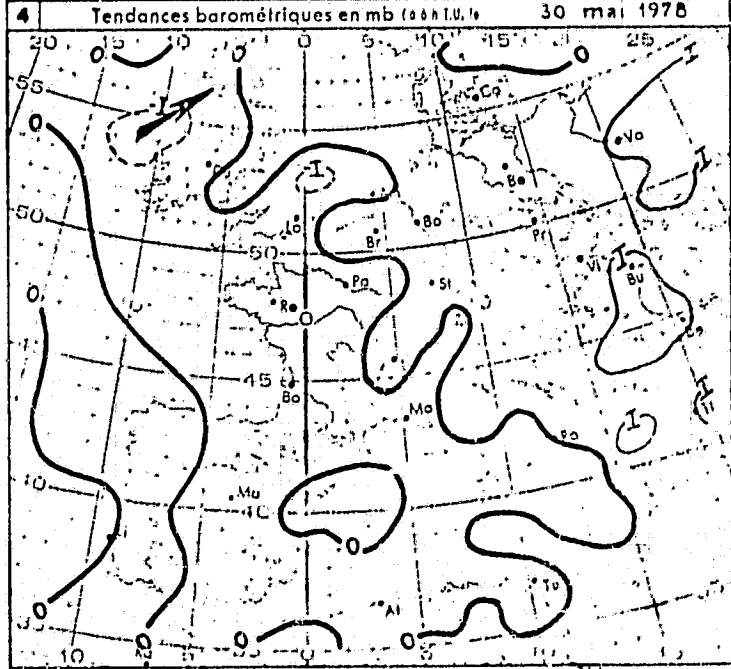
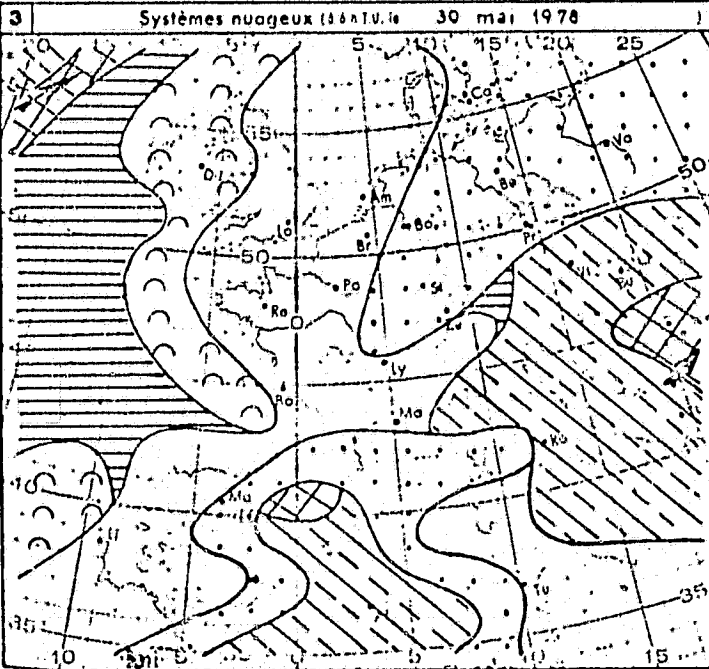
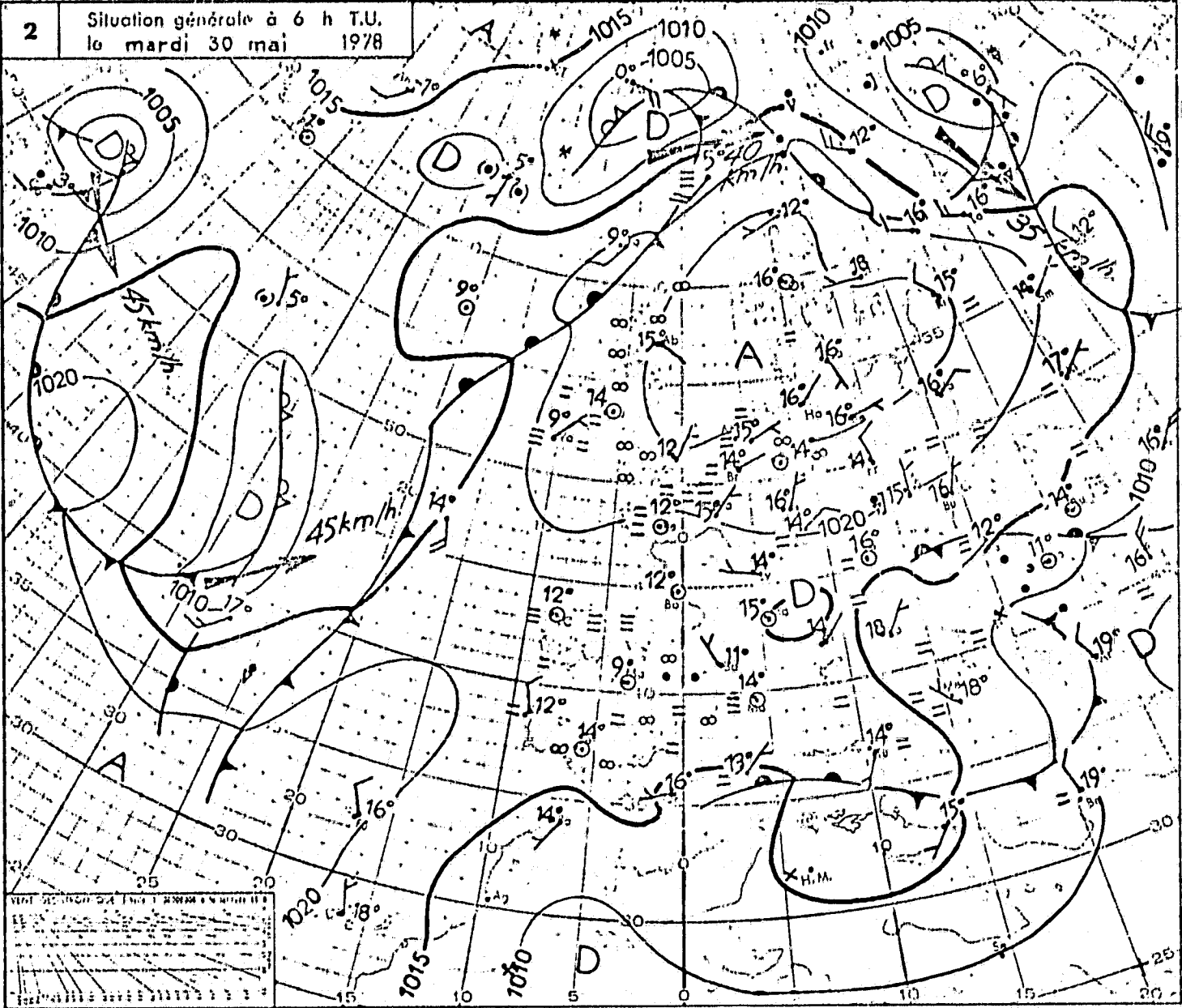
ORIGINAL PAGE IS
OF POOR QUALITY

FIG. 2b



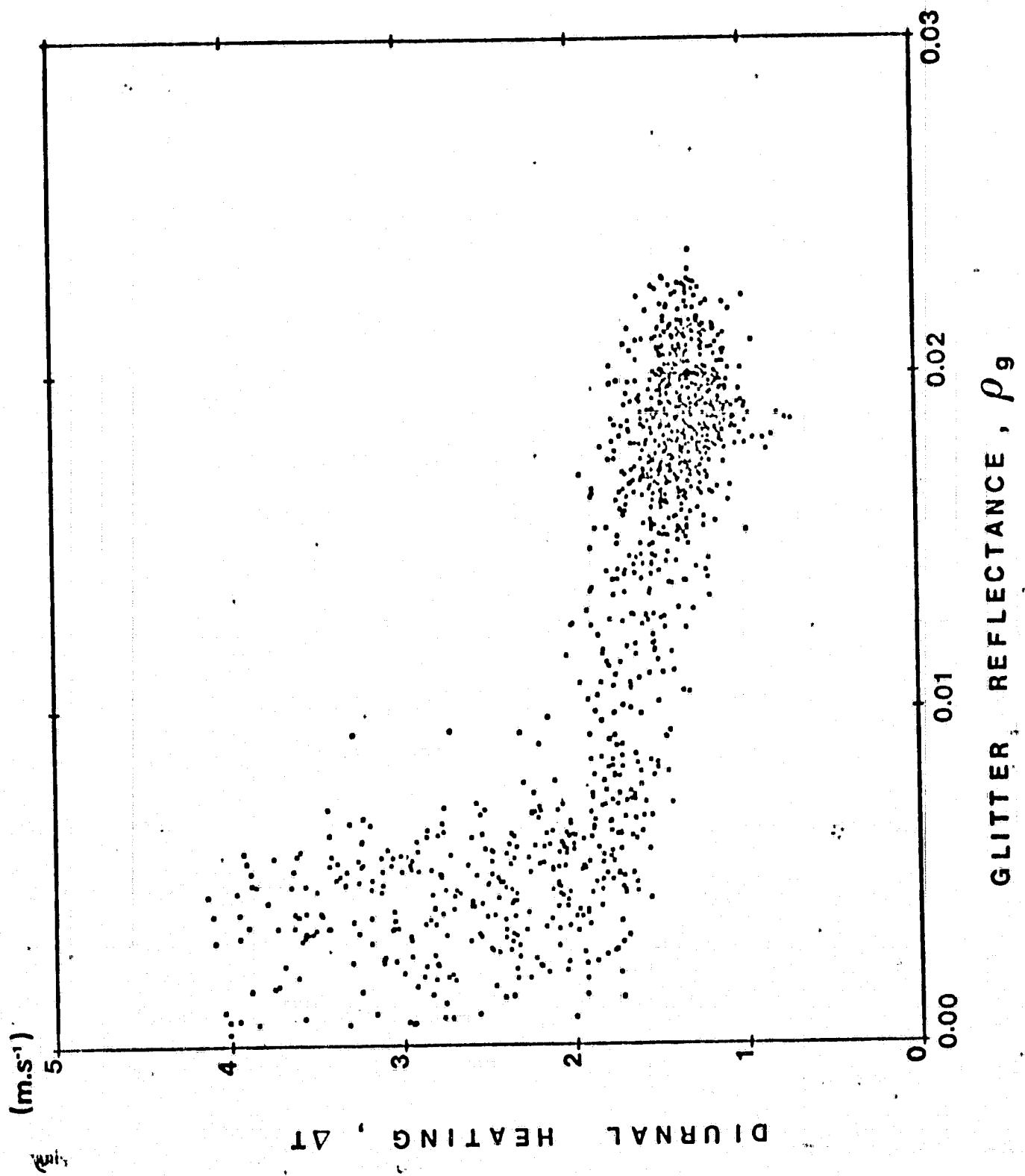
201

FIG. 2c



ORIGINAL PAGE IS
IN POOR QUALITY

FIG. 3



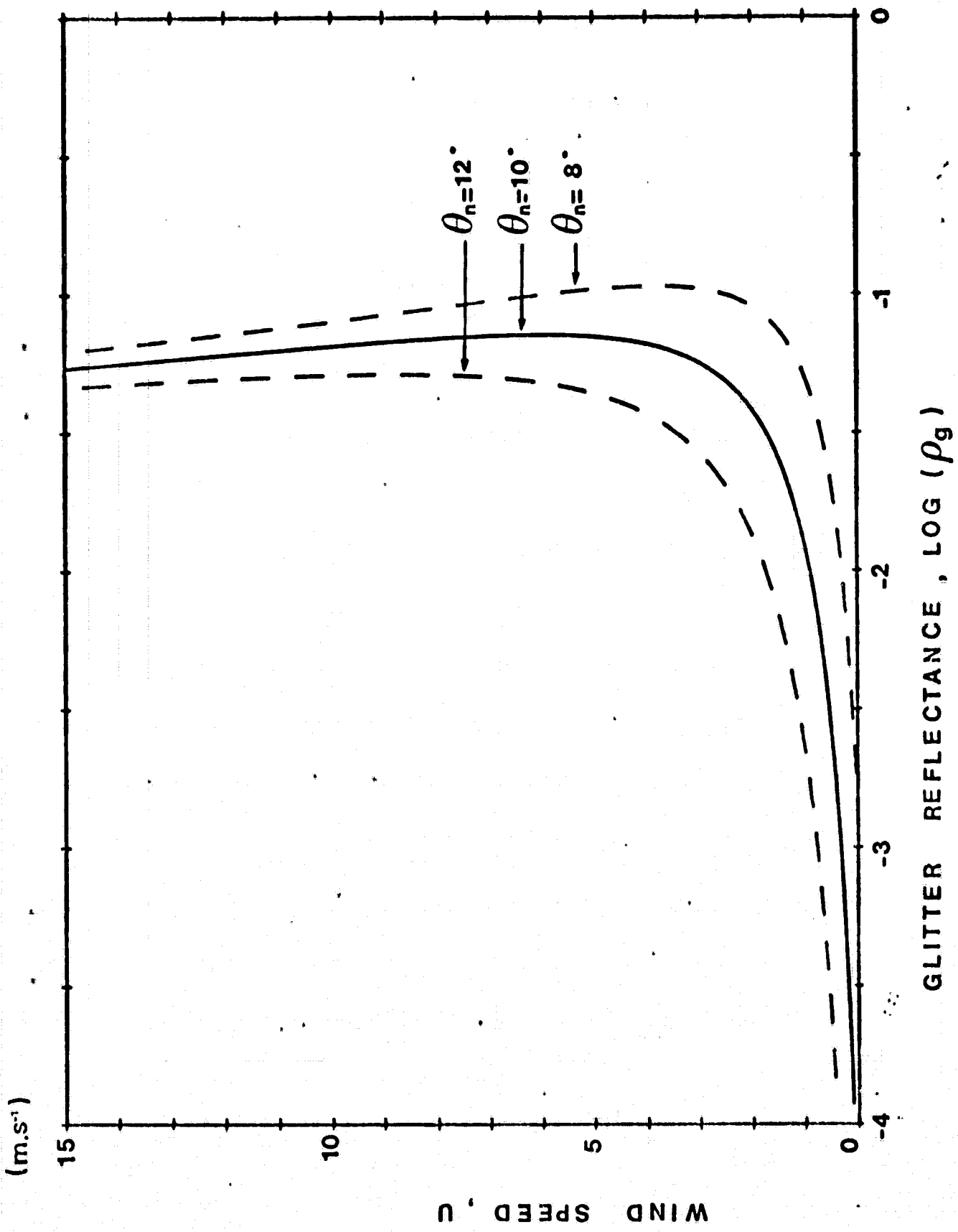


FIG. 5

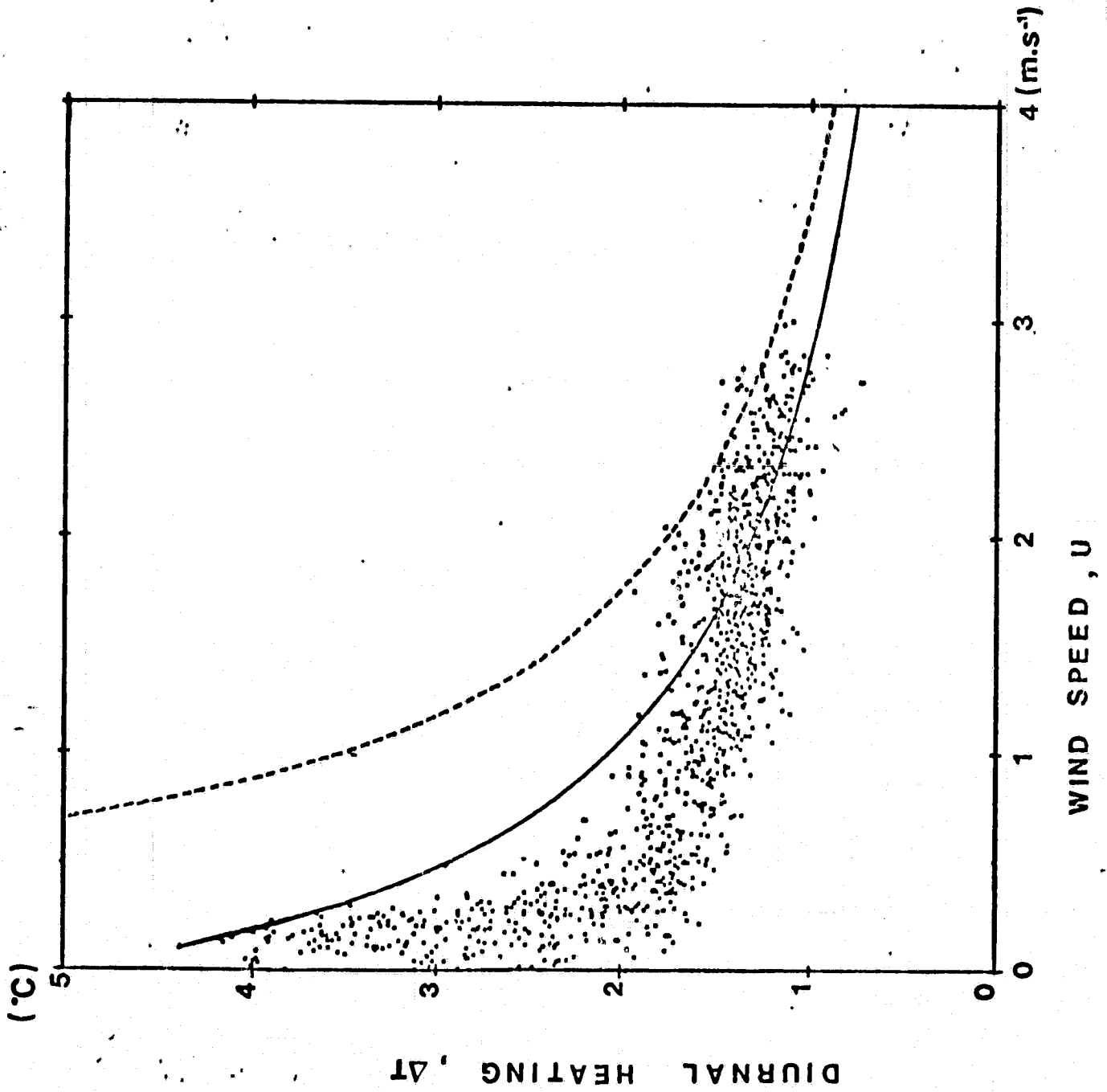
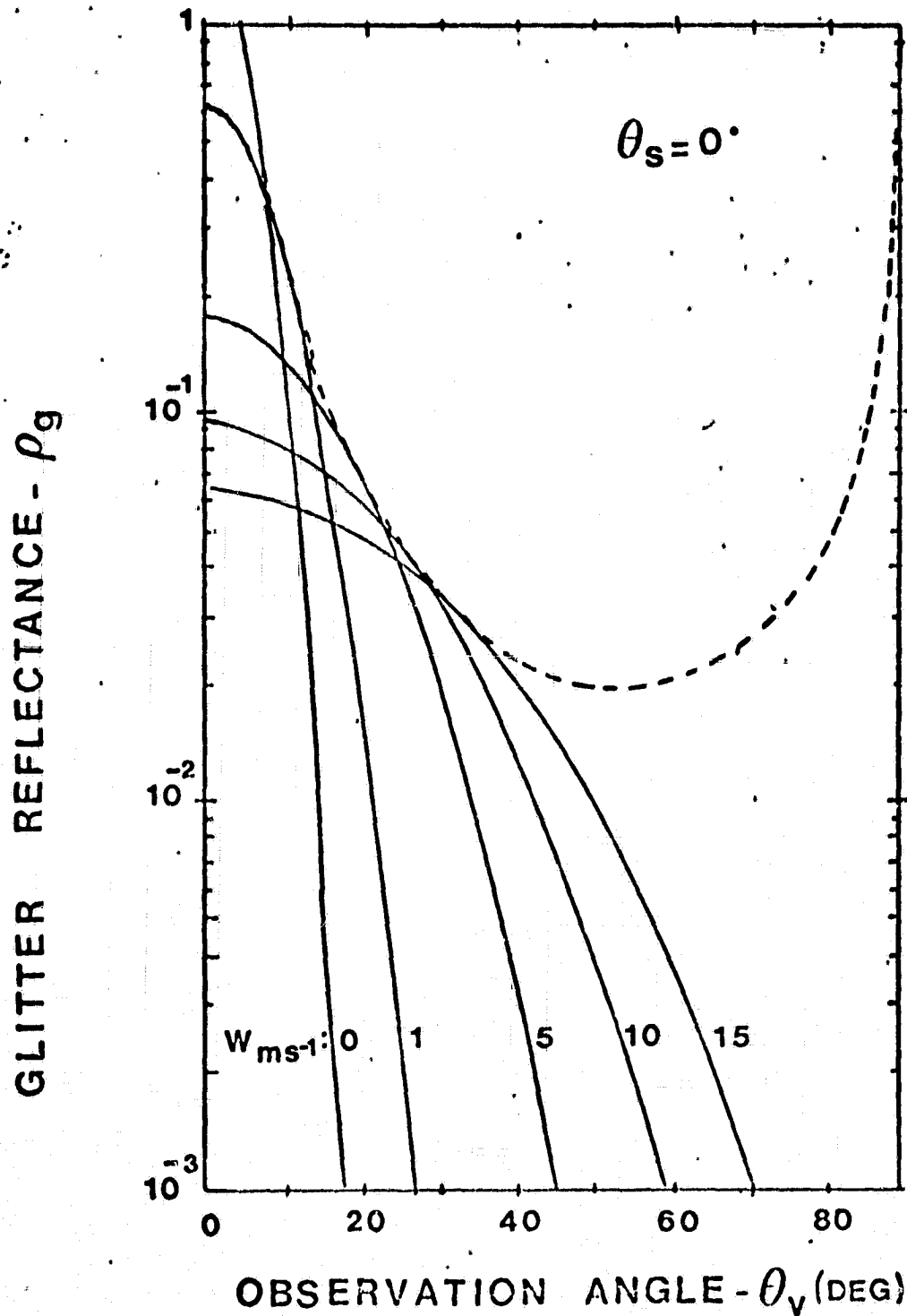


Fig. 6



anti
anti

The following listing give the date, identification and location of center of image of HCMM scenes received from NASA by the Principal Investigator. The last column "ETAT" give the status of the corresponding digital data :

- R : received
- IR : received but not readable
- C : requested but not received.

DATE	IDENTIFICATION	LOCATION	SCENE	BDE	ETAT	DST	PM
11MAY78	15-2540-3	53.32N 3.43W					
11MAY78	15-2550-3	47.29N 6.08W	303	R	M	2	
11MAY78	15-2560-3	45.29N 6.08W	303	R	M	8	
11MAY78	15-2564-3	41.10N 8.45W					
11MAY78	15-2570-3	41.26N 8.08W	303	R	M	5	
11MAY78	15-3000-3	32.50N 10.00W					
11MAY78	15-13510-1	40.35N 4.53W	318	R	M	8	
11MAY78	15-13510-2	40.35N 4.53W	318	R	M	11	
11MAY78	15-13530-1	46.38N 6.52W	318	R	M	2	
11MAY78	15-13530-2	46.38N 6.52W	318	R	M	5	
11MAY78	15-13550-1	52.40N 9.14W					
11MAY78	15-13550-2	52.40N 9.14W					
13MAY78	17-1570-3	38.02N 5.56E	318	R	M	14	
13MAY78	17-12510-1	41.29N 9.56E	318	R	M	17	
13MAY78	17-12510-2	41.29N 9.56E	318	R	M	20	
13MAY78	17-12540-1	53.34N 5.29E					
13MAY78	17-12540-2	53.34N 5.29E					
14MAY78	18-2140-3	44.02N 7.10E			C		
14MAY78	18-2150-3	37.56N 1.19E			C		
14MAY78	18-13060-1	39.07N 6.02E	312	R	M	8	
14MAY78	18-13060-2	39.07N 6.02E	312	R	M	11	
14MAY78	18-13100-1	45.11N 4.08E	312	R	M	2	
14MAY78	18-13100-2	45.11N 4.08E	312	R	M	5	
16MAY78	20-2480-3	51.39N 3.11W	318	R	M	23	
16MAY78	20-2500-3	45.36N 5.28W	318	R	M	26	
18MAY78	22-3251-3	50.16N 12.55W					
18MAY78	22-12460-1	44.55N 10.11E					
18MAY78	22-12460-2	44.55N 10.11E					
18MAY78	22-12470-1	50.58N 7.57E	312	R	M	14	
18MAY78	22-12470-2	50.58N 7.57E	312	R	M	17	
19MAY78	23-2050-3	55.24N 9.04E					
19MAY78	23-2080-3	43.19N 4.20E					
19MAY78	23-2100-3	37.13N 2.31E					
19MAY78	23-13050-2	50.25N 7.35E					
20MAY78	24-13200-1	38.07N 3.07E					
20MAY78	24-13200-1	36.32N 3.34E					
20MAY78	24-13200-2	38.07N 3.07E					
20MAY78	24-13200-2	36.32N 3.34E					
20MAY78	24-13220-1	44.11N 1.15E					
20MAY78	24-13220-2	44.11N 1.15E					
20MAY78	24-13230-1	48.40N .19E	293	R	M	6	
20MAY78	24-13230-1	50.13N .56E	293	R	M	2	
20MAY78	24-13230-2	48.40N .19E	293	R	M	11	
20MAY78	24-13230-2	50.13N .56E	293	R	M	5	
20MAY78	24-13250-1	54.40N 2.52W	293	R	M	20	
20MAY78	24-13250-1	56.14N 7.37W	293	R	M	14	
20MAY78	24-13250-2	54.40N 2.52W	293	R	M	23	
20MAY78	24-13250-2	56.14N 7.37W	293	R	M	17	
21MAY78	25-13300-1	35.53N .52E					
21MAY78	25-13300-2	35.53N .52E					

ORIGINAL PAGE IS
OF POOR QUALITY

DATE	IDENTIFICATION	LOCATION	SCENE	BDE	ETAT	DST	PM
21MAY78	25-13390-1	41.58N	2.38W				
21MAY78	25-13390-2	41.58N	2.38W				
21MAY78	25-13410-1	48.01N	4.41W	312	R	M	20
21MAY78	25-13410-2	48.01N	4.41W	312	R	M	23
21MAY78	25-13430-1	54.04N	7.08E				
21MAY78	25-13430-2	54.04N	7.08E				
22MAY78	26- 3000-3	52.30N	6.02W			C	
22MAY78	26- 3020-3	46.27N	8.23W			C	
23MAY78	27- 1440-3	42.47N	10.07E				
23MAY78	27- 1440-3	42.28N	10.01E				
23MAY78	27- 1450-3	36.40N	8.19E				
23MAY78	27- 1450-3	36.22N	8.14E				
23MAY78	27- 3180-3	52.55N	10.27W				
23MAY78	27- 3200-3	46.52N	12.50W	318	R	M	29
24MAY78	28- 2020-3	43.47N	5.49E	320	R	M	2
24MAY78	28- 2030-3	37.41N	3.58E				
24MAY78	28-12550-1	36.16N	9.35E				
24MAY78	28-12550-2	36.16N	9.35E				
24MAY78	28-12570-1	42.40N	7.47E	312	R	M	20
24MAY78	28-12570-2	42.40N	7.47E	312	R	M	29
25MAY78	29- 2210-3	39.37N	1.02E	320	R	M	5
25MAY78	29-13140-1	37.22N	4.40E				
25MAY78	29-13140-1	37.40N	4.35E				
25MAY78	29-13140-2	37.22N	4.40E				
25MAY78	29-13140-2	37.40N	4.35E				
25MAY78	29-13150-1	43.26N	2.50E			C	
25MAY78	29-13150-2	43.26N	2.50E			C	
25MAY78	29-13170-1	49.29N	1.42E				
25MAY78	29-13170-1	49.47N	1.35E	310	R	M	20
25MAY78	29-13170-2	49.29N	1.42E				
25MAY78	29-13170-2	49.47N	1.35E	310	R	M	29
26MAY78	30- 2370-3	48.31N	1.41W	320	R	M	8
26MAY78	30- 2380-3	42.26N	3.45W	320	R	M	11
26MAY78	30-13310-1	35.27N	1.39E				
26MAY78	30-13310-2	35.27N	1.39E				
26MAY78	30-13330-1	41.32N	1.06W				
26MAY78	30-13330-2	41.32N	1.06W				
26MAY78	30-13350-1	47.36N	3.08W			C	
26MAY78	30-13350-2	47.36N	3.08W			C	
26MAY78	30-13360-1	53.38N	5.34W				
26MAY78	30-13360-2	53.38N	5.34W				
27MAY78	31- 2540-3	50.25N	5.32W	320	R	M	14
27MAY78	31- 2560-3	44.21N	7.44E	320	R	M	17
27MAY78	31-13510-1	40.50N	5.28E				
27MAY78	31-13510-2	40.50N	5.28E				
27MAY78	31-13530-1	46.54N	7.27W			C	
27MAY78	31-13530-2	46.54N	7.27W			C	
27MAY78	31-13540-1	52.56N	9.50W				
27MAY78	31-13540-2	52.56N	9.50W				
28MAY78	32- 3120-3	57.05N	9.00W				

DATE	IDENTIFICATION	LOCATION	SCENE	BDE	ETAT	DST	PM
28MAY78	32-3180-3	47.02N 11.23W					
28MAY78	32-12350-1	50.08N 11.02E					
28MAY78	32-12350-4	51.38N 10.26E					
28MAY78	32-12350-2	50.08N 11.02E					
28MAY78	32-12350-2	51.38N 10.26E					
28MAY78	32-12360-1	56.08N 8.22E		320	R	M	20
28MAY78	32-12360-2	56.08N 8.22E		320	R	M	23
28MAY78	32-14110-1	46.49N 12.01W					
28MAY78	32-14110-2	46.49N 12.01W					
29MAY78	33-1550-3	43.35N 7.08E		303	R	M	11
29MAY78	33-1570-3	37.29N 5.18E					
29MAY78	33-12500-1	39.56N 9.57E		293	R	M	26
29MAY78	33-12500-2	39.56N 9.57E		293	R	M	29
29MAY78	33-12520-1	46.01N 7.59E		294	R	M	2
29MAY78	33-12520-2	46.01N 7.59E		294	R	M	5
29MAY78	33-12530-1	52.03N 5.40E		320	R	M	26
29MAY78	33-12530-2	52.03N 5.40E		320	R	M	29
30MAY78	34-2120-3	50.41N 5.06E		303	R	M	14
30MAY78	34-2120-4	43.32N 4.14E		328	R	M	7
30MAY78	34-2120-5	43.32N 4.14E		328	R	M	10
30MAY78	34-2120-6	43.32N 4.14E		333	R	M	2
30MAY78	34-2120-7	43.32N 4.14E		333	R	M	5
30MAY78	34-2120-8	36.56N 2.36E		328	R	M	4
30MAY78	34-2130-3	44.37N 2.53E		303	R	M	17
30MAY78	34-2130-3	50.05N 4.30E					
30MAY78	34-2140-3	44.37N 2.53E			C		
30MAY78	34-2150-3	38.31N 1.02E					
30MAY78	34-2280-3	56.13N 3.00E			C		
30MAY78	34-13070-1	36.17N 6.25E					
30MAY78	34-13070-2	36.17N 6.25E					
30MAY78	34-13080-1	38.50N 5.41E		294	R	M	8
30MAY78	34-13080-2	38.50N 5.41E		294	R	M	11
30MAY78	34-13090-1	44.55N 3.47E		304	R	M	5
30MAY78	34-13090-1	42.22N 4.37E		304	R	M	2
30MAY78	34-13090-2	44.55N 3.47E		304	R	M	8
30MAY78	34-13090-2	42.22N 4.37E					
30MAY78	34-13100-1	48.26N 2.32E		303	R	M	26
30MAY78	34-13100-2	48.26N 2.32E		303	R	M	29
30MAY78	34-13110-1	50.58N 1.33E		321	R	M	2
30MAY78	34-13110-2	50.58N 1.33E		321	R	M	5
30MAY78	34-13120-1	54.27N 0.01E		303	R	M	20
30MAY78	34-13120-2	54.27N 0.01E		303	R	M	23
31MAY78	35-2280-3	56.13N 3.00E		313	R	M	14
31MAY78	35-2300-3	50.47N 1.34E		313	R	M	17
31MAY78	35-2300-3	50.11N 1.19E			C		
31MAY78	35-2310-3	44.43N 1.38E			C		
31MAY78	35-2320-3	44.07N 1.50E			C		
31MAY78	35-2330-3	38.01N 3.41E					
31MAY78	35-2330-3	38.37N 3.30E					
31MAY78	35-21320-1	55.40N 110.30W		304	R	M	11

DATE	IDENTIFICATION	LOCATION	SCENE	RDE	ETAT	DST	PM	
31MAY78	35-21320-2	35.40N 119.30W		304	R	M	14	
1JUN78	36-2480-3	31.25N 3.44W						
1JUN78	36-2490-3	45.21N 6.00W						
1JUN78	36-13440-1	38.45N 3.23W		321	R	M	14	
1JUN78	36-13440-2	38.35N 3.23W		321	R	M	17	
1JUN78	36-13460-1	42.00N 4.25W						
1JUN78	36-13460-1	44.40N 5.17W		321	R	M	8	
1JUN78	36-13460-2	42.00N 4.25W						
1JUN78	36-13460-2	44.40N 5.17W		321	R	M	11	
1JUN78	36-13470-1	50.43N 7.31W						
1JUN78	36-13470-2	50.43N 7.31W						
2JUN78	37-3060-3	51.12N 8.25W						
2JUN78	37-3080-3	45.08N 10.41W						
3JUN78	38-1480-4	43.39N 10.11E		331	R	M	7	****
3JUN78	38-1480-5	43.39N 10.11E		334	R	M	4	****
3JUN78	38-1480-6	43.39N 10.11E		330	R	M	5	****
3JUN78	38-1480-7	43.39N 10.11E		330	R	M	8	****
3JUN78	38-1480-8	34.52N 5.59E		331	R	M	4	****
3JUN78	38-1490-3	41.46N 7.56E		294	R	M	14	
3JUN78	38-1510-3	35.39N 6.11E						
3JUN78	38-12440-1	40.54N 11.04E		304	R	M	29	
3JUN78	38-12440-2	40.54N 11.04E			C			
3JUN78	38-12460-1	46.59N 9.04E		304	R	M	23	
3JUN78	38-12460-2	46.59N 9.04E		304	R	M	26	
3JUN78	38-12470-1	53.01N 6.40E		304	R	M	17	
3JUN78	38-12470-2	53.01N 6.40E		304	R	M	20	
4JUN78	39-2040-3	55.46N 8.44E						
4JUN78	39-2050-3	49.44N 6.06E						
4JUN78	39-2070-3	43.39N 3.57E						
4JUN78	39-2090-3	37.32N 2.07E						
4JUN78	39-13020-1	39.56N 6.47E			C			
4JUN78	39-13020-2	39.56N 6.47E			C			
4JUN78	39-13030-1	46.01N 4.49E						
4JUN78	39-13030-2	46.01N 4.49E						
4JUN78	39-13050-1	52.03N 2.29E			C			
4JUN78	39-13050-2	52.03N 2.29E			C			
5JUN78	40-2220-3	55.30N 4.03E			C			
5JUN78	40-2250-3	43.23N 4.41E						
5JUN78	40-2270-3	37.16N 2.30W						
5JUN78	40-13200-1	40.52N 1.56E						
5JUN78	40-13200-2	40.52N 1.56E						
5JUN78	40-13220-1	46.56N 0.02E						
5JUN78	40-13220-2	46.56N 0.02E						
5JUN78	40-13240-1	52.59N 2.26W						
5JUN78	40-13240-2	52.59N 2.26W						
6JUN78	41-13370-1	55.23N 1.05W						C
6JUN78	41-13370-2	55.23N 1.05W						C
6JUN78	41-13390-1	41.29N 2.51W						
6JUN78	41-13390-2	41.29N 2.51W						
6JUN78	41-13400-1	47.33N 4.53W						C

ORIGINAL PAGE IS
OF POOR QUALITY

DATE	IDENTIFICATION	LOCATION	SCENE	BDE	ETAT	DST	PM
6 JUN 78	41-13400-2	47.33N 4.53W					C
7 JUN 78	42-3020-3	42.24N 10.08W					
8 JUN 78	43-3190-3	46.00N 13.32W					
8 JUN 78	43-12370-1	54.45N 14.15E					
8 JUN 78	43-12380-1	41.20N 12.20E		294	R	M	17
8 JUN 78	43-12380-2	41.20N 12.20E		294	R	M	20
9 JUN 78	44-1590-3	50.04N 7.40E					
9 JUN 78	44-2010-3	43.59N 5.30E					
9 JUN 78	44-2020-3	37.53N 3.40E					
9 JUN 78	44-12250-1	38.41N 8.34E					
9 JUN 78	44-12550-2	39.41N 8.34E					
9 JUN 78	44-12570-1	44.46N 6.40E					
9 JUN 78	44-12570-2	44.46N 6.40E					
9 JUN 78	44-12580-1	50.50N 4.26E					
9 JUN 78	44-12580-2	50.50N 4.26E					
10 JUN 78	45-13130-1	36.36N 4.35E					
10 JUN 78	45-13130-2	36.36N 4.35E					
10 JUN 78	45-13140-1	42.41N 2.46E					
10 JUN 78	45-13140-2	42.41N 2.46E					
10 JUN 78	45-13160-1	48.46N .40E		307	R	M	2
10 JUN 78	45-13160-2	48.46N .40E		307	R	M	5
10 JUN 78	45-13180-1	54.47N 1.52W					
10 JUN 78	45-13180-2	54.47N 1.52W					
11 JUN 78	46-13310-1	35.45N .16E		313	R	M	20
11 JUN 78	46-13310-2	35.45N .16E		313	R	M	29
11 JUN 78	46-13320-1	41.50N 1.29E					
11 JUN 78	46-13320-2	41.50N 1.29W					
11 JUN 78	46-13340-1	47.55N 3.33W		313	R	M	20
11 JUN 78	46-13340-2	47.55N 3.33W		313	R	M	23
11 JUN 78	46-13360-1	53.57N 6.02W					
11 JUN 78	46-13360-2	53.57N 6.02W					
12 JUN 78	47-13500-1	42.12N 6.13W					
12 JUN 78	47-13500-2	42.12N 6.13W					
12 JUN 78	47-13520-1	48.16N 8.17W					
12 JUN 78	47-13520-2	48.16N 8.17W					
13 JUN 78	48-1370-3	41.26N 10.41E					
13 JUN 78	48-3110-3	52.49N 9.28W					
13 JUN 78	48-3120-3	46.46N 11.51W					
13 JUN 78	48-12350-1	55.26N 8.24E					
13 JUN 78	48-12350-2	55.26N 8.24E					
14 JUN 78	49-12490-1	40.04N 9.38E					
14 JUN 78	49-12490-2	40.04N 9.38E					
14 JUN 78	49-12510-1	46.09N 7.40E					
14 JUN 78	49-12510-2	46.09N 7.40E					
14 JUN 78	49-12520-1	52.12N 5.20E					
14 JUN 78	49-12520-2	52.12N 5.20E					
15 JUN 78	50-2090-3	55.49N 7.03E					
15 JUN 78	50-2110-3	49.47N 4.25E					
15 JUN 78	50-2120-3	43.42N 2.16E					
15 JUN 78	50-2140-3	37.35N .26E					

DATE	IDENTIFICATION	LOCATION	SCENE	SDE	ETAT	DST	PM
15 JUN 78	50-13070-1	40.05N 5.03E					C
15 JUN 78	50-13100-1	52.13N 4.46E					
15 JUN 78	50-13100-2	52.13N 4.46E					
15 JUN 78	50-13120-2	58.14N 2.30E					
16 JUN 78	51-2270-3	56.20N 2.47E					
16 JUN 78	51-2320-3	58.07N 2.59W		307	R	M	8
16 JUN 78	51-13240-1	57.00N 1.23E					C
16 JUN 78	51-13240-2	57.00N 1.23E					C
16 JUN 78	51-13260-1	43.06N 1.26E					
16 JUN 78	51-13260-2	43.06N 1.26E					
16 JUN 78	51-13280-1	49.10N 2.34W					
16 JUN 78	51-13280-2	49.10N 2.34W					
17 JUN 78	52-2450-3	55.38N 2.10W					
17 JUN 78	52-2470-3	49.35N 4.47W					
17 JUN 78	52-2490-3	43.31N 6.55W					
17 JUN 78	52-13430-1	57.35N 3.20W					
17 JUN 78	52-13460-1	49.45N 7.20W					
17 JUN 78	52-13460-2	49.45N 7.20W					
18 JUN 78	53-3050-3	51.35N 8.33W					C
18 JUN 78	53-3060-3	45.31N 10.50W					C
18 JUN 78	53-14030-1	46.05N 10.34W		305	R	M	8
18 JUN 78	53-14030-2	46.05N 10.34W		305	R	M	11
18 JUN 78	53-14050-1	52.09N 12.54W		305	R	M	2
18 JUN 78	53-14050-2	52.09N 12.54W		305	R	M	5
19 JUN 78	54-1470-3	45.45N 8.58E		305	R	M	14
19 JUN 78	54-1490-3	59.40N 7.02E		305	R	M	17
19 JUN 78	54-12430-1	42.46N 10.16E		294	R	M	23
19 JUN 78	54-12430-2	42.46N 10.16E		294	R	M	26
19 JUN 78	54-12450-1	48.51N 8.10E					
19 JUN 78	54-12450-2	48.51N 8.10E					
19 JUN 78	54-12470-1	54.53N 5.35E		321	R	M	20
19 JUN 78	54-12470-2	54.53N 5.35E		321	R	M	23
20 JUN 78	55-2030-3	52.43N 7.05E					
20 JUN 78	55-2030-3	52.58N 7.11E		296	R	M	26
20 JUN 78	55-2040-3	52.00N 6.46E					
20 JUN 78	55-2050-3	46.40N 4.43E					C
20 JUN 78	55-2050-3	45.56N 4.27E					
20 JUN 78	55-2050-3	46.54N 4.47E		296	R	M	29
20 JUN 78	55-2070-3	40.48N 2.47E					
20 JUN 78	55-2070-3	40.34N 2.43E					
20 JUN 78	55-2070-3	59.49N 2.30E					C
20 JUN 78	55-13000-1	59.00N 6.50E		294	R	M	29
20 JUN 78	55-13000-2	59.00N 6.50E					C
20 JUN 78	55-13020-1	45.05N 4.55E		295	R	M	2
20 JUN 78	55-13020-2	45.05N 4.55E		295	R	M	5
20 JUN 78	55-13040-1	51.10N 2.39E		295	R	M	8
20 JUN 78	55-13040-2	51.10N 2.39E		295	R	M	11
21 JUN 78	56-2210-7	56.11N 4.04E					
21 JUN 78	56-2220-3	50.09N 1.26E					
21 JUN 78	56-2240-3	44.04N 1.43E					

DATE	IDENTIFICATION	LOCATION	SCENE	BDE	ETAT	DST	PM
21 JUN 78	56-2260-3	37.58N	2.34W		295	R	H 29
21 JUN 78	56-13180-1	36.42N	2.55E			C	
21 JUN 78	56-13180-2	36.42N	2.55E			C	
21 JUN 78	56-13190-1	42.49N	1.07E			C	
21 JUN 78	56-13190-2	42.49N	1.07E			C	
22 JUN 78	57-13350-1	35.02N	1.10W		321	R	M 26
22 JUN 78	57-13350-2	35.02N	1.10W		321	R	M 29
22 JUN 78	57-13370-1	41.08N	2.56W				
22 JUN 78	57-13370-2	41.08N	2.56W				
22 JUN 78	57-13390-1	47.13N	4.58W				
22 JUN 78	57-13390-2	47.13N	4.58W				
22 JUN 78	57-13400-1	53.17N	7.23W				
22 JUN 78	57-13400-2	53.17N	7.23W				
23 JUN 78	58-2590-3	47.49N	9.34W				
23 JUN 78	58-13550-1	41.11N	7.30W				
23 JUN 78	58-13550-2	41.11N	7.30W				
23 JUN 78	58-13570-1	47.17N	9.31W				
23 JUN 78	58-13570-2	47.17N	9.31W				
24 JUN 78	59-1410-3	42.31N	9.22E		322	R	M 2
24 JUN 78	59-1430-3	36.24N	7.35E		322	R	M 5
24 JUN 78	59-3160-3	52.22N	11.20W				
24 JUN 78	59-3180-3	46.18N	13.40W				
24 JUN 78	59-12370-1	42.34N	11.47E		322	R	M 8
24 JUN 78	59-12370-2	42.34N	11.47E		322	R	M 11
24 JUN 78	59-12400-1	54.41N	7.07E				
24 JUN 78	59-12400-2	54.41N	7.07E				
25 JUN 78	60-1560-3	54.26N	9.19E				
25 JUN 78	60-1580-3	48.23N	6.49E				
25 JUN 78	60-2000-3	42.17N	4.45E				
25 JUN 78	60-2010-3	36.11N	2.59E				
25 JUN 78	60-12540-1	41.16N	7.39E				
25 JUN 78	60-12540-2	41.16N	7.39E				
25 JUN 78	60-12560-1	47.21N	5.38E				
25 JUN 78	60-12560-2	47.21N	5.38E				
26 JUN 78	61-2160-3	49.14N	2.34E				
26 JUN 78	61-2170-3	43.10N	.27E				
26 JUN 78	61-2190-3	37.01N	1.20W		322	R	M 14
26 JUN 78	61-13110-1	36.55N	4.21E		322	R	M 17
26 JUN 78	61-13110-2	36.55N	4.21E		322	R	M 20
26 JUN 78	61-13130-1	43.01N	2.32E				
26 JUN 78	61-13130-2	43.01N	2.32E				
26 JUN 78	61-13150-1	49.05N	2.25E				
26 JUN 78	61-13150-2	49.06N	2.25E				
26 JUN 78	61-13160-1	55.08N	2.10W				
26 JUN 78	61-13160-2	55.08N	2.10W				
27 JUN 78	62-13290-1	35.01N	.19E		322	R	M 26
27 JUN 78	62-13290-2	35.01N	.19E		322	R	M 29
27 JUN 78	62-13300-1	41.08N	1.25W				
27 JUN 78	62-13300-2	41.08N	1.25W				
28 JUN 78	63-2510-3	51.35N	5.36W				

DATE	IDENTIFICATION	LOCATION	SCENE	BDE	ETAT	DST	PM
28 JUN 78	63-2530-3	45.32N 7.52W					
28 JUN 78	63-13490-1	43.33N 6.46W		323	R	M	2
28 JUN 78	63-13490-2	43.33N 6.46W		323	R	M	5
29 JUN 78	64-14080-1	44.41N 11.40W					
29 JUN 78	64-14080-2	44.41N 11.40W					
30 JUN 78	65-1500-3	54.07N 10.39E					
30 JUN 78	65-1530-3	41.59N 6.08E		305	R	M	20
30 JUN 78	65-1550-3	55.53N 4.23E					
30 JUN 78	65-12470-1	39.22N 9.43E					
30 JUN 78	65-12470-2	39.22N 9.43E					
30 JUN 78	65-12490-1	45.79N 7.47E					
30 JUN 78	65-12490-2	45.49N 7.47E					
1 JUL 78	66-13050-1	38.10N 5.30E				C	
1 JUL 78	66-13050-2	38.10N 5.30E				C	
1 JUL 78	66-13080-1	50.21N 1.25E					
1 JUL 78	66-13080-2	50.21N 1.25E					
2 JUL 78	67-2270-3	50.36N 0.02E					
2 JUL 78	67-2280-3	44.32N 2.09W					
2 JUL 78	67-2300-3	38.26N 4.01W				C	
4 JUL 78	69-14000-1	41.18N 9.05W					
4 JUL 78	69-14000-2	41.18N 9.05W					
5 JUL 78	70-1460-3	43.16N 8.04E					
5 JUL 78	70-1460-3	42.29N 7.49E					
5 JUL 78	70-1470-3	57.10N 6.15E					
5 JUL 78	70-1480-3	56.73N 6.02E					
5 JUL 78	70-12410-1	43.01N 10.08E		332	R	M	26
5 JUL 78	70-12410-1	43.34N 9.58E					
5 JUL 78	70-12410-2	43.01N 10.08E		332	R	M	29
5 JUL 78	70-12410-2	43.34N 9.58E					
5 JUL 78	70-12450-1	55.09N 5.25E					
5 JUL 78	70-12450-1	55.41N 5.08E					
5 JUL 78	70-12450-2	55.09N 5.25E					
5 JUL 78	70-12450-2	55.41N 5.08E					
6 JUL 78	71-2020-3	48.26N 5.17E					
6 JUL 78	71-2040-3	42.22N 7.13E		305	R	M	23
6 JUL 78	71-2060-3	36.16N 1.27E					
6 JUL 78	71-12570-1	36.10N 7.38E					
6 JUL 78	71-12570-2	36.10N 7.38E					
6 JUL 78	71-12590-1	42.16N 5.49E		323	R	M	8
6 JUL 78	71-12590-2	42.16N 5.49E		323	R	M	11
7 JUL 78	72-2210-3	46.31N 0.02E		295	R	M	14
7 JUL 78	72-2230-3	40.25N 1.54W					
7 JUL 78	72-13170-1	40.08N 1.54E					
7 JUL 78	72-13170-1	40.05N 1.55E		295	R	M	17
7 JUL 78	72-13170-2	40.08N 1.54E					
7 JUL 78	72-13170-2	40.05N 1.55E		295	R	M	20
7 JUL 78	72-13180-1	46.14N 0.03E					
7 JUL 78	72-13180-1	46.11N 0.02E		295	R	M	23
7 JUL 78	72-13180-2	46.14N 0.03E					
7 JUL 78	72-13180-2	46.11N 0.02E		295	R	M	26

DATE	IDENTIFICATION	LOCATION	SCENE	BDE	ETAT	DST	PM
8JUL78	73-2370-3	52.33N 2.10W					
8JUL78	73-13350-1	40.53N 2.50W					
8JUL78	73-13350-2	40.53N 2.50W					
8JUL78	73-13360-1	46.59N 4.51W		296	R	M	2
8JUL78	73-13360-2	46.59N 4.51W		296	R	M	5
10JUL78	75-1390-3	42.20N 9.21E		296	R	M	8
10JUL78	75-1410-3	36.44N 7.35E		296	R	M	11
10JUL78	75-12350-1	45.02N 11.01E		323	R	M	14
10JUL78	75-12350-2	45.02N 11.01E		323	R	M	17
10JUL78	75-12370-1	51.07N 8.46E					
10JUL78	75-12370-2	51.07N 8.46E					
11JUL78	76-1540-3	52.29N 8.27E					
11JUL78	76-1550-3	49.03N 7.04E					
11JUL78	76-1560-3	46.26N 6.07E					
11JUL78	76-1570-3	42.59N 4.58E		296	R	M	14
11JUL78	76-1580-3	40.22N 4.10E			C		
11JUL78	76-1590-3	36.53N 3.10E		296	R	M	17
11JUL78	76-12520-1	40.33N 7.52E		323	R	M	20
11JUL78	76-12520-2	40.33N 7.52E		323	R	M	23
11JUL78	76-12530-1	46.40N 5.54E					
11JUL78	76-12530-2	46.40N 5.54E					
11JUL78	76-12550-1	52.43N 3.32E					
11JUL78	76-12550-2	52.43N 3.32E					
12JUL78	77-2130-3	51.37N 3.33E					
12JUL78	77-2140-3	45.34N 1.17E		296	R	M	40
12JUL78	77-2160-3	39.29N .37E		296	R	M	23
13JUL78	78-2310-3	51.45N .56E					
13JUL78	78-2320-3	45.42N 3.13W		322	R	M	23
16JUL78	81-1500-3	45.08N 7.15E		323	R	M	26
16JUL78	81-1510-3	39.04N 5.22E		323	R	M	29
17JUL78	82-1540-3	.00N .00E			C		
17JUL78	82-2060-3	51.24N 5.02E					
17JUL78	82-2080-3	45.21N 2.47E		297	R	M	2
17JUL78	82-2090-3	39.17N .53E					
17JUL78	82-13020-1	39.22N 5.15E			C		
17JUL78	82-13020-2	39.22N 5.15E			C		
17JUL78	82-13040-1	45.29N 3.19E			C		
17JUL78	82-13040-2	45.29N 3.19E			C		
17JUL78	82-13060-1	51.33N 1.02E					
17JUL78	82-13060-2	51.33N 1.02E					
18JUL78	83-2270-3	39.41N 3.39W					
18JUL78	83-2440-3	51.22N .29E					
20JUL78	85-3010-3	46.39N 10.22W					
21JUL78	86-1450-3	36.18N 6.12E					
21JUL78	86-12380-1	42.55N 10.17E		297	R	M	5
21JUL78	86-12380-2	42.55N 10.17E		297	R	M	8
22JUL78	87-2020-3	47.02N 4.59E					
22JUL78	87-2020-3	40.58N 3.00E			L		
23JUL78	88-2200-3	40.08N 1.47W					
25JUL78	90-2530-3	51.47N 6.47W		324	R	M	2

DATE	IDENTIFICATION	LOCATION	SCENE	BDE	ETAT	DST	PM
25 JUL 78	90- 2540-3	45.44N	9.04W	324	R	M	5
26 JUL 78	91- 1370-3	41.00N	9.14E	297	R	M	11
27 JUL 78	92- 1510-3	54.28N	9.41E				
27 JUL 78	92- 1530-3	48.27N	1.11E				
27 JUL 78	92- 1540-3	42.23N	5.07E	307	R	M	11
27 JUL 78	92- 1560-3	36.19N	3.20E				
24 SEP 78	93- 2080-4	41.41N	6.03E	329	R	M	7 ***
24 SEP 78	93- 2080-5	41.41N	6.03E	329	R	M	10 ***
24 SEP 78	93- 2080-6	41.41N	6.03E	326	R	M	2 ***
24 SEP 79	93- 2080-7	41.41N	6.03E	326	R	M	5 ***
28 JUL 78	93- 2080-8	41.08N	.11E	329	R	M	4 ***
28 JUL 78	93- 2100-3	50.54N	3.35E				
28 JUL 78	93- 2120-3	44.52N	1.22E			C	
28 JUL 78	93- 2130-3	38.47N	.30E				
28 JUL 78	93-13060-1	37.03N	4.29E	297	R	M	14
28 JUL 78	93-13060-2	37.03N	4.29E	297	R	M	17
28 JUL 78	93-13070-1	43.10N	2.40E	297	R	M	20
28 JUL 78	93-13070-2	43.10N	2.40E	297	R	M	23
28 JUL 78	93-13090-1	49.14N	.33E	297	R	M	26
28 JUL 78	93-13090-2	49.14N	.33E	297	R	M	29
28 JUL 78	93-13110-1	55.17N	2.01W				
28 JUL 78	93-13110-2	55.17N	2.01W				
29 JUL 78	94- 2280-3	51.50N	.31E	324	R	M	8
29 JUL 78	94- 2290-3	45.48N	2.49W	324	R	M	11
29 JUL 78	94-13230-1	36.00N	.16E				
29 JUL 78	94-13230-2	36.00N	.16E				
29 JUL 78	94-13250-1	42.07N	1.29W				
29 JUL 78	94-13250-2	42.07N	1.29W				
29 JUL 78	94-13270-1	48.11N	3.34W				
29 JUL 78	94-13270-2	48.11N	3.34W				
29 JUL 78	94-13280-1	54.14N	6.04W				
29 JUL 78	94-13280-2	54.14N	6.04W				
30 JUL 78	95- 2470-3	46.04N	7.16W				
30 JUL 78	95-13430-1	42.46N	6.16W				
30 JUL 78	95-13430-2	42.46N	6.16W				
30 JUL 78	95-13450-1	48.50N	8.22W				
30 JUL 78	95-13450-2	48.50N	8.22W				
31 JUL 78	96- 3040-3	51.54N	9.34W				
31 JUL 78	96- 3050-3	45.42N	11.52W				
31 JUL 78	96-12260-1	50.27N	10.45E				
31 JUL 78	96-12260-2	50.27N	10.45E				
31 JUL 78	96-12280-1	56.28N	8.01E				
31 JUL 78	96-12280-2	56.28N	8.01E				
31 JUL 78	96-14010-1	41.13N	10.17W				
31 JUL 78	96-14010-2	41.13N	10.17W				
31 JUL 78	96-14020-1	47.18N	12.19W				
31 JUL 78	96-14020-2	47.18N	12.19W				
1 AUG 78	97- 1470-3	43.46N	7.11E	296	R	M	2
1 AUG 78	97- 1480-3	37.42N	5.21E				
5 AUG 78	101- 2580-3	46.08N	10.08W				

ORIGINAL PAGE IS
OF POOR QUALITY

DATE	IDENTIFICATION	LOCATION	SCENE	BDE	ETAT	DST	PM
7AUG78	103-1580-3	42.59N	4.01E				
7AUG78	103-1590-3	36.54N	2.12E				
7AUG78	103-12520-1	39.58N	6.54E				
7AUG78	103-12520-2	39.58N	6.54E				
8AUG78	104-2140-3	49.55N	1.57E				
8AUG78	104-2150-3	43.52N	.12E				
8AUG78	104-2170-3	37.47N	2.02W				
8AUG78	104-13100-1	39.41N	2.25E				
8AUG78	104-13100-2	39.41N	2.25E				
8AUG78	104-13120-1	43.46N	.29E				
8AUG78	104-13120-2	43.46N	.29E				
9AUG78	105-13290-1	44.46N	3.41W				
9AUG78	105-13290-2	44.46N	3.41W				
9AUG78	105-13310-1	50.50N	5.55W				
9AUG78	105-13310-2	50.50N	5.55W				
11AUG78	107-1320-3	42.53N	10.11E				
11AUG78	107-13340-3	36.48N	8.23E				
11AUG78	107-3070-3	33.08N	10.17W				
11AUG78	107-3090-3	47.07N	12.21W				
12AUG78	108-1510-3	41.31N	5.13E				
12AUG78	108-1530-3	35.26N	3.28E				
12AUG78	108-12450-1	40.34N	8.19E	324	R	M	20
12AUG78	108-12450-2	40.34N	8.19E	324	R	M	23
12AUG78	108-12470-1	46.39N	6.21E	324	R	M	14
12AUG78	108-12470-2	46.39N	6.21E	324	R	M	17
13AUG78	109-2070-3	49.19N	3.22E				
13AUG78	109-2080-3	43.17N	1.13E				
13AUG78	109-2100-3	37.12N	.33E				
14AUG78	110-2270-3	42.36N	3.29W				
14AUG78	110-13210-1	40.07N	.34E				
14AUG78	110-13210-2	40.07N	.34E				
14AUG78	110-13220-1	46.11N	2.31W				
14AUG78	110-13220-2	46.11N	2.31W				
17AUG78	113-12380-1	40.49N	9.54E	325	R	M	26
17AUG78	113-12380-1	40.16N	9.27E	324	R	M	26
17AUG78	113-12380-2	40.49N	9.54E	325	R	M	29
17AUG78	113-12380-2	42.16N	9.27E	324	R	M	29
17AUG78	113-12390-1	46.53N	7.55E				
17AUG78	113-12390-2	46.53N	7.55E				
17AUG78	113-12410-1	52.55N	5.31E	298	R	M	5
17AUG78	113-12410-2	52.55N	5.31E	298	R	M	8
18AUG78	114-12550-1	37.48N	6.16E	325	R	M	2
18AUG78	114-12550-2	37.48N	6.16E	325	R	M	5
18AUG78	114-12570-1	43.53N	4.25E	298	R	M	11
18AUG78	114-12570-2	43.53N	4.25E	298	R	M	14
19AUG78	115-2170-3	51.58N	1.35E				
19AUG78	115-2180-3	45.56N	.42E				
19AUG78	115-2180-3	45.56N	.42E	307	R	M	14
19AUG78	115-2200-3	39.52N	0.39W				
19AUG78	115-13130-1	37.32N	1.49E	325	R	M	6

DATE	IDENTIFICATION	LOCATION	SCENE	BDE	ETAT	DST	PM
19AUG78	115-13130-2	37.32N 1.49E		325	R	M	11
19AUG78	115-13140-1	43.37N .00E		313	R	M	8
19AUG78	115-13140-2	43.37N .00E		313	R	M	11
19AUG78	115-13160-1	49.40N 2.09W		313	R	M	2
19AUG78	115-13160-2	49.40N 2.09W		313	R	M	5
20AUG78	116-13300-3	41.25N 6.43W					
20AUG78	116-13320-1	40.44N 3.38W					
20AUG78	116-13320-2	40.44N 3.38W					
20AUG78	116-13330-1	46.49N 5.37W					
20AUG78	116-13330-2	46.49N 5.37W					
20AUG78	116-13350-1	52.50N 8.00W					
20AUG78	116-13350-2	52.50N 8.00W					
21AUG78	117-13500-1	43.35N 9.04W		325	R	M	20
21AUG78	117-13500-2	43.35N 9.04W		325	R	M	23
21AUG78	117-13520-1	49.38N 11.13W		325	R	M	14
21AUG78	117-13520-2	49.38N 11.13W		325	R	M	17
22AUG78	118-13550-3	45.16N 9.47E		298	R	M	17
22AUG78	118-12310-1	41.30N 11.21E		332	R	M	2
22AUG78	118-12310-2	41.30N 11.21E		332	R	M	5
22AUG78	118-12340-1	53.35N 6.53E					
22AUG78	118-12340-2	53.35N 6.53E					
23AUG78	119-1510-3	54.52N 9.06E					
23AUG78	119-1540-3	42.48N 4.26E					
23AUG78	119-1560-3	56.43N 2.38E					
24AUG78	120-2110-3	47.10N 1.22E					
24AUG78	120-2120-3	41.06N .37E					
24AUG78	120-13060-1	40.34N 2.34E		307	R	M	23
24AUG78	120-13060-2	40.34N 2.34E		307	R	M	26
24AUG78	120-13080-1	46.38N .36E		307	R	M	17
24AUG78	120-13080-2	46.38N .36E		307	R	M	20
25AUG78	121-13240-1	40.43N 2.01W					
25AUG78	121-13240-2	40.43N 2.01W					
25AUG78	121-13260-1	46.47N 4.00W					
25AUG78	121-13260-2	46.47N 4.00W					
25AUG78	121-13280-1	52.49N 6.22W					
25AUG78	121-13280-2	52.49N 6.22W					
26AUG78	122-13440-1	43.50N 7.34W					
26AUG78	122-13440-2	43.50N 7.34W					
26AUG78	122-13450-1	49.53N 9.43W					
26AUG78	122-13450-2	49.53N 9.43W					
27AUG78	123-1290-3	44.15N 10.58E					
27AUG78	123-1300-3	58.10N 9.05E					
28AUG78	124-1460-3	49.26N 8.13E					
28AUG78	124-12410-1	59.00N 9.00E					
28AUG78	124-12410-2	59.00N 9.00E					
28AUG78	124-12430-1	55.05N 7.07E		296	R	M	20
28AUG78	124-12430-2	55.05N 7.07E		296	R	M	23
28AUG78	124-12450-1	51.07N 4.52E		296	R	M	26
28AUG78	124-12450-2	51.07N 4.52E		296	R	M	29
30AUG78	126-13160-1	50.44N .41E					

DATE	IDENTIFICATION	LOCATION	SCENE	BDE	ETAT	DST	PM
30AUG78	126-13180-2	40.44N	2.41E				C
30AUG78	126-13200-1	46.47N	2.40W				C
30AUG78	126-13200-2	46.47N	2.40W				C
30AUG78	126-13220-1	52.49N	5.02W				
30AUG78	126-13220-2	52.49N	5.02W				
31AUG78	127-2401-3	50.15N	5.14W				C
31AUG78	127-2421-3	44.12N	7.26W				
31AUG78	127-13380-1	45.05N	6.39W	308	R	M	17
31AUG78	127-13380-2	45.05N	6.39W	308	R	M	20
1SEP78	128-12220-1	56.23N	8.22E				
1SEP78	128-12220-2	56.23N	8.22E				
1SEP78	128-13550-1	41.23N	10.02W				
1SEP78	128-13550-2	41.23N	10.02W				
2SEP78	129-1410-3	45.22N	8.06E	299	R	M	2
2SEP78	129-1420-3	39.17N	6.11E				
2SEP78	129-12370-1	45.29N	8.19E				C
2SEP78	129-12370-2	45.29N	8.19E				C
3SEP78	130-1590-3	42.55N	2.41E				
3SEP78	130-12540-1	38.57N	5.48E				
3SEP78	130-12540-2	38.57N	5.48E				
3SEP78	130-12550-1	45.01N	7.54E	308	R	M	8
3SEP78	130-12550-2	45.01N	7.54E	308	R	M	11
3SEP78	130-12570-1	51.04N	4.39E	308	IR		2
3SEP78	130-12570-2	51.04N	4.39E	308	R	M	5
4SEP78	131-2150-3	51.40N	4.19E	308	R	M	14
4SEP78	131-2170-3	45.37N	5.8E				
5SEP78	132-2340-3	50.22N	3.49W				
5SEP78	132-2750-3	44.18N	6.02W				
5SEP78	132-13300-1	49.34N	3.32W				
5SEP78	132-13300-2	49.34N	3.32W				
6SEP78	133-13490-1	43.30N	9.20W				
6SEP78	133-13490-2	43.30N	9.20W				
7SEP78	134-1370-3	55.29N	6.31E				
7SEP78	134-3090-3	53.38N	11.36W				
7SEP78	134-12300-1	43.44N	10.16E				
7SEP78	134-12300-1	43.29N	10.21E				
7SEP78	134-12300-2	43.29N	10.21E				
7SEP78	134-12300-2	43.44N	10.16E				
7SEP78	134-12340-1	55.32N	5.35E				
7SEP78	134-12340-1	55.47N	5.29E				
7SEP78	134-12340-2	55.47N	5.29E				
7SEP78	134-12340-2	55.32N	5.35E				
8SEP78	135-1550-3	56.49N	2.15E				C
8SEP78	135-12470-1	47.32N	7.35E				C
8SEP78	135-12470-2	47.32N	7.35E				C
8SEP78	135-12490-1	47.37N	5.44E				C
8SEP78	135-12490-2	47.37N	5.44E				C
8SEP78	135-12500-1	49.40N	7.35E				
8SEP78	135-12500-2	49.40N	7.35E				
9SEP78	136-2100-3	46.40N	4.44E				

DATE	IDENTIFICATION	LOCATION	SCENE	BDE	ETAT	DST	PH
9SEP78	136-2120-3	40.43N	1.14W				
9SEP78	136-13050-1	36.32N	3.17E				C
9SEP78	136-13050-2	36.32N	3.17E				C
9SEP78	136-13070-1	42.37N	1.29E				C
9SEP78	136-13070-2	42.37N	1.29E				C
9SEP78	136-13080-1	48.40N	3.35E				
9SEP78	136-13080-2	48.40N	3.35E				
10SEP78	137-2290-3	44.37N	4.32W				
10SEP78	137-13240-1	40.06N	2.18W				
10SEP78	137-13240-2	40.06N	2.18W				
10SEP78	137-13260-1	46.10N	4.14W				C
10SEP78	137-13260-2	46.10N	4.14W				C
11SEP78	138-2460-3	50.07N	7.07W				
12SEP78	139-1290-3	42.48N	9.59E				
12SEP78	139-1300-3	36.41N	8.11E				
13SEP78	140-1450-3	31.05N	8.26E				
14SEP78	141-2050-3	41.38N	2.28E	309	R	M	20
14SEP78	141-12580-1	36.02N	4.49E				
14SEP78	141-12580-1	36.10N	4.47E	309	R	M	14
14SEP78	141-12580-2	36.02N	4.49E				
14SEP78	141-12580-2	36.10N	4.47E	309	R	M	17
14SEP78	141-13000-1	42.07N	3.02E				
14SEP78	141-13000-1	42.15N	3.00E	309	R	M	8
14SEP78	141-13000-2	42.07N	3.02E				
14SEP78	141-13000-2	42.15N	3.00E	309	R	M	11
14SEP78	141-13020-1	48.18N	5.56E	309	R	M	2
14SEP78	141-13020-1	48.11N	5.59E				
14SEP78	141-13020-2	48.11N	5.59E				
14SEP78	141-13020-2	48.18N	5.56E	309	R	M	5
14SEP78	141-13030-1	54.12N	1.30W				
14SEP78	141-13030-1	54.19N	1.33W				
14SEP78	141-13030-2	54.19N	1.33W				
14SEP78	141-13030-2	54.12N	1.30W				
15SEP78	142-2210-3	52.02N	2.22E				
15SEP78	142-2210-3	51.55N	2.25E	302	R	M	23
15SEP78	142-2220-3	45.52N	2.43W				C
15SEP78	142-2220-3	45.59N	2.41W				
15SEP78	142-13180-1	40.21N	5.58E	302	R	M	11
15SEP78	142-13180-2	40.21N	5.58E	302	R	M	14
15SEP78	142-13190-1	46.25N	2.55W	302	R	M	17
15SEP78	142-13190-2	46.25N	2.55W	302	R	M	20
15SEP78	142-13210-1	52.27N	5.16W				
15SEP78	142-13210-2	52.27N	5.16W				
16SEP78	143-2390-3	52.49N	4.34W				
16SEP78	143-2400-3	46.46N	6.57W				
17SEP78	144-12210-1	55.17N	8.33E				
17SEP78	144-12210-2	55.17N	8.33E				
17SEP78	144-13550-1	46.05N	14.58W				
17SEP78	144-13550-2	46.05N	14.58W				
17SEP78	144-13570-1	52.08N	14.17W				

ORIGINAL PAGE IS
OF POOR QUALITY

DATE	IDENTIFICATION	LOCATION	SCENE	BDE	ETAT	DST	PM
17SEP78	144-13570-2	52.08N 14.17W					
18SEP78	145-12360-1	42.16N 9.00E		302	R	M	26
18SEP78	145-12360-2	42.16N 9.00E		302	R	M	29
18SEP78	145-12370-1	48.19N 6.56E					
18SEP78	145-12370-2	48.19N 6.56E					
18SEP78	145-12390-1	54.20N 4.26E					
18SEP78	145-12390-2	54.20N 4.26E					
19SEP78	146- 1570-3	50.44N 5.07E					C
19SEP78	146- 1580-3	44.41N 2.53E					C
19SEP78	146- 2000-3	38.35N .59E					C
21SEP78	148- 2340-3	45.48N 5.52W					
21SEP78	148-13280-1	36.19N 2.58W					C
21SEP78	148-13280-2	36.19N 2.58W					C
21SEP78	148-13300-1	42.25N 4.44W					C
21SEP78	148-13300-2	42.25N 4.44W					C
21SEP78	148-13320-1	48.28N 6.49W					C
22SEP78	149- 2520-3	46.25N 10.13W					C
22SEP78	149-13480-1	40.49N 8.49W					C
22SEP78	149-13480-2	40.49N 8.49W					C
22SEP78	149-13490-1	46.53N 10.48W					C
22SEP78	149-13490-2	46.53N 10.48W					C
23SEP78	150-12300-1	46.19N 9.07E					
23SEP78	150-12300-2	46.19N 9.07E					
23SEP78	150-12320-1	52.22N 6.47E					
24SEP78	151-12460-1	39.07N 6.50E					
24SEP78	151-12460-2	39.07N 6.50E					
24SEP78	151-12480-1	45.11N 4.56E					
24SEP78	151-12480-2	45.11N 4.56E					
24SEP78	151-12500-1	51.14N 2.41E					
24SEP78	151-12500-2	51.14N 2.41E					
25SEP78	152- 2080-3	50.33N 1.54E					C
25SEP78	152- 2100-3	44.28N .18E					C
25SEP78	152- 2120-3	38.22N 2.11W					C
26SEP78	153-13220-1	37.49N 1.54W					
26SEP78	153-13220-2	37.49N 1.54W					
26SEP78	153-13240-1	43.54N 3.45W		310	R	M	20
26SEP78	153-13240-2	43.54N 3.45W		310	R	M	23
26SEP78	153-13260-1	49.57N 5.55W		310	R	M	14
26SEP78	153-13260-2	49.57N 5.55W		310	R	M	17
27SEP78	154- 2450-3	49.29N 7.38W					
27SEP78	154- 2460-3	43.25N 9.47W					
27SEP78	154-13420-1	43.26N 8.09W					C
27SEP78	154-13420-2	43.26N 8.09W					C
28SEP78	155- 1280-3	42.18N 9.35E					
28SEP78	155- 1290-3	36.11N 7.48E					
28SEP78	155-12220-1	42.50N 11.44E					
28SEP78	155-12230-2	42.50N 11.44E					
28SEP78	155-12260-1	34.55N 7.05E					
28SEP78	155-12260-2	34.55N 7.05E					
29SEP78	155- 1460-3	41.52N 4.53E					

DATE	IDENTIFICATION	LOCATION	SCENE	BDE	ETAT	DST	PM
29SEP78	156-1480-3	35.45N	3.07E				
29SEP78	156-12400-1	37.51N	8.40E				C
29SEP78	156-12400-2	37.51N	8.40E				C
29SEP78	156-12410-1	43.56N	6.49E				C
29SEP78	156-12410-2	43.56N	6.49E				C
30SEP78	157-2030-3	44.17N	1.04E				
30SEP78	157-2040-3	43.11N	4.3E				
30SEP78	157-2050-3	37.04N	1.05W				
30SEP78	157-2050-3	38.10N	4.7E				
20OCT78	159-2400-3	44.11N	8.03W				
20OCT78	159-13360-1	44.32N	7.01W				
20OCT78	159-13360-2	44.32N	7.01W				
30OCT78	160-13530-1	43.29N	11.13W				
30OCT78	160-13530-2	43.29N	11.13W				
30OCT78	160-13550-1	49.32N	13.21W				
30OCT78	160-13550-2	49.32N	13.21W				
50OCT78	162-12520-1	40.38N	4.49E				
50OCT78	162-12520-2	40.38N	4.49E				
50OCT78	162-12530-1	46.43N	2.50E				
50OCT78	162-12530-2	46.43N	2.50E				
80OCT78	165-13460-1	42.28N	9.23W				
80OCT78	165-13460-2	42.28N	9.23W				
80OCT78	165-13480-1	48.32N	11.27W				
80OCT78	165-13480-2	48.32N	11.27W				
90OCT78	166-12270-1	41.44N	10.35E				C
90OCT78	166-12270-2	41.44N	10.35E				C
90OCT78	166-12290-1	47.49N	8.34E				
90OCT78	166-12290-2	47.49N	8.34E				
90OCT78	166-12300-1	53.52N	6.05E				
90OCT78	166-12300-2	53.52N	6.05E				
100OCT78	167-12450-1	39.56N	6.35E	299	R	M	5
100OCT78	167-12450-2	39.56N	6.35E	299	R	M	8
100OCT78	167-12460-1	46.02N	4.38E	299	R	M	23
100OCT78	167-12460-2	46.02N	4.38E	299	R	M	26
110OCT78	168-2050-3	55.40N	4.09E				
110OCT78	168-2060-3	49.37N	1.30E				
110OCT78	168-2080-3	43.32N	3.38E				
110OCT78	168-2100-3	37.26N	2.26W				
110OCT78	168-13030-1	40.32N	1.52E				
110OCT78	168-13030-2	40.32N	1.52E				
110OCT78	168-13040-1	46.38N	0.05E				
110OCT78	168-13040-2	46.38N	0.05E				
110OCT78	168-13060-1	52.41N	2.27W				
110OCT78	168-13060-2	52.41N	2.27W				
120OCT78	169-13210-1	39.46N	2.26W				
120OCT78	169-13210-2	39.46N	2.26W				
120OCT78	169-13220-1	45.52N	4.22W				
120OCT78	169-13220-2	45.52N	4.22W				
120OCT78	169-13240-1	51.55N	6.40W				
120OCT78	169-13240-2	51.55N	6.40W				

DATE IDENTIFICATION LOCATION SCENE BDE ETAT DST PM

DATE	IDENTIFICATION	LOCATION	SCENE	BDE	ETAT	DST	PM
13OCT78	170-13390-1	41.38N	7.32W				
13OCT78	170-13390-2	41.38N	7.32W				
13OCT78	170-13410-1	47.43N	9.34W				
13OCT78	170-13410-2	47.43N	9.34W				
14OCT78	171-12210-1	43.46N	11.31E				C
14OCT78	171-12210-2	43.46N	11.31E				C
14OCT78	171-12220-1	49.51N	9.22E				
14OCT78	171-12220-2	49.51N	9.22E				
15OCT78	172-12380-1	41.04N	7.50E				
15OCT78	172-12380-2	41.04N	7.50E				
15OCT78	172-12400-1	47.09N	5.50E				
15OCT78	172-12400-2	47.09N	5.50E				
16OCT78	173-12550-1	37.14N	4.24E				
16OCT78	173-12550-2	37.14N	4.24E				
16OCT78	173-12570-1	43.20N	2.35E				
16OCT78	173-12570-2	43.20N	2.35E				
17OCT78	174-13140-1	39.54N	.53E				
17OCT78	174-13140-1	39.43N	.50E				
17OCT78	174-13140-2	39.54N	.53E				
17OCT78	174-13140-2	39.43N	.50E				
17OCT78	174-13170-1	32.04N	5.08W				
17OCT78	174-13170-1	31.53N	5.04W				
17OCT78	174-13170-2	32.04N	5.08W				
17OCT78	174-13170-2	31.53N	5.04W				
18OCT78	175-13320-1	42.42N	6.16W				
18OCT78	175-13320-2	42.42N	6.16W				
19OCT78	176-12150-1	31.03N	10.30E				
19OCT78	176-12150-2	31.03N	10.30E				
20OCT78	177-12320-1	47.28N	7.21E				
20OCT78	177-12320-2	47.28N	7.21E				
21OCT78	178-12480-1	39.02N	5.32E				C
21OCT78	178-12480-2	39.02N	5.32E				C
21OCT78	178-12500-1	45.08N	3.38E				C
21OCT78	178-12500-2	45.08N	3.38E				C
22OCT78	178-13080-1	46.28N	1.20W				
22OCT78	178-13080-2	46.28N	1.20W				
22OCT78	179-13060-1	40.22N	.37E				C
22OCT78	179-13060-2	40.22N	.37E				C
23OCT78	180-12270-3	32.22N	3.10W				
24OCT78	181-13430-1	42.10N	8.57W	305	R	M	27
24OCT78	181-13430-2	42.10N	8.57W	305	R	M	30
24OCT78	181-13450-1	48.15N	11.01W	308	R	M	23
24OCT78	181-13450-2	48.15N	11.01W	308	R	M	26
25OCT78	182-12231-1	41.37N	10.58E				
25OCT78	182-12231-2	41.37N	10.58E				
25OCT78	182-12250-1	48.04N	8.48E				
25OCT78	182-12251-1	47.42N	8.56E				
25OCT78	182-12251-2	47.42N	8.56E				
25OCT78	182-12270-1	34.07N	6.19E				
25OCT78	182-12270-2	34.07N	6.19E				

DATE	IDENTIFICATION	LOCATION	SCENE	BDE	ETAT	DST	PM
25OCT78	182-12271-1	53.46N	6.28E				
25OCT78	182-12271-2	53.46N	6.28E				
26OCT78	183-12410-1	38.50N	7.16E				
26OCT78	183-12410-2	38.50N	7.16E				
26OCT78	183-12420-1	44.57N	5.22E				
26OCT78	183-12420-2	44.57N	5.22E				
27OCT78	184-12580-1	35.14N	3.45E				C
27OCT78	184-12580-2	35.14N	3.45E				C
27OCT78	184-12590-1	41.22N	2.01E				
27OCT78	184-12590-2	41.22N	2.01E				C
27OCT78	184-12590-3	40.45N	2.11E				C
27OCT78	184-13010-1	47.28N	.00E				C
27OCT78	184-13010-2	47.28N	.00E				C
27OCT78	184-13010-3	46.51N	.13E				
27OCT78	184-13020-3	52.55N	2.10W				
27OCT78	184-13030-1	53.31N	2.26W				
27OCT78	184-13030-2	53.31N	2.26W				
28OCT78	185-13160-1	37.49N	1.26W	306	R	M	26
28OCT78	185-13160-2	37.49N	1.26W		C		
28OCT78	185-13180-1	43.56N	3.17W	306	R	M	8
28OCT78	185-13180-2	43.56N	3.17W	306	R	M	11
28OCT78	185-13200-1	50.01N	5.27W	306	R	M	2
28OCT78	185-13200-2	50.01N	5.27W	306	R	M	5
29OCT78	186-13360-1	45.09N	8.13W		C		
29OCT78	186-13360-2	45.09N	8.13W		C		
29OCT78	186-13380-1	51.13N	10.28W				
29OCT78	186-13380-2	51.13N	10.28W				
30OCT78	187-12170-1	44.34N	11.44E	309	R	M	23
30OCT78	187-12170-2	44.34N	11.44E	309	R	M	26
30OCT78	187-12180-1	50.36N	9.31E				
31OCT78	188-1370-3	49.13N	8.01E				
31OCT78	188-1390-3	43.08N	5.53E				C
31OCT78	188-1410-3	57.03N	4.04E				C
1NOV78	189-1550-3	51.14N	4.19E				
1NOV78	189-1560-3	45.10N	2.04E				C
1NOV78	189-1580-3	50.05N	.08E				C
1NOV78	189-12500-1	36.01N	5.17E				C
1NOV78	189-12500-2	36.01N	5.17E				C
1NOV78	189-12520-1	42.08N	3.31E				C
1NOV78	189-12520-2	42.08N	3.31E				C
1NOV78	189-12530-1	48.13N	1.28E				C
1NOV78	189-12530-2	48.13N	1.28E				C
1NOV78	189-12550-1	54.16N	1.02W				
1NOV78	189-12550-2	54.16N	1.02W				
2NOV78	190-13090-1	40.23N	.26E				
2NOV78	190-13090-2	40.23N	.26E				
2NOV78	190-13110-1	46.29N	2.24W	299	R	M	11
2NOV78	190-13110-2	46.29N	2.24W	299	R	M	14
2NOV78	190-13130-1	52.33N	4.46W				
2NOV78	190-13130-2	52.32N	4.46W				

ORIGINAL PAGE IS
OF POOR QUALITY

DATE	IDENTIFICATION	LOCATION	SCENE	BDE	ETAT	DST	PM
3NOV78	191-13280-1	45.13N 6.28W					
3NOV78	191-13280-2	45.13N 6.28W					
5NOV78	193-12260-1	40.37N 10.16E					
5NOV78	193-12260-2	40.37N 10.16E					
5NOV78	193-12270-1	46.43N 8.17E					
5NOV78	193-12270-2	46.43N 8.17E					
5NOV78	193-12290-1	52.47N 5.55E					
5NOV78	193-12290-2	52.47N 5.55E					
6NOV78	194-12430-1	38.22N 6.25E					C
6NOV78	194-12430-2	38.22N 6.25E					C
6NOV78	194-12450-1	44.29N 4.34E					C
6NOV78	194-12450-2	44.29N 4.34E					C
6NOV78	194-12460-1	50.34N 2.21E					
6NOV78	194-12460-2	50.34N 2.21E					
7NOV78	195- 2050-1	48.22N .31E		310	R	M	8
7NOV78	195- 2050-3	48.50N .41E		310	IP		2
7NOV78	195- 2070-1	42.17N 1.33W		310	R	M	11
7NOV78	195- 2070-3	42.47N 1.24W		310	R	M	5
7NOV78	195- 2080-1	36.41N 3.13W					
7NOV78	195-13010-1	40.49N 1.13E					
7NOV78	195-13010-2	40.49N 1.13E					
7NOV78	195-13030-1	46.55N .45E					
7NOV78	195-13030-2	46.55N .45E					
7NOV78	195-13050-1	52.59N 3.09W					
7NOV78	195-13050-2	52.59N 3.09W					
8NOV78	196- 2240-1	46.32N 4.36W					
9NOV78	197- 2400-1	52.53N 6.38W		306	R	M	29
9NOV78	197- 2420-1	46.52N 9.02W					C
10NOV78	198- 1240-1	40.59N 8.43E					
10NOV78	198-12190-1	42.10N 11.25E					
10NOV78	198-12190-2	42.10N 11.25E					
10NOV78	198-12210-1	48.14N 9.21E					
10NOV78	198-12210-2	48.14N 9.21E					
11NOV78	199- 1420-1	44.27N 5.11E					
11NOV78	199- 1430-1	38.22N 7.19E					
11NOV78	199-12360-1	36.19N 8.31E					
11NOV78	199-12360-2	36.19N 8.31E					
11NOV78	199-12370-1	42.25N 6.43E					
11NOV78	199-12370-2	42.25N 6.43E					
11NOV78	199-12390-1	48.31N 4.38E					
11NOV78	199-12390-2	48.31N 4.38E					
11NOV78	199-12410-1	54.33N 2.07E					
11NOV78	199-12410-2	54.33N 2.07E					
12NOV78	200- 2000-1	44.50N .43E		299	R	M	17
12NOV78	200- 2010-1	38.46N 1.10W		299	R	M	20
12NOV78	200-12540-1	35.33N 4.07E					
12NOV78	200-12540-2	35.33N 4.07E					
12NOV78	200-12550-1	41.40N 2.21E					
12NOV78	200-12550-2	41.40N 2.21E					
12NOV78	200-12570-1	47.46N .19E		300	R	M	2

DATE	IDENTIFICATION	LOCATION	SCENE	BDE	ETAT	DST	PM
12NOV78	200-12570-2	47.46N .19E		300	R	M	5
14NOV78	202-13330-1	45.35N 8.06W			C		
14NOV78	202-13330-2	45.35N 8.06W			C		
15NOV78	203-1180-3	42.13N 10.22E			C		
15NOV78	203-1200-3	36.08N 8.35E			C		
16NOV78	204-1340-3	49.53N 8.28E					
16NOV78	204-1360-3	43.50N 6.17E		300	R	M	8
16NOV78	204-1380-3	37.46N 4.26E					
17NOV78	205-1520-3	51.40N 4.35E					
17NOV78	205-1540-3	45.37N 2.17E		300	R	M	11
19NOV78	207-2290-3	50.32N 5.04W					
19NOV78	207-2310-3	44.29N 7.17W			C		
21NOV78	209-1310-3	39.49N 6.22E					
22NOV78	210-1450-3	55.23N 7.38E					
22NOV78	210-1470-3	49.23N 5.01E					
22NOV78	210-1480-3	43.20N 2.52E			C		
22NOV78	210-1500-3	37.16N 1.02E			C		
23NOV78	211-2060-3	45.59N .50E			C		
23NOV78	211-2080-3	39.55N 2.46W					
24NOV78	212-2230-3	49.37N 4.27W			C		
24NOV78	212-2250-3	42.34N 6.32W					
28NOV78	216-2020-3	37.38N 2.05W					
28NOV78	216-12540-1	36.58N 3.12E					
28NOV78	216-12540-1	36.39N 3.17E					
28NOV78	216-12540-2	36.58N 3.12E					
28NOV78	216-12540-2	36.39N 3.17E					
28NOV78	216-12560-1	43.05N 1.18E					
28NOV78	216-12560-1	42.47N 1.24E					
28NOV78	216-12560-2	43.05N 1.18E					
28NOV78	216-12560-2	42.47N 1.24E					
28NOV78	216-12570-1	48.50N .39E		300	R	M	14
28NOV78	216-12570-2	48.50N .39E		300	R	M	17
28NOV78	216-12580-1	49.09N .46E					
28NOV78	216-12580-2	49.09N .46E					
28NOV78	216-12590-1	54.52N 3.12W					
28NOV78	216-12590-2	54.52N 3.12W					
30NOV78	218-2340-3	52.04N 6.16W					
30NOV78	218-13320-1	42.13N 7.32W					
30NOV78	218-13320-2	42.13N 7.32W					
30NOV78	218-13340-1	50.46N 10.33W		300	R	M	20
30NOV78	218-13340-1	48.17N 9.35W		300	R	M	26
30NOV78	218-13340-2	50.46N 10.33W		300	R	M	23
30NOV78	218-13340-2	48.17N 9.35W		300	R	M	29
5DEC78	223-13260-1	42.02N 6.01W					
5DEC78	223-13260-2	42.02N 6.01W					
6DEC78	224-12090-1	49.58N 10.45E					
6DEC78	224-12090-2	49.58N 10.54E					
6DEC78	224-12100-1	55.59N 9.14E					
6DEC78	224-12100-2	55.59N 9.14E					
6DEC78	224-13440-1	43.20N 11.02W					

DATE	IDENTIFICATION	LOCATION	SCENE	BDE	ETAT	DST	PM
6DEC78	224-13440-2	43.20N 11.02W					
6DEC78	224-13460-1	49.24N 13.10W					
6DEC78	224-13460-2	49.24N 13.10W					
7DEC78	225-12230-1	37.05N 10.32E					
7DEC78	225-12230-2	37.05N 10.32E					
7DEC78	225-12250-1	42.01N 9.05E		306	R	M	20
7DEC78	225-12250-1	43.11N 8.44E					
7DEC78	225-12250-2	42.01N 9.05E		306	R	M	23
7DEC78	225-12250-2	43.11N 8.44E					
7DEC78	225-12260-1	48.05N 7.02E					
7DEC78	225-12260-2	48.05N 7.02E					
7DEC78	225-12270-1	49.14N 6.37E					
7DEC78	225-12270-2	49.14N 6.37E					
7DEC78	225-12280-1	54.07N 4.34E		306	R	M	14
7DEC78	225-12280-2	54.07N 4.34E		306	R	M	17
8DEC78	226-12410-1	36.38N 6.06E					
8DEC78	226-12410-2	36.38N 6.06E					
9DEC78	227-12590-1	35.49N 1.46E					
9DEC78	227-12590-2	35.49N 1.46E					
9DEC78	227-13010-1	41.54N .00E		301	R	M	2
9DEC78	227-13010-2	41.54N .00E		301	R	M	5
9DEC78	227-13030-1	47.58N 2.01W		301	R	M	8
9DEC78	227-13030-2	47.58N 2.01W		301	R	M	11
9DEC78	227-13040-1	34.00N 4.29W					
9DEC78	227-13040-2	34.00N 4.29W					
10DEC78	228-13170-1	34.58N 2.34W					
10DEC78	228-13170-2	34.58N 2.34W					
10DEC78	228-13190-1	41.04N 4.17W					
10DEC78	228-13190-2	41.04N 4.17W					
10DEC78	228-13220-1	33.10N 8.41W					
10DEC78	228-13220-2	33.10N 8.41W					
11DEC78	229-13400-1	30.35N 12.09W					
11DEC78	229-13400-2	30.35N 12.09W					
13DEC78	231-12350-1	33.01N 7.11E					
13DEC78	231-12350-2	33.01N 7.11E					
14DEC78	232-12530-1	35.27N 3.20E					
14DEC78	232-12530-2	35.27N 3.20E					
14DEC78	232-12540-1	41.33N 1.35E					
14DEC78	232-12540-2	41.33N 1.35E					
14DEC78	232-12560-1	47.37N .25E					
14DEC78	232-12560-2	47.37N .25E					
14DEC78	232-12580-1	33.38N 2.50W					
14DEC78	232-12580-2	33.38N 2.50W					
16DEC78	234-13320-1	48.27N 9.50W					
16DEC78	234-13320-2	48.27N 9.50W					
17DEC78	235-12120-1	42.37N 11.53E					
17DEC78	235-12120-2	42.37N 11.53E					
17DEC78	235-12130-1	43.41N 9.49E					

C
C

DATE	IDENTIFICATION	LOCATION	SCENE	BDE	ETAT	DST	PM
17DEC78	235-12130-2	48.41N	9.49E				
17DEC78	235-12150-1	54.42N	7.17E				
17DEC78	235-12150-2	54.42N	7.17E				
18DEC78	236-12280-1	36.24N	9.10E				
18DEC78	236-12280-2	36.24N	9.10E				
18DEC78	236-12310-1	48.32N	5.19E				
18DEC78	236-12310-2	48.32N	5.19E				
18DEC78	236-12330-1	54.34N	2.47E				
18DEC78	236-12330-2	54.34N	2.47E				
19DEC78	237-12460-1	36.07N	4.41E				
19DEC78	237-12460-2	36.07N	4.41E				
19DEC78	237-12480-1	42.12N	2.55E				
19DEC78	237-12480-2	42.12N	2.55E				
19DEC78	237-12490-1	48.16N	.52E				C
19DEC78	237-12490-2	48.16N	.52E				C
19DEC78	237-12510-1	54.16N	1.36W				C
19DEC78	237-12510-2	54.16N	1.36W				C
20DEC78	238-4380-2	37.20S	138.04E				
21DEC78	239-2290-3	44.08N	7.54W				
21DEC78	239-2290-3	43.49N	8.00W				
21DEC78	239-13250-1	45.08N	7.04W				
21DEC78	239-13250-2	45.08N	7.04W				
22DEC78	240-13440-1	49.37N	13.16W				
22DEC78	240-13440-2	49.37N	13.16W				
23DEC78	241-12230-1	42.34N	8.55E				
23DEC78	241-12230-2	42.34N	8.55E				
24DEC78	242-12400-1	39.18N	5.22E				
25DEC78	243-2040-3	44.19N	1.42W	301	R	M	20
25DEC78	243-12580-1	39.57N	.37E				
25DEC78	243-12580-2	39.57N	.37E				
25DEC78	243-13000-1	46.01N	1.18W	301	R	M	14
25DEC78	243-13000-2	46.01N	1.18W	301	R	M	17
25DEC78	243-13020-1	52.04N	3.36W				
25DEC78	243-13020-2	52.04N	3.36W				
26DEC78	244-2210-3	45.24N	5.53W	301	R	M	23
27DEC78	245-2400-3	44.00N	10.55W				
28DEC78	246-1210-3	40.52N	7.52E				C
28DEC78	246-12160-1	43.31N	10.11E				C
28DEC78	246-12160-2	43.31N	10.11E				C
29DEC78	247-1400-3	37.10N	2.14E				
29DEC78	247-12360-3	48.43N	7.51E				
29DEC78	247-12370-3	54.44N	1.19E				
30DEC78	248-12500-1	35.55N	3.20E				
30DEC78	248-12520-1	42.01N	1.36E				
30DEC78	248-12520-2	42.01N	1.36E				
31DEC78	249-1120-1	45.53N	4.07W				
31DEC78	249-13140-1	45.41N	4.07W				
31DEC78	249-13130-2	51.43N	6.24W				
3JAN79	252-1320-3	41.33N	5.07E				
3JAN79	252-1340-3	35.27N	7.22E				

DATE	IDENTIFICATION	LOCATION	SCENE	BDE	ETAT	DST	PM
3 JAN 79	252-12260-1	39.56N	8.25E				
3 JAN 79	252-12260-2	39.56N	8.25E				
3 JAN 79	252-12280-1	46.00N	6.29E				
3 JAN 79	252-12280-2	46.00N	6.29E				
3 JAN 79	252-12290-1	52.02N	4.11E				
3 JAN 79	252-12290-2	52.02N	4.11E				
6 JAN 79	255-2260-3	42.50N	8.04W				
6 JAN 79	255-13210-1	44.07N	6.27W				
6 JAN 79	255-13210-2	44.07N	6.27W				
7 JAN 79	256-1060-3	42.58N	11.44E				
7 JAN 79	256-2410-3	53.47N	8.29W				
7 JAN 79	256-13390-1	43.02N	10.38W				
7 JAN 79	256-13390-2	43.02N	10.38W				
10 JAN 79	259-1570-3	53.19N	2.31E				
10 JAN 79	259-2010-3	41.10N	1.55W				
11 JAN 79	260-2150-3	53.31N	1.49W				
12 JAN 79	261-2330-3	54.42N	5.48W				
13 JAN 79	262-1170-3	41.26N	8.50E	R	301	R	M 26
13 JAN 79	262-1190-3	35.19N	7.04E				
13 JAN 79	262-2520-3	50.31N	12.05W				
14 JAN 79	263-1320-3	52.05N	8.13E		302	R	M 2
14 JAN 79	263-1360-3	59.55N	7.55E		302	R	M 5
15 JAN 79	264-1500-3	53.47N	4.25E				
15 JAN 79	264-1510-3	47.44N	1.57E			C	
15 JAN 79	264-1530-3	41.39N	.00E			C	
16 JAN 79	265-2090-3	48.14N	2.15W			C	
16 JAN 79	265-2110-3	42.10N	4.20W			C	
17 JAN 79	266-2260-3	52.40N	4.57W				
17 JAN 79	266-2270-3	46.37N	7.20W			C	
17 JAN 79	266-13230-1	40.42N	5.56W				
17 JAN 79	266-13230-2	40.42N	5.56W				
17 JAN 79	266-13250-1	46.46N	7.55W				
17 JAN 79	266-13250-2	46.46N	7.55W				
17 JAN 79	266-13260-1	52.49N	10.18W				
17 JAN 79	266-13260-2	52.49N	10.18W				
18 JAN 79	267-13420-1	42.58N	11.08W				
18 JAN 79	267-13420-2	42.58N	11.08W				
19 JAN 79	268-1290-3	35.34N	4.32E				
21 JAN 79	270-2010-3	51.18N	1.36E				
21 JAN 79	270-2010-3	51.18N	1.36E				
21 JAN 79	270-2030-3	45.14N	1.40W			C	
21 JAN 79	270-2040-3	59.08N	3.35W				
21 JAN 79	270-13000-1	46.10N	1.36W				
21 JAN 79	270-13000-2	46.10N	1.36W				
21 JAN 79	270-13010-1	52.12N	3.56W				
21 JAN 79	270-13010-2	52.12N	3.56W				
23 JAN 79	272-12000-1	51.13N	11.05E				
23 JAN 79	272-12000-2	51.13N	11.05E				
23 JAN 79	272-13360-1	44.39N	10.47W				
23 JAN 79	272-13360-2	44.39N	10.47W				

DATE	IDENTIFICATION	LOCATION	SCENE	BDE	ETAT	DST	PM
23JAN79	272-13370-1	50.43N	13.01W				
23JAN79	272-13370-2	50.43N	13.01W				
24JAN79	273-1210-3	41.20N	7.01E				C
24JAN79	273-1230-3	35.13N	5.16E				
25JAN79	274-12340-2	40.39N	5.33E				
25JAN79	274-12360-1	46.44N	3.34E				
25JAN79	274-12360-2	46.44N	3.34E				
25JAN79	274-12370-1	52.47N	1.11E				
25JAN79	274-12370-2	52.47N	1.11E				
26JAN79	275-1590-3	38.38N	2.57W				
26JAN79	275-12520-1	39.40N	1.14E				
26JAN79	275-12520-2	39.40N	1.14E				
26JAN79	275-12550-1	51.49N	2.58W				
26JAN79	275-12550-2	51.49N	2.58W				
27JAN79	276-2140-3	50.40N	3.29W				
28JAN79	277-2330-3	47.36N	9.16W				
28JAN79	277-13300-1	44.29N	9.26W				
28JAN79	277-13300-2	44.29N	9.26W				
28JAN79	277-13320-1	50.33N	11.39W				
28JAN79	277-13320-2	50.33N	11.39W				
29JAN79	278-1170-3	36.12N	6.51E				
30JAN79	279-1330-3	43.00N	4.16E				C
30JAN79	279-1350-3	36.54N	2.28E				C
30JAN79	279-12280-1	40.38N	6.51E				
30JAN79	279-12280-2	40.38N	6.51E				
31JAN79	280-1490-3	51.37N	2.49E				C
31JAN79	280-1510-3	45.33N	3.31E				C
31JAN79	280-1530-3	39.28N	1.23W				C
1FEB79	281-2060-3	51.26N	1.50W				
1FEB79	281-2090-3	45.23N	4.07W				
2FEB79	282-2261-3	49.15N	7.19W				
3FEB79	283-1090-3	42.47N	10.08E				
3FEB79	283-1110-3	36.41N	8.20E				C
4FEB79	284-1250-3	50.26N	8.16E				
4FEB79	284-1270-3	44.22N	6.04E				C
4FEB79	284-1290-3	38.16N	4.11E				C
4FEB79	284-12220-1	39.01N	8.41E				C
4FEB79	284-12220-2	39.01N	8.41E				C
5FEB79	285-1430-3	50.50N	3.50E				
5FEB79	285-1450-3	44.46N	1.37E				
5FEB79	285-1470-3	38.41N	.16E				
5FEB79	285-12400-1	38.01N	4.24E				C
5FEB79	285-12400-2	38.01N	4.24E				C
5FEB79	285-12430-1	50.11N	.22E				
5FEB79	285-12430-2	50.11N	.22E				
6FEB79	286-2010-3	37.41N	.28E				C
6FEB79	286-2020-3	47.38N	1.59W				C
6FEB79	286-12570-1	36.03N	.20E				
6FEB79	286-12570-2	36.03N	.20E				
7FEB79	287-13160-1	32.37N	5.13W				

ORIGINAL PAGE IS
OF POOR QUALITY

DATE IDENTIFICATION LOCATION SCENE BDE ETAT DST PM

DATE	IDENTIFICATION	LOCATION	SCENE	BDE	ETAT	DST	PM
7FEB79	287-13160-2	39.37N	5.13W				
7FEB79	287-13180-1	45.43N	7.08W				
7FEB79	287-13180-2	45.43N	7.08W				
10FEB79	290-1370-3	49.51N	5.27W				
14FEB79	294-12090-1	42.04N	11.14E				
14FEB79	294-12090-2	42.04N	11.14E				
15FEB79	295-12260-1	38.46N	7.40E				
15FEB79	295-12260-2	38.46N	7.40E				
16FEB79	296-12450-1	40.41N	2.32E				
17FEB79	297-13020-1	38.04N	1.13W				
17FEB79	297-13020-2	38.04N	1.13W				
17FEB79	297-13040-1	44.10N	3.04W				
17FEB79	297-13040-2	44.10N	3.04W				
20FEB79	300-12190-1	38.49N	9.13E				
20FEB79	300-12190-2	38.49N	9.13E				
20FEB79	300-12210-1	44.55N	7.20E				
20FEB79	300-12210-2	44.55N	7.20E				
20FEB79	300-12230-1	50.59N	5.05E				
20FEB79	300-12230-2	50.59N	5.05E				
21FEB79	301-12380-1	41.35N	3.53E				C
21FEB79	301-12380-2	41.35N	3.53E				C
21FEB79	301-12400-1	47.40N	1.50E				C
21FEB79	301-12400-2	47.40N	1.50E				C
22FEB79	302-12550-1	38.53N	.08E				
22FEB79	302-12550-2	38.53N	.08E				C
22FEB79	302-12590-1	51.04N	4.00W				C
22FEB79	302-12590-2	51.04N	4.00W				
23FEB79	303-13150-1	44.11N	6.00W				C
23FEB79	303-13150-2	44.11N	6.00W				C
23FEB79	303-13160-1	50.16N	8.12W				C
23FEB79	303-13160-2	50.16N	8.12W				C
24FEB79	304-11580-1	52.42N	10.33E				
24FEB79	304-11580-2	52.42N	10.33E				
24FEB79	304-13330-1	44.39N	10.40W				
24FEB79	304-13330-2	44.39N	10.40W				
25FEB79	305-12130-1	42.46N	9.42E				
25FEB79	305-12130-2	42.46N	9.42E				
25FEB79	305-12150-1	48.52N	7.36E				
25FEB79	305-12150-2	48.52N	7.36E				
25FEB79	305-12160-1	54.54N	5.02E				
25FEB79	305-12160-2	54.54N	5.02E				
26FEB79	306-12300-1	39.14N	6.16E				
26FEB79	306-12300-2	39.14N	6.16E				
26FEB79	306-12320-1	45.20N	4.21E				
26FEB79	306-12320-2	45.20N	4.21E				
26FEB79	306-12330-1	51.24N	2.04E				
26FEB79	306-12330-2	51.24N	2.04E				
27FEB79	307-1530-2	45.35N	.51E				C
27FEB79	307-1550-3	39.30N	2.46W				
27FEB79	307-12480-1	38.01N	2.06E				

DATE	IDENTIFICATION	LOCATION	SCENE	BDE	ETAT	DST	PM
27FEB79	307-12480-2	38.01N	2.06E				
27FEB79	307-12490-1	44.07N	.14E				C
27FEB79	307-12490-2	44.07N	.14E				C
27FEB79	307-12510-1	50.11N	1.56W				C
27FEB79	307-12510-2	50.11N	1.56W				C
1MAR79	309-13250-1	45.01N	9.03W				
1MAR79	309-13250-2	45.01N	9.03W				
14MAR79	322-12270-1	38.42N	6.07E				C
14MAR79	322-12270-2	38.42N	6.07E				C
14MAR79	322-12290-2	44.47N	4.13E				C
15MAR79	323-12460-1	39.55N	1.08E				
15MAR79	323-12460-2	39.55N	1.08E				
16MAR79	324-13040-1	39.04N	3.11W				
16MAR79	324-13040-2	39.04N	3.11W				
16MAR79	324-13050-1	45.09N	5.05W				C
16MAR79	324-13050-2	45.09N	5.05W				C
17MAR79	325-13230-1	41.02N	8.20W				
17MAR79	325-13230-2	41.02N	8.20W				
17MAR79	325-13240-1	47.07N	10.20W				
17MAR79	325-13240-2	47.07N	10.20W				
18MAR79	326-12040-1	43.29N	10.35E				C
18MAR79	326-12040-2	43.29N	10.35E				C
18MAR79	326-12080-1	55.34N	5.50E				
18MAR79	326-12080-2	55.34N	5.50E				
19MAR79	327-12210-1	37.19N	7.52E				C
19MAR79	327-12210-2	37.19N	7.52E				C
19MAR79	327-12220-1	43.25N	6.03E				
19MAR79	327-12220-2	43.25N	6.03E				
19MAR79	327-12260-1	55.30N	1.17L				
19MAR79	327-12260-2	55.30N	1.17E				
20MAR79	328-12390-1	36.41N	3.28E				C
20MAR79	328-12390-2	36.41N	3.28E				C
20MAR79	328-12400-1	42.47N	1.40E				C
20MAR79	328-12400-2	42.47N	1.40E				C
20MAR79	328-12420-1	48.51N	.25E				C
20MAR79	328-12420-2	48.51N	.25E				C
21MAR79	329-12570-1	38.56N	1.43W				
21MAR79	329-12570-2	38.56N	1.43W				
21MAR79	329-12590-1	45.01N	3.37W				
21MAR79	329-12590-2	45.01N	3.37W				
21MAR79	329-13010-1	51.04N	5.51W				
21MAR79	329-13010-2	51.04N	5.51W				
23MAR79	331-11580-1	43.29N	12.02E				
23MAR79	331-11580-2	43.29N	12.02E				
23MAR79	331-11590-1	49.32N	9.53E				
23MAR79	331-11590-2	49.32N	9.53E				
23MAR79	331-12040-1	55.34N	7.16E				C
23MAR79	331-12040-2	55.34N	7.16E				C
24MAR79	332-12150-1	59.07N	9.49E				C
24MAR79	332-12150-2	59.07N	9.49E				C

DATE	IDENTIFICATION	LOCATION	SCENE	BDE	ETAT	DST	PM
24MAR79	332-12160-1	45.12N	6.56E				C
24MAR79	332-12160-2	45.12N	6.56E				C
24MAR79	332-12180-1	51.15N	4.41E				C
24MAR79	332-12180-2	51.15N	4.41E				C
25MAR79	333-12330-1	38.09N	4.32E				
25MAR79	333-12330-2	38.09N	4.32E				
26MAR79	334-12530-1	46.59N	2.47W				
26MAR79	334-12530-2	46.59N	2.47W				
27MAR79	335-13090-1	39.46N	5.00W				
27MAR79	335-13090-2	39.46N	5.00W				
30MAR79	338-12260-1	38.02N	6.10E				
30MAR79	338-12260-2	38.02N	6.10E				
30MAR79	338-12270-1	44.07N	4.19E				
30MAR79	338-12270-2	44.07N	4.19E				
1APR79	340-13010-1	37.32N	2.13W				
1APR79	340-13010-2	37.32N	2.13W				
1APR79	340-13030-1	43.37N	4.04W				
1APR79	340-13030-2	43.37N	4.04W				
1APR79	340-13050-1	49.40N	6.14W				
1APR79	340-13050-2	49.40N	6.14W				
2APR79	341-13210-1	41.59N	8.05W				
2APR79	341-13210-2	41.59N	8.05W				
2APR79	341-13220-1	48.03N	10.08W				
2APR79	341-13220-2	48.03N	10.08W				
7APR79	346-13130-1	43.41N	7.21W				
7APR79	346-13130-2	43.41N	7.21W				
7APR79	346-13150-1	49.45N	9.31W				
7APR79	346-13150-2	49.45N	9.31W				
8APR79	347- 590-1	41.38N	10.23E	302	R	M	6
8APR79	347-13330-1	49.01N	13.43W				
8APR79	347-13330-2	49.01N	13.43W				
10APR79	349-12290-1	39.14N	4.48E				
10APR79	349-12290-2	39.14N	4.48E				
10APR79	349-12320-1	51.22N	.37E				C
10APR79	349-12320-2	51.22N	.37E				C
11APR79	350-12460-1	39.40N	.11E				
11APR79	350-12460-2	39.40N	.11E				
11APR79	350-12480-1	45.45N	1.44W				
11APR79	350-12480-2	45.45N	1.44W				
12APR79	351-13050-1	39.13N	4.18W				
12APR79	351-13050-2	39.13N	4.18W				
12APR79	351-13060-1	45.17N	6.12W				C
12APR79	351-13060-2	45.17N	6.12W				C
13APR79	352-11490-1	50.39N	11.28E				
13APR79	352-11490-2	50.39N	11.28E				
13APR79	352-11500-1	53.04N	10.26E				
13APR79	352-11500-2	53.04N	10.26E				
13APR79	352-11510-1	56.40N	9.43E				
13APR79	352-11510-2	56.40N	9.43E				
17APR79	356-13000-1	39.13N	3.11W				C

DATE	IDENTIFICATION	LOCATION	SCENE	BDE	ETAT	DST	PM
17APR79	356-13000-2	59.13N 3.11W					C
17APR79	356-13010-1	45.17N 5.06W					C
17APR79	356-13010-2	45.17N 5.06W					
17APR79	356-13030-1	51.20N 7.22W					C
17APR79	356-13030-2	51.20N 7.22W					C
18APR79	357-13200-1	45.06N 9.41W					
18APR79	357-13200-2	45.06N 9.41W					
19APR79	358-12000-1	41.25N 11.10E					
19APR79	358-12000-2	41.25N 11.10E					
19APR79	358-12030-1	53.30N 6.43E					
19APR79	358-12030-2	53.30N 6.43E					
21APR79	360-12370-1	40.30N 2.10E					
21APR79	360-12370-2	40.30N 2.10E					
23APR79	362-13160-1	49.34N 10.08W					
23APR79	362-13160-2	49.34N 10.08W					
25APR79	364-1180-1	50.47N 8.08E					
25APR79	364-1180-2	44.43N 5.56E					C
26APR79	365-1350-1	48.31N 2.40E					
26APR79	365-1370-1	42.26N .35E					
26APR79	365-12310-1	40.06N 3.28E					C
26APR79	365-12310-2	40.06N 3.28E					C
26APR79	365-12330-1	46.10N 4.32E					
26APR79	365-12330-2	46.10N 4.32E					
26APR79	365-12340-1	52.13N .47E					
29APR79	368-540-3	43.11N 11.18E					
1MAY79	370-1310-3	41.56N 1.40E					C
1MAY79	370-12250-1	37.28N 5.29E		332	R	M	20
1MAY79	370-12250-2	37.28N 5.29E		332	R	M	23
1MAY79	370-12260-1	43.34N 3.38E		332	R	M	14
1MAY79	370-12260-2	43.34N 3.38E		332	R	M	17
2MAY79	371-1480-1	46.58N 4.15W					
2MAY79	371-1500-1	40.53N 3.14W					
3MAY79	372-2040-1	55.53N 2.08W					
3MAY79	372-2060-1	49.50N 4.47W					
5MAY79	374-1060-1	45.37N 8.46E					C
6MAY79	375-1230-1	50.43N 6.04E					
6MAY79	375-1250-1	44.38N 3.51E					C
6MAY79	375-12200-1	39.50N 6.04E		332	R	M	8
6MAY79	375-12200-2	39.50N 6.04E		332	R	M	11
6MAY79	375-12210-1	45.56N 4.08E					
6MAY79	375-12210-2	45.56N 4.08E					
7MAY79	376-1420-1	46.56N .01E					C
7MAY79	376-1440-1	40.50N 1.57W					
7MAY79	376-12380-1	41.03N 4.09E					C
7MAY79	376-12380-2	41.03N 4.09E					C
8MAY79	377-2000-1	48.56N 3.50W					
10MAY79	379-1010-1	41.72N 6.48E					C
11MAY79	380-1180-1	45.22N 5.26E					C
11MAY79	380-12130-1	38.41N 7.46E					C
11MAY79	380-12130-2	38.41N 7.46E					C

ORIGINAL PAGE 1
OF POOR QUALITY

DATE	IDENTIFICATION	LOCATION	SCENE	BDE	ETAT	DST	PM
11MAY79	380-12150-1	44.46N 5.53E					C
11MAY79	380-12150-2	44.46N 5.53E					C

ORIGINAL PAGE IS
OF POOR QUALITY